Optimization and Functionallization of Nanofibrous Mats/Membranes Prepared by Electrospinning

2005

Bin Ding

CONTENTS

CHAPTER 1

Introduction

1.1 Background

Nanoscale materials can be rationally designed to exhibit novel and significantly improved physical, chemical, and biological properties, phenomena, and processes because of their size [1]. When the diameters of polymeric fiber materials are decreased from micrometers to sub-micrometers or nanometers, they present some unique characteristics such as super large surface area to volume ratio (this ratio for a nanofiber can be as large as 10^3 times of that of a microfiber), flexibility in surface functionalities, and superior mechanical performance (e.g. stiffness and tensile strength) compared with any other known form of the materials [2]. These noticeable properties make the polymeric nanofibers to be optimal candidates for many important applications.

The electrospinning technique has been known since 1930s. Formalas published a series of patents to describe an experimental setup for the production of polymeric nanofibrous mats using an electrostatic force [3-7]. It is a useful way to produce the polymeric nanofibers through the action of an external electric field imposed on a polymer solution or melt. The polymeric nanofibers are formed, from the solution, between two electrodes bearing electrical charges of opposite polarity. One of the electrodes is placed into the solution and the other onto a collector. Once eject out of a metal spinnerette with a small hole, the charged solution jets evaporate to become fibers which are collected on the collector [8-15].

Since 1990s and especially in recent years, the electrospinning process has regained more attention probably due in part to a surging interest in nanotechnology as ultrafine fibers or fibrous structures of various polymers with diameters down to sub-micrometers or nanometers can be easily fabricated with this technique. Up to date, it is generally believed that more than one hundred different polymers have been successfully electrospun into nanofibers by this technique, such as poly(vinyl alcohol) (PVA) [16-18], polycarbonate

(PC) [19,20], nylon [20,21], polyurethane (PU) [20,22], polymethacrylate (PMA) [23,24], poly(ethylene oxide) (PEO) [9,10,16,23,25,26], polyaniline (PAN) [27,28], collagen [13,29,30], polystyrene (PS) [23,31-34], poly(vinyl phenol) (PVP) [35], poly(vinyl chloride) (PVC) [36,37], cellulose acetate (CA) [18,38], polycaprolactone (PCL) [39-41], poly(ethylene-co-vinyl alcohol) (EVAL) [42], poly(ethylene terephthalate) (PET) [14], etc. An investigation of open publications related with electrospinning in the past 10 years is given in Fig. 1-1. These literature data are obtained based on a SciFinder Scholar search system. The data clearly demonstrate that the electrospinning has attracted increasing attentions recently.

The typical polymeric nanofibers have a distribution of fiber diameters and the fibers are randomly oriented as a porous mat. The application fields based on electrospun polymeric nanofibers have been steadily extended especially in recent years. The applications which have been targeted include filtration [16-18,24,43-45], composite materials [46-56], tissue engineering [13,30,39,57-62], cosmetology [13,62,63], sensor system [64-67], and other industrial applications [27,28]. The extended or perspective applications are summarized in Fig. 1-2.

1.2 Process and Governing Parameters of Electrospinning

The schematic of electrospining process is shown in Fig. 1-3. There are basically three components to perform the electrospinning process: a high voltage power source, a syringe with a pipette or needle of small diameter and a metallic collector. In the electrospinning process, a high voltage is used to create an electrically charged jet of polymer solution or melt out of the pipette. Before reaching the collector, the solution jet evaporates or solidifies, and is collected as an interconnected web of small fibers [43].

One electrode is placed into the spinning solution/melt and the other attached to the collector. In most cases, the collector is simply grounded. The electric field is subjected to the end of the syringe that contains the solution fluid held by its surface tension. This induces a charge on the surface of the liquid. Mutual charge repulsion and the contraction of the surface charges to the counter electrode cause a force directly opposite to the surface

tension [68]. As the intensity of the electric field is increased, the hemispherical surface of the fluid at the tip of the syringe elongates to form a conical shape known as the Taylor cone [69]. Further increasing the electric field, a critical value is attained with which the repulsive electrostatic force overcomes the surface tension and the charged jet of the fluid is ejected from the tip of the Taylor cone. The discharged polymer solution jet undergoes an instability and elongation process, which allows the jet to become very long and thin. Meanwhile, the solvent evaporates, leaving behind a charged polymer fiber. In the case of the melt the discharged jet solidifies when it travels in the air [2].

Polymers, molten in high temperature, can also be made into nanofibers through electrospinning. Instead of a solution, the polymer melt is introduced into the syringe. However, different from the case of polymer solution, the electrospinning process for a polymer melt has to be performed in a vacuum condition [15,70,71]. Namely, the syringe, the traveling of the charged melt fluid jet, and the metal collector must be encapsulated within a vacuum.

Many parameters can affect the transformation of polymer solutions into nanofibers through electrospinning. These parameters include (i) the solution properties such as viscosity, elasticity, conductivity, temperature, and surface tension, (ii) governing variables such as hydrostatic pressure in the syringe, electric potential at the syringe tip, and the gap (distance between the tip and the collector), and (iii) ambient parameters such as humidity, air temperature and velocity in the electrospinning chamber [72]. The spinnibility of different polymers is investigated by some researchers. Fong et al [25] found that the electrospinning is prohibited because of the instability of flow caused by the high cohesiveness of the high viscous solution. Droplets are formed when the viscosity is too low. And the viscosity range of a different polymer solution which is spinnable is different [40]. A higher viscosity results in a large fiber diameter [73-75]. Another parameter which affects the fiber diameter to a remarkable extent is the applied electrical voltage. In general, a higher applied voltage ejects more fluid in a jet, resulting in a larger fiber diameter [9,76-78]. When the distance between the tip and the collector is short, electrospun fibers tend to stick to the collector as well as to each other, due to incomplete solvent evaporation.

As long as a polymer can be electrospun into nanofibers, ideal targets would be in that: (i) the diameters of the fibers be consistent and controllable, (ii) the fiber surface be defect-free or defect-controllable, and (iii) continuous single nanofibers be collectable.

1.3 Composite and Inorganic Nanofibers

It is well known that the new materials, called nanocomposites or organic-inorganic hybrids, have the possibility to become new materials such as lightweight, flexibility, and good moldability, and of inorganic materials such as high strength, heat-stable, and chemical reisistance. These composites are expected to be applied for scrath- and abrasive-resistant hard coating [79], nonlinear optical materials [80], contact lenses [81], and reinforcement of elastomers and plastics [82].

A number of processing techniques combined with electrospinning have been employed to prepare the composite nanofibers. These approaches include (i) electrospinning the blend solution of mixed polymers, (ii) electrospinning the blend solution of polymer and sol-gel, (iii) electrospinning the sol-gel, (iv) electrospinning the blend solution of polymer with nanoparticles, carbon nanotubes (CNTs), liquid crystal, enzyme, DNA, virus, and aqueous inorganic salts, (v) coating the functional materials on nanofibers by chemical vapor deposition (CVD), sol-gel deposition, liquid-phase deposition (LPD), and “in situ doping polymerization”.

The multi-component polymeric nanofibers are obtained by electrospinning the solution of mixed polymers. Won et al [83] prepared the composite nanofibers of PEO/poly(acrylic acid) (PAA) and PEO/poly(allylamine hydrochloride) (PAH). The average diameters of electrospun PEO fibers from PEO/water solutions are decreased and their distributions are narrowed by adding PAH and PAA due to the increased charge density in solutions. The addition of PAH and PAA lower the minimum concentration for electrospinning of a PEO/water solution. Many research groups have tried to produce the other blend polymeric nanofibers in recent years, in making PEO/PAN [84], poly(l-lactide) (PLLA)/PVP [64], PVC/PU [85], PEO/silk [86], and collagen/PEO [87], respectively. The mechanical properties of composite polymeric nanofibers can be adjust by controlling the content of

each component. Additionally, Gupta et al [37] prepared composite nanofibers of bicomponent system by using a side-by-side electrospinning fashion under fixed state. Unfortunately, no reports have been found to fabricate composite nanofibrous mats with multi-component polymers which cannot be dissolved in the same solvent or kept in the same container such as, polyanion and polycation. Meanwhile, there is a demand to increase the dispersibility of multi-component in the composite nanofibrous mats in order to get uniform properties of composite nanofibrous mats.

The idea of incorporating nanoscale fillers into polymer solution to electrospin composite nanofibers has been extended to prepare a composite solution of organic and inorganic materials for electrospinning. Shao et al fabricated many kinds of composite nanofibers using sol-gel processing and electrospinning technique such as PVA/Mn_3O_4 [88], PVA/Co_3O_4 [89], PVA/NiO [90], PVA/CuO [50], etc. Other research groups also used the same way to obtain composite nanofibers such as poly(vinyl acetate) (PVAc)/TiO_2-SiO_2 [91], PAN/Ag_2O [92], PVP/TiO_2 [93], PVA/SiO_2 [52], PVA/Al_2O_3 [94], PVA/ZnO [48,95], PVAc/$MgTiO_3$ [47], PVP/$NiFe_2O_4$ [96], PVAc/V_2O_3-V_2O_5 [97], and so on. The precursor of the metal oxide is the corresponded metal alkoxide. The matrix polymers are regarded as fiber template during the electrospinning process. The properties of polymer solutions have been found greatly changed by blending with sol-gel. It is observed that the morphology, crystalline phase, swelling, thermal, and mechanical properties of composite nanofibers are strongly related with the content of sol-gel in electrospinning solutions.

Under appropriate conditions, the alkoxide precursor could be rapidly hydrolyzed by the moisture in air to generate an amorphous oxide as the liquid jets are accelerated toward the collector. The amorphous oxide could then be transformed into a polycrystalline structure as the polymer matrix is selectively removed by calcining the composite nanofibers in air at elevated temperature. If the percentage of the alkoxide precursor is sufficiently high, it is possible to obtain continuous ceramic nanofibers made of various polycrystalline metal oxides. Up to date, various kinds of ceramic nanofiber have been obtained by this template method such as Mn_3O_4 [88], Co_3O_4 [89], NiO [90], CuO [50], TiO_2-SiO_2 [91], Ag_2O [92], TiO_2 [93], SiO_2 [52], Al_2O_3 [94], ZnO [48,95], $MgTiO_3$ [47], $NiFe_2O_4$ [96], V_2O_3-V_2O_5

[97], etc. The morphology and crystalline phase of the obtained ceramic nanofibers have been proved to be strongly related with the calcination temperature and the content of metal oxides in composite nanofibers.

Wang et al [98] obtained a new nanofiber by electrospinning the sol-gel. They synthesized micro/nanoscopic $Pb(Zr_{0.52}Ti_{0.48})O_3$ fibers from commercially available zirconium n-propoxide, titanium isopropoxide, and lead 2-ethylhexanoate. Using xylene as a solvent, they are mixed to form a precursor solution with a suitable viscosity for electrospinning. Ultra-fine fibers are electrostatically drawn from the precursor solution. The as-deposited materials are sintered at various elevated temperaure. Sintered fibers have diameters varying from 100 to 500 nm. Choi et al also produced the silica nanofibers by eletrospinning the sol-gel [99].

Another attempt has been tried to fabricate the composite nanofibers by electrospinning the polymer solution with fine particles. Luu et al [62] fabricated synthetic polymer/DNA composite scaffolds by electrospinning for therapeutic application in gene delivery for tissue engineering. Results indicate that DNA release directly from these electrospun scaffolds is indeed intact, capable of cellular transfection, and successfully encoded the protein beta-galactosidase. When test under tensile loads, the electrospun polymer/DNA composite scaffolds exhibit tensile moduli of similar to 35 MPa, with similar to 45% strain initially. These values approximate those of skin and cartilage. Moreover, other composite nanofibers with biomaterials such as enzyme [31,100] and virus [101] also are successfully produced.

PVA/Pt–TiO_2 composite nanofiber aggregate is prepared by electrospinning the polymer solution with TiO_2 particles, and the photocatalytic degradation of solid-phase PVA is investigated by He and Gong [53]. The experimental results show that the photocatalytic technique is effective for the degradation of solid-phase PVA in this fiber. Kataphinan et al [102] obtained the fibers from glass/ceramic (tetraethylorthosilicate-SiO) and fire-blanket (polydiphenoxyphosphazene-PDPP) precursors by electrospinning. The SiO fibers are smaller in diameter and more uniform than the PDPP fibers, and stable to higher temperatures. Moreover, they coat these fiber systems with several rare-earth nitrates, and

find that these coatings can be used to selectively modify optical properties of the electrospun fibers.

Carbon nanotubes (CNTs) possess several unique mechanical, electronic, and other kinds of characteristics. Unfortunately, CNTs are difficult to be aligned when they are used as reinforcement in composite fabrication. The resulting nanocomposite cannot exhibit the mechanical properties as much as one would expect. Thus, several research groups have tried to incorporate CNTs into polymeric nanofibers produced through electrospinning [55,103-105]. The spinning process is expected to align CNTs or their bundles along the fiber direction due to combination of dielectrophoretic forces caused by dielectric or conductivity mismatch between CNTs and the polymer solution and high shear forces induced by the spinning. They characterized the structure, composition, and physical properties of the resulting nanocomposite fibrils.

Gong et al prepared composite nanofibers of PVA/$H_3PW_{12}O_{40}$ [106], PVA/$H_4SiW_{12}O_{40}$ [107], and PVA/$H_4SiMo_{12}O_{40}$ [108] by electrospinning the solution of template polymer and aqueous inorganic salt. The average diameter of the fibers is about 285-600 nm. The effects of the viscosity and conductivity of the PVA/inorganic salt solution on the morphologies of the fiber mats are investigated. The swelling properties of the fiber mats in water are also studied. Furthermore, the pure $H_4SiW_{12}O_{40}$ ultra-fine fiber mats are prepared by calcining the PVA/$H_4SiW_{12}O_{40}$ fiber mats at 380 ^oC for 4 h.

The approach of using electrospun polymeric nanofibers as templates provides great versatility for the design of tubular materials with controlled dimensions. Hou et al [109] reported fabricating poly(p-xylylene) nanotubes by CVD coating and solvent extraction removal of ultrathin polymer template fibers, so-called TUFT process (TUFT = tubes by fiber templates). Metal oxide nanocoating can be achieved using sol-gel process. Coating with metal oxide is achieved by soaking the template in the metal alkoxide solution and then a water/alchohol solution for hydrolysis and condensation reactions. The composite material is heated to remove the organic material and crystallize the metal oxide, leaving a porous inorganic structure that retains the initial polymer gel or membrane morphology. Caruso et al [110] prepared TiO_2 nanotubes with the help of PLLA template fiber using the above method. Drew et al [56] obtained TiO_2 coated with polyacrylontrile nanofibers

prepared by immersing the electrospun nanofibers into an aqueous solution of titanium halide salts and halogen scavengers (LPD). Sub-micrometer conducting polyaniline tubes [111] are prepared by “in situ doping polymerization” from polymeric fiber template. Unfortunately, these coating techniques still have the disadvantages for mass production such as, harsh coating condition of CVD and “in situ doping polymerization” process, and elevated temperature treatment to adjust the crystalline phase for sol-gel process. Moreover, these above methods produced the coating layers with uncontrollable thickness. Hence, there is a demand to make a coating on electrospun using a simple, inexpensive, clean, and thickness controllable method.

On the other hand, Wang et al [112-114] and other researchers [115,116] produced carbon nanofibers derived from a polyacrylonitrile (PAN)/N,N-dimethyl formamide (DMF) precursor solution using electrospinning and vacuum pyrolysis techniques. Their conductivity, sigma, is measured at temperatures between 1.9 and 300 K and transverse magnetic field between -9 and 9 T. Zero magnetic field conductivity sigma (0, T) is found to increase monotonically with the temperature with a convex sigma (0, T) versus T curve. Conductivity increases with the external transverse magnetic field, revealing a negative magnetoresistance at temperatures between 1.9 and 10 K, with a maximum magnetoresistance of -75% at 1.9 K and 9 T. The magnetic field dependence of the conductivity and the temperature dependence of the zero-field conductivity are best described using the two-dimensional weak localization effect.

1.4 Purpose of the Present Study

Electrospinning has been recognized as an efficient way for the fabrication of polymeric nanofibers with high surface-to-volume ratio. The electrospun nanofibers typically has a length > 100 μm and diameters in the range of 30-2000 nm. Polymeric nanofibers have a broad range of potential applications such as, tissue engineering, sensor, cosmetology, filtration, composite materials, and other industrial applications. After the studying of electrospinning for decades, a number of polymers have been electrospun into polymeric nanofibers with various morphologies, thermal, and mechanical properties. However, there

are still some challenges left in the electrospinning process and the functionallization of electrospun nanofibers.

No reports have been given to fabricate composite nanofibrous mats with multi-component polymers which cannot be dissolved in the same solvent or kept in the same container such as, polyanion and polycation. Meanwhile, there are also no reports to increase the dispersibility of multi-component in the composite nanofibrous mats in order to get uniform properties of composite nanofibrous mats. Therefore, we want to design a multi-jet electrospinning device to afford the opportunity for electrospinning not only bicomponent but also multi-component which cannot be dissolved in the same solvent or kept in the same container. Meanwhile, the movable multi-jet and rotatable grounded tubular layer is adopted to get the uniform thickness of blend nanofibrous mats with good dispersibility of multi-component. Two kinds of polymers which cannot be dissolved in the same solvent are chosen as a typical model for this novel electrospinning fashion. The morphology, composition, dispersibility, and mechanical properties of composite nanofibrous mats will be studied in Chapter 3.

It is unsatisfied that those coating techniques which have been used for electrospun nanofibers still have the various disadvantages. We want to find a novel coating approach to avoid the harsh coating condition, the irregular transformations of crystalline phase, the growths of crystal size, and the damages to other functional materials in the precursor during the sintering process. Moreover, this novel approach should produce the coating layers with controllable thickness. The electrostatic layer-by-layer (LBL) self-assembly technique, based on alternate adsorption of oppositely charged polyelectrolytes, shows the advantage of allowing stable films to be produced in air with the use of a simple and inexpensive apparatus and many different substrates. We design to prepare the functional materials coated nanofibers by combination of electrospinning and electrostatic LBL self-assembly techniques. The LBL structured films of TiO_2 nanoparticles and PAA on electrospun nanofibers will be fabricated in Chapter 4.

Based on the above approach, we want to fabricate the self-assembled polyelectrolyte multilayered (PEM) films on electrospun CA nanofibers via the electrostatic LBL adsorption of oppositely charged poly(allylamine hydrochloride) (PAH) and PAA. The

growth of PEM films on CA nanofibers was studied by regulating the pH value of polyelectrolyte solutions and the number of PAH/PAA bilayers. The influence of pH conditions of polyelectrolytes solution and the amount of bilayers on the formation of LBL film on nanofibers will be studied in Chapter 5.

Furthermore, we want to fabricate the Keggin-type polyoxometalate ($H_4SiW_{12}O_{40}$) nanotubes by calcining the LBL structured ultrathin hybrid films coated electrospun fibrous mats. The hybrid films coated electrospun fibrous mats can be obtained from the alternate deposition of positively charged PAH and negatively charged $H_4SiW_{12}O_{40}$ on the surface of negatively charged CA nanofibers using the electrostatic LBL self-assembly technique. The fabrication of $H_4SiW_{12}O_{40}$ nanotubes from LBL coating and thermal removal of electrospun nanofibers will be discussed in Chapter 6.

Most of known sensors composed of electrospun nanofibers are fluorescence quenching-based optical chemical sensors [65,66] for metal ions (Fe^{3+} and Hg^{2+}) and 2,4-dinitrotoluene (DNT). These sensors show high sensitivities due to the high surface area-to-volume ratio of the nanofibrous membrane structures. Encouraged by the polyelectrolytes and quartz crystal microbalance (QCM) study in our lab, we want to build up a new gas sensor model based on QCM and electrospun nanofibrous polyelectrolytes. Polyelectrolytes (polyanion and polycation) have the interactions with oppositely charged gases. In order to make the electrospun fibers stick to the collector (the electrode of QCM), a short distance is adopted between the tip and the collector, due to incomplete solvent evaporation. Sensing experiments are examined by measuring the resonance frequency shifts of QCM which due to the additional mass loading. These issues will be evaluated in Chapter 7.

Encouraged with our built gas sensor model, we want to fabricate a sensor to detect ammonia at ppb level by modifying the sensing materials. Meanwhile, the relation between sensor performance and the morphology of the fibrous membranes, concentration of ammonia, coating load of the fibrous membranes on QCM, and relative humidity will be discussed in Chapter 8.

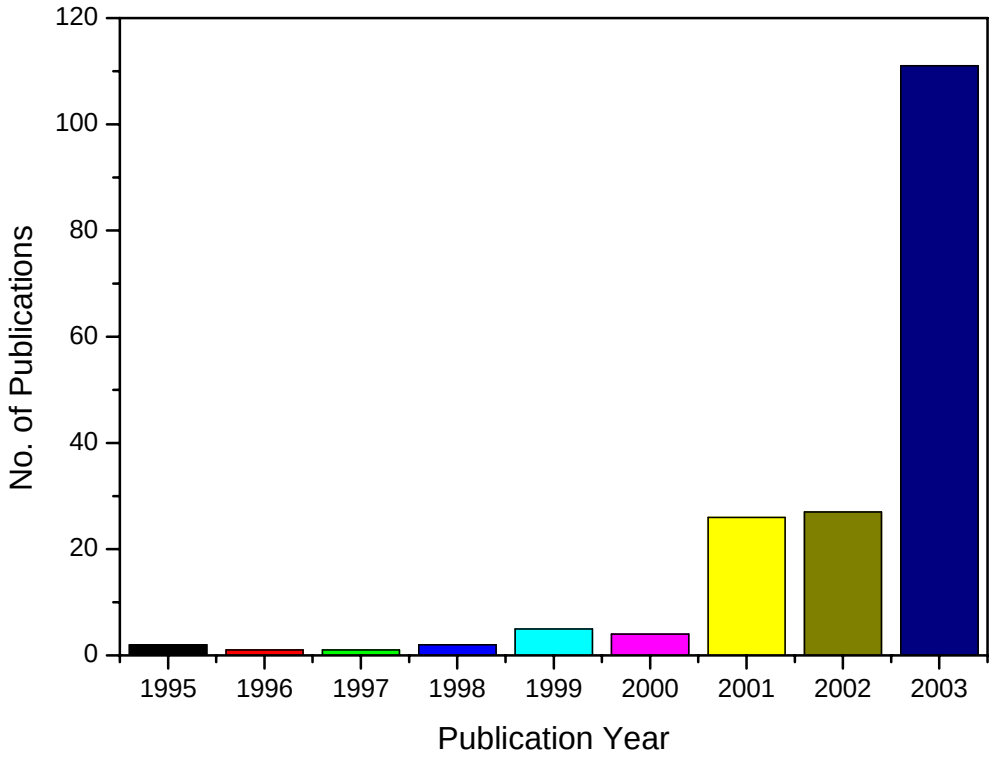

Fig. 1-1. Comparison of the annual number of scientific publications since the term of "electrospinning" was introduced in 1995. (Data analysis of publications is done using the SciFinder Scholar search system with the term "Electrospinning", as at 2004).

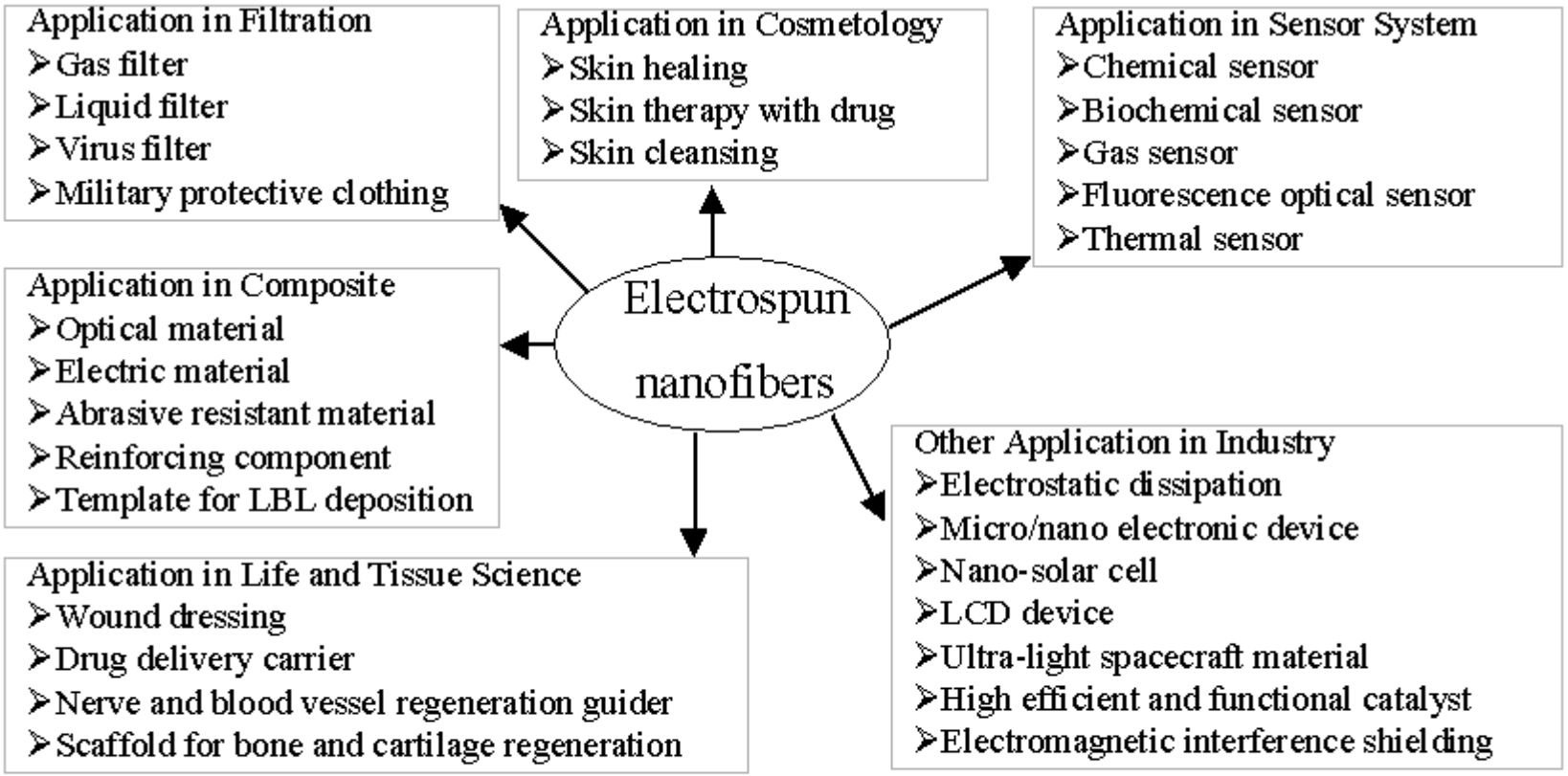

Fig. 1-2. Potential applications of electrospun nanofibers.

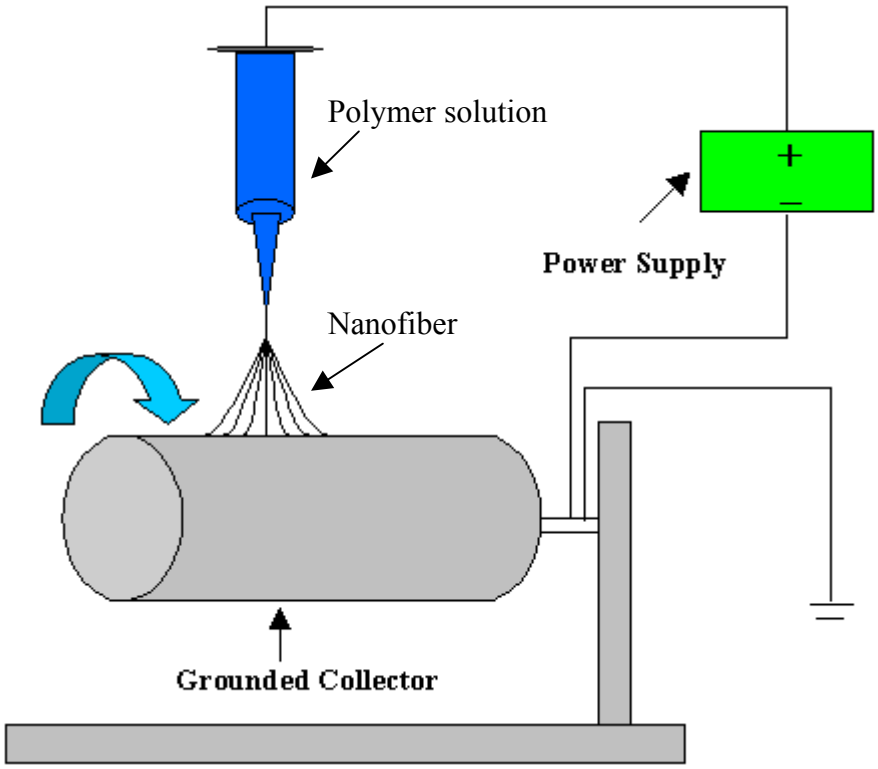

Fig. 1-3. A schematic of electrospinning process.

References

[1-1] V.E. Borisenko and A.B. Filonor, Physics, Chemistry and Application of Nanostructures, World Scientific: Singapore, 1999.

[1-2] Z.M. Huang, Y.Z. Zhang, M. Kotaki and S. Ramakrishna, *Compos. Sci. Technol.* 63 (2003) 2223.

[1-3] A. Formhals, US patent 1,975,504, 1934.

[1-4] A. Formhals US patent 2,160,962, 1939.

[1-5] A. Formhals US patent, 2,187,306, 1940.

[1-6] A. Formhals US patent, 2,323,025, 1943.

[1-7] A. Formhals US patent, 2,349,950, 1944.

[1-8] D.H. Reneker and I. Chun, *Nanotechnology* 7 (1996) 216.

[1-9] J.M. Deitzel, J. Kleinmeyer, D. Harris and T.N.C. Beck, *Polymer* 42 (2001) 261.

[1-10] Y.M. Shin, M.M. Hohman, M.P. Brenner and G.C. Rutledge, *Polymer* 42 (2001) 9955.

[1-11] D.H. Reneker, A.L. Yarin, H. Fong and S. Koombhongse, *J. Appl. Phys.* 87 (2000) 4531.

[1-12] A.L. Yarin, S. Koombhongse and D.H. Reneker, *J. Appl. Phys.* 89 (2001) 3018.

[1-13] J.A. Matthews, G.E. Wnek, D.G. Simpson and G.L. Bowlin, *Biomacromolecules* 3 (2002) 232.

[1-14] J.S. Kim and D.S. Lee, *Polym. J.* 32 (2000) 616.

[1-15] R.M. Larrondo and J. St, *J. Polym. Sci.: Polym. Phys. Ed.* 19 (1981) 921.

[1-16] B. Ding, H.Y. Kim, S.C. Lee, C.L. Shao, D.R. Lee and S.J. Park, *J. Polym. Sci.: Polym. Phys.* 40 (2002) 1261.

[1-17] L. Yao, T.W. Haas, A. Guiseppi-Elie, D.G. Simpson, G.L. Bowlin and G.E. Wnek, *Chem. Mater.* 15 (2003) 1860.

[1-18] B. Ding , E. Kimura , T. Sato , S. Fujita and S. Shiratori, *Polymer* 45 (2004) 1895.

[1-19] M. Bognitzki, H. Hou, M. Ishaque, T. Frese, M. Hellwig and C. Schwarte, *Adv. Mater.* 12 (2000) 637.

[1-20] H.L. Schreuder-Gibson, P. Gibson, K. Senecal, M. Sennett, J. Walker and W.

Yeomans, *J. Adv. Mater.* 34 (2002) 44.

[1-21] Y.J. Ryu, H.Y. Kim, K.H. Lee, H.C. Park and D.R. Lee, *Eur. Polym. J.* 39 (2003) 1883.

[1-22] A. Pedicini and R.J. Farris, *Polymer* 44 (2003) 6857.

[1-23] S. Megelski, J.S. Stephens, J.F. Rabolt and C.D. Bruce, *Macromolecules* 35 (2002) 8456.

[1-24] J.M. Deitzel, W. Kosik, S.H. McKnight, N.C.B. Ten, J.M. Desimone and S. Crette, *Polymer* 43 (2002) 1025.

[1-25] H. Fong, I. Chun and D.H. Reneker, *Polymer* 40 (1999) 4585.

[1-26] A. Theron, E. Zussman and A.L. Yarin, *Nanotechnology* 12 (2001) 384.

[1-27] A.G. MacDiarmid, W.E. Ones, I.D. Norris, J. Gao, A.T. Johnson and N.J. Pinto, *Synthetic Met.* 119 (2001) 27.

[1-28] I.D. Norris, M.M. Shaker, F.K. Ko and A.G. Macdiarmid, *Synthetic Met.* 114 (2000) 109.

[1-29] H. Yoshimoto, Y.M. Shin, H. Terai and J.P. Vacanti, *Biomaterials* 24 (2003) 2077.

[1-30] G.E. Wnek, M.E. Carr, D.G. Simpson and G.L. Bowlin, *Nano Lett.* 3 (2003) 213.

[1-31] H.F. Jia, G.Y. Zhu, B. Vugrinovich, W. Kataphinan, D.H. Reneker and P. Wang, *Biotechnol. Progr.* 18 (2002) 1027.

[1-32] J.S. Stephens, S. Frisk, S. Meglski, J.F. Rabolt and D.B. Chase, *Appl. Spectrosc.* 55 (2001) 1287.

[1-33] S. Koombhongse, W.X. Liu and D.H. Reneker, *J. Polym. Sci.: Polym. Phys.* 39 (2001) 2598.

[1-34] K.H. Lee, H.Y. Kim, H.J. Bang, Y.H. Jung and S.G. Lee, *Polymer* 44 (2003) 4029.

[1-35] K.H. Lee, H.Y. Kim, Y.M. La, D.R. Lee and N.H. Sung, *J. Polym. Sci.: Polym. Phys.* 40 (2002) 2259.

[1-36] E.R. Kenawy and Y.R. Abdel-Fattah, *Macromol. Biosci.* 2 (2002) 261.

[1-37] P. Gupta and G.L. Wilkes, *Polymer* 44 (2003) 6353.

[1-38] H.Q. Liu and Y.L. Hsieh, *J. Polym. Sci.: Polym. Phys.* 40 (2002) 2119.

[1-39] M. Shin, O. Ishii, T. Sueda and J.P. Vacanti, *Biomaterials* 25 (2004) 3717.

[1-40] S.A. Theron , E. Zussman and A.L. Yarin, *Polymer* 45 (2004) 2017.

[1-41] K.H. Lee, H.Y. Kim, M.S. Khil, Y.M. Ra and D.R. Lee, *Polymer* 44 (2003) 1287.

[1-42] E.R. Kenawy, J.M. Layman, J.R. Watkins, G.L. Bowlin, J.A. Matthews and D.G. Simpson, *Biomaterials* 24 (2003) 907.

[1-43] J.M. Deitzel, J. Kleinmeyer, J.K. Hirvonen and T.N.C. Beck, *Polymer* 42 (2001) 8163.

[1-44] P.W. Gibson, H.L. Schreuder-Gibson and D. Rivin, *AIChE J.* 45 (1999) 190.

[1-45] M.G. Hajra, K. Mehta and G.G. Chase, *Sep. Purif. Technol.* 30 (2003) 79.

[1-46] C. Shao, X. Yang, H. Guan, Y. Liu and J. Gong, *Inorg. Chem. Commun.* 7 (2004) 625.

[1-47] N. Dharmaraj, H.C. Park, B.M. Lee, P. Viswanathamurthi, H.Y. Kim and D.R. Lee, *Inorg. Chem. Commun.* 7 (2004) 431.

[1-48] X. Yang, C. Shao, H. Guan, X. Li and J. Gong, *Inorg. Chem. Commun.* 7 (2004) 176.

[1-49] H. Guan, C. Shao, S. Wen, B. Chen, J. Gong and X. Yang, *Mater. Chem. Phys.* 82 (2003) 1002.

[1-50] H. Guan, C. Shao, B. Chen, J. Gong and X. Yang, *Inorg. Chem.Commun.* 6 (2003) 1409.

[1-51] H. Guan, C. Shao, S. Wen, B. Chen, J. Gong and X. Yang, *Inorg. Chem. Commun.* 6 (2003) 1302.

[1-52] C. Shao, H.Y. Kim, J. Gong, B. Ding, D.R. Lee and S.J. Park, *Mater. Lett.* 57 (2003) 1579.

[1-53] C.H. He and J. Gong, *Polym. Degrad. Stabil.* 81 (2003) 117.

[1-54] D. Li and Y. Xia, *Nano Lett.* 4 (2004) 933.

[1-55] R. Sen, B. Zhao, D. Perea, M.E. Itkis, H. Hu, J. Love, E. Bekyarova and R.C. Haddon, *Nano Lett.* 4 **(**2004) 459.

[1-56] C. Drew, X. Liu, D. Ziegler, X. Wang, F.F. Bruno, J. Whitten, L.A. Samuelson and J. Kumar, *Nano Lett.* 3 **(**2003) 143.

[1-57] W.J. Li, C.T. Laurencin, E.J. Caterson, R.S. Tuan and F.K. Ko, *J. Biomed. Mater. Res.* 60 (2002) 613.

[1-58] M.S. Khil, D.I. Cha, H.Y. Kim, I.S. Kim and N. Bhattarai, *J. Biomed. Mater. Res. Appl. Biomater.* 67B (2003) 675.

[1-59] H.J. Jin, J. Chen, V. Karageorgiou, G.H. Altman and D.L. Kaplan, *Biomaterials* 25 (2004) 1039.

[1-60] B.M. Min, G. Lee, S.H. Kim, Y.S. Nam, T.S. Lee and W.H. Park, *Biomaterials* 25 (2004) 1289.

[1-61] W.J. Li, R. Tuli, C. Okafor, A. Derfoul, K.G. Danielson, D.J. Hall and R.S. Tuan, *Biomaterials* 26 (2005) 599.

[1-62] Y.K. Luu, K. Kim, B.S. Hsiao, B. Chu and M. Hadjiargyrou, *J. Control. Release* 89 (2003) 341.

[1-63] W.J. Li, K.G. Danielson, P.G. Alexander and R.S. Tuan, *J. Biomed. Mater. Res.* 67 (2003) 1105.

[1-64] M. Bognitzki, T. Frese, M. Steinhart, A. Greiner, J.H. Wendorff, A. Schaper and M. Hellwig, *Polym. Eng. Sci.* 41 (2001) 982.

[1-65] X. Wang, C. Drew, S.H. Lee, K.J. Senecal, J. Kumar and L.A.Samuelson, *Nano Lett.* 2 (2002) 1273.

[1-66] X. Wang, Y.G. Kim, C. Drew, B.C. Ku, J. Kumar and L.A.Samuelson, *Nano Lett.* 4 (2004) 331.

[1-67] H. Liu, J. Kameoka, D.A. Czaplewski and H.G. Craighead, *Nano Lett.* 4 (2004) 671.

[1-68] X. Fang and D.H. Reneker, *J. Macromolecular Sci. Phys.* B 36 (1997) 169.

[1-69] G.I. Taylor, *Proc. R. Soc. London, Ser. A* 313 (1969) 453.

[1-70] R.M. Larrondo and J. St, *J. Polym. Sci.: Polym. Phys. Ed.* 19 (1981) 909.

[1-71] R.M. Larrondo and J. St, *J. Polym. Sci.: Polym. Phys. Ed.* 19 (1981) 933.

[1-72] J. Doshi and D.H. Reneker, *J. Electrostat.* 35 (1995) 151.

[1-73] M.G. McKee, G.L. Wilkes, R.H. Colby and T.E. Long, *Macromolecules* 37 **(**2004) 1760.

[1-74] X. Zong, K. Kim, D. Fang, S. Ran, B.S. Hsiao and B. Chu, *Polymer* 43 (2002) 4403.

[1-75] S. Zhao, X. Wu, L. Wang and Y. Huang, *J. Appl. Polym. Sci.* 91 (2004) 242.

[1-76] S.J. Kim, K.M. Shin and S.I. Kim, *Scripta Mater.* 51 (2004) 31.

[1-77] H. Jiang, D. Fang, B.S. Hsiao, B. Chu and W. Chen, *Biomacromolecules* 5 (2004) 326.

[1-78] X.M. Mo, C.Y. Xu, M. Kotaki and S. Ramakrishna, *Biomaterials* 25 (2004) 1883.

[1-79] J. Wen, V.J. Vasudevan and G.L. Wilkes, *J. Sol-gel Sci. Technol.* 5 (1995) 115.

[1-80] C.J. Wang, Y. Pang and P.N. Prasad, *Polymer* 32 (1991) 605.

[1-81] H. Schmidt, H. Scholze and G. Tunker, *J. Non-cryst. Solids* 80 (1986) 557.

[1-82] Y. Kojima, A. Usuki, M. Kawasumi, A. Okada, T. Kurauchi and O. Kamigaitio, *J. Polym. Chem.* 31 (1993) 983.

[1-83] W.K. Son, J.H. Youk, T.S. Lee and W.H. Park, *Polymer* 45 (2004) 2959.

[1-84] P.K. Kahol and N.J. Pinto, *Synthetic Met.* 140 (2004) 269.

[1-85] K.H. Lee, H.Y. Kim, Y.J. Ryu, K.W. Kim and S.W. Choi, *J. Polym. Sci.: Polym. Phys.* 41 (2003) 1256.

[1-86] H.J. Jin, S.V. Fridrikh, G.C. Rutledge and D.L. Kaplan, *Biomolecules* 3 (2002) 1233.

[1-87] L. Huang, K. Nagapudi, R.P. Apkarian and E.L. Chaikof, *J. Biomater. Sci. Polym. Ed.* 12 (2001) 979.

[1-88] C.L. Shao, H.Y. Guan, S.B. Wen, B. Chen, X.H. Yang and J. Gong, *Chinese Chem. Lett.* 15 (2004) 471.

[1-89] C.L. Shao, H.Y. Guan, S.B. Wen, B. Chen, X.H. Yang, J. Gong and Y.C. Liu, *Chinese Chem. Lett.* 15 (2004) 492.

[1-90] C.L. Shao, H.Y. Guan, S.B. Wen, B. Chen, X.H. Yang and J. Gong, *Chinese Chem. Lett.* 15 (2004) 365.

[1-91] B. Ding, H. Kim, C. Kim, M. Khil and S. Park, *Nanotechnology* 14 (2003) 532.

[1-92] Q.B. Yang, D.M. Li, Y.L. Hong, Z.Y. Li, C. Wang, S.L. Qiu and Y. Wei, *Synthetic Met.* 137 (2003) 973.

[1-93] D. Li and Y.N. Xia, *Nano Lett.* 3 (2003) 555.

[1-94] H.Q. Dai, J. Gong, H. Kim and D. Lee, *Nanotechnology* 13 (2002) 674.

[1-95] P. Viswanathamurthi, N. Bhattarai, H.Y. Kim and D.R. Lee, *Nanotechnology* 15 (2004) 320.

[1-96] D. Li, T. Herricks and Y.N. Xia, *Appl. Phys. Lett.* 83 (2003) 4586.

[1-97] P. Viswanathamurthi, N. Bhattarai, H.Y. Kim and D.R. Lee, *Scripta Mater.* 49 (2003) 577.

[1-98] Y. Wang, R. Furlan, I. Ramos and J.J. Santiago-Aviles, Appl. Phys. A-Mater. 78 (2004) 1043.

[1-99] S.S. Choi, S.G. Lee, S.S. Im, S.H. Kim and Y.L. Joo, *J. Mater. Sci. Lett.* 22 (2003) 891.

[1-100] J.B. Xie and Y.L. Hsieh, *J. Mater. Sci.* 38 (2003) 2125.

[1-101] S.W. Lee and A.M. Belcher, *Nano Lett.* 4 (2004) 387.

[1-102] W. Kataphinan, R. Teye-Mensah, E.A. Evans, R.D. Ramsier, D.H. Reneker and D.J. Smith, *J. Vac. Sci. Technol. A* 21 (2003) 1574.

[1-103] Y. Dror, W. Salalha, R.L. Khalfin, Y. Cohen, A.L. Yarin and E. Zussman, *Langmuir* 19 (2003) 7012.

[1-104] F. Ko, Y. Gogotsi, A. Ali, N. Naguib, H.H. Ye, G.L. Yang, C. Li and P. Willis, *Adv. Mater.* 15 (2003) 1161.

[1-105] C. Seoul, Y.T. Kim and C.K. Baek, *J. Polym. Sci.: Polym. Phys.* 41 (2003) 1572.

[1-106] J. Gong, C.L. Shao, G.C. Yang, Y. Pan and L.Y. Qu, *Chinese Chem. Lett.* 15 (2004) 330.

[1-107] J. Gong, C.L. Shao, G.C. Yang, Y. Pan and L.Y. Qu, *Inorg. Chem. Commun.* 6 (2003) 916.

[1-108] J. Gong, X.D. Li, B. Ding, D.R.Lee and H.Y. Kim, *J. Appl. Polym. Sci.* 89 (2003) 1573.

[1-109] H. Hou, Z. Jun, A. Reuning, A. Schaper, J.H. Wendorff and A. Greiner, *Macromolecules* 35 (2002) 2429.

[1-110] R.A. Caruso, J.H. Schattka and A. Greiner, *Adv. Mater.* 13 (2001) 1577.

[1-111] H. Dong, S. Prasad and V. Nyame, *Chem. Mater.* 16 (2004) 371.

[1-112] Y. Wang and J.J. Santiago-Aviles, *J. Appl. Phys.* 94 (2003) 1721.

[1-113] Y. Wang, S. Serrano and J.J. Santiago-Aviles, *Synthetic Met.* 138 (2003) 423.

[1-114] Y. Wang, J.J. Santiago-Aviles, R. Furlan and I. Ramos, *IEEE T. Nanotechnol.* 2 (2003) 39.

[1-115] K.S. Yang, D.D. Edie, D.Y. Lim, Y.M. Kim and Y.O. Choi, *Carbon* 41 (2003) 2039.

[1-116] C. Kim and K.S. Yang, *Appl. Phys. Lett.* 83 (2003) 1216.

CHAPTER 2

Experimental Procedure

2.1 Starting Materials

2.1.1 Polymer sources for electrospinning

The polymers for electrospinning included poly(vinyl alcohol) (PVA) (M_n 66 000, 86-90 % hydrolyzed, Wako Pure Chemical Industries, Ltd., Japan), cellulose acetate (CA) with a degree of substitution of 2.45 (M_n 40 000, Teijin co. Ltd., Japan), and poly(acrylic acid) (PAA) (M_w 90 000, Aldrich, and M_w 250 000, Wako Pure Chemical Industries, Ltd, Japan).

2.1.2 Coating materials

The materials used for electrostatic layer-by-layer (LBL) self-assembly coating included a 25 wt% aqueous solution of PAA (M_w 90 000, Polysciences Co., Ltd.), poly(allylamine hydrochloride) (PAH) (M_w 70 000, Aldrich), TiO_2 (anatase) colloid solution of 30 wt% with a pH of 1.5 (Ishihara Co., Ltd., Japan), and $H_4SiW_{12}O_{40}\cdot 25\text{-}26H_2O$ (Aldrich). The diameter of TiO_2 particles was 7 nm.

2.1.3 Solvents

Acetone, N,N-Dimethylacetamide (DMAc), ethanol, and distilled water were employed as solvents for making electrospinning solutions and LBL coating solutions.

2.1.4 Substrates for electrospinning

Carbon paper (Gokura Co., Ltd., Japan) and quartz crystal microbalance (QCM) (10

MHz, AT-cut quartz crystal with Ag electrodes) were used as substrate for collecting nanofibers during electrospinning process.

2.2 Sample Preparation

2.2.1 Preparation of electrospinning solutions

A 10 wt% PVA solution was prepared from PVA powder and distilled water at 80 ^{o}C with vigorous stirring. CA solution was produced in acetone and DMAc, the weight ratio of acetone to DMAc was 2:1. The concentration of CA solution tested was 10 wt% [1]. PAA (M_w 90 000) was dissolved in distilled water at 12.5 wt%. The blend solutions were obtained by blending the PVA and PAA (M_w 90 000) solutions at room temperature. The weight percentage of PAA (M_w 90 000) to PVA in blend solutions was 0, 11, 18, 25, and 33 wt%, respectively [2]. Various PAA (M_w 250 000) solutions were prepared with H_2O/ethanol weight ratios of 100/0, 50/50, and 0/100. The concentration of PAA (M_w 250 000) solution was 6 wt% [3].

2.2.2 Generation of electrospun nanofibers

The schematic of the electrospinning process was shown in Fig. 2-1. A grounded stainless tubular layer was covered by a piece of carbon paper and rotated at 100 rpm. A multi-jet containing four plastic syringes (5 ml) were clamped to a stand which can be moved with the speed of 20 m/min along the track. The distance between two tips was 3 cm. The velocity of the rotatable tubular layer and the movable stand can be controlled by computer. The PVA and CA solutions were placed in different syringes according to the requirement. The positive electrode of a high voltage power supply (FC30P4, Glassman High Voltage Inc., USA) was connected with copper wires which immersed in polymer solutions. The voltage was 20 kV, and tip-to-collector distance (TCD) was 15 cm. The number ratio of jets of PVA/CA was controlled with 4/0, 3/1, 2/2, and 0/4 to get blend nanofibrous mats with different weight ratio of PVA/CA. The homogenous nanofibrous

nonwoven mats were collected on the surface of carbon paper and dried at 80 ^{o}C in vacuum for 24 h. The samples in Chapter 3 were prepared in this way [1].

The blend solutions of PAA and PVA were placed in a plastic capillary. The plastic capillary was then clamped to a stand which was above a grounded QCM (10 MHz, AT-cut quartz crystal with Ag electrodes). The applied voltage was 15 kV, and the tip-to-QCM distance was 10 cm. The droplet instantly disintegrated into nanofibers that were drawn to the QCM. Nanofibrous membranes were incontinuously collected on the surface of QCM until about 10 000 Hz frequency shift was got. The resonance frequencies were measured by a frequency counter (Hewlett Packard 53131 A). Then, the NMCQCMS were dried at 80 ^{o}C in vacuum for 2 h to remove the trace solvent and crosslink the PVA and PAA [4]. The samples in Chapter 7 were obtained in the above method [2].

The positive electrode of a high voltage power supply was immersed into a syringe containing PAA solution. The syringe was fixed to a stand which was above a grounded QCM (10 MHz, AT-cut quartz crystal with Ag electrodes), and the distance from the tip of syringe to the electrode of QCM was 5 cm. The applied voltage was kept at 20 kV. To minimize falling drops at the tip of syringe, the syringe was tilted at 15^{o} from the horizontal. Fibrous PAA membranes were in continuously collected on the electrode of QCM until the required frequency shift was got. The resonance frequencies were measured by a frequency counter (Hewlett Packard 53131 A). The coating load of the fibrous PAA membranes on QCM were about 5 000, 10 000, 15 000, and 20 000 Hz, respectively. Then, the FM-QCMs were dried for 2 h at 80 ^{o}C under vacuum prior to the subsequent characterizations. The detailed illustration was shown in Chapter 8 [3].

2.2.3 Preparation of LBL coating solutions

PAA and PAH were dissolved in distilled water under vigorous stirring, respectively. The concentration of the solutions tested was set as 10^{-2} M (based on the repeat unit molecular weight) and their pH values were adjusted according to the requirements with either HCl or NaOH solution [5-7]. The TiO_2 colloid solution, having positively charged $–TiOH_2^+$ surface [8], was diluted into 0.1 wt% with a pH of 2.5 and a zeta potential of 35.5

mV [5]. The concentration of the aqueous $H_4SiW_{12}O_{40}$ solution was 10^{-3} M and its pH was controlled at 2.5 [7].

2.2.4 LBL deposition process

In the deposition process, the negatively charged CA nanofibrous mats were immersed into the following solutions separately for different time periods: (a) the cationic TiO_2 colloid solution for 15 min, (b) the pure water three times, 1.5 min for each time, (c) the anionic PAA solution for 15 min, (d) the pure water three times, 1.5 min for each time. Steps (a) to (d) were repeated until 5 bilayers of TiO_2/PAA films were deposited. These processes were performed on an automatic dipping machine with the controlled dipping time in each bath by a personal computer. The schematic illustration of the experiment setup for preparation of LBL films was shown in Fig. 2-2. The detailed description for LBL deposition process was discussed in our previous work [9-11]. The LBL films coated fibrous mats were dried 24 h at 80 ^oC under vacuum for prior to the subsequent characterizations. In Chapter 3, the samples were fabricated by this method [5].

The hydrophilic and negatively charged CA nanofibrous mats were used for substrate material after immersion in distilled water. The self-assembled LBL films of PAH/PAA were generated according to the following procedure: (1) the CA nanofibrous mats were immersed in the cationic PAH solution for 15 min; (2) the fibrous mats were immersed into distilled water three times, 1.5 min for each; (3) the fibrous mats were immersed into the anionic PAA solution for 15 min; (d) the fibrous mats were immersed into distilled water three times, 1.5 min for each. Steps (1) to (4) were repeated until 5, 10, 15, 20, and 25 bilayers of PAH/PAA films were obtained on the fiber surface. Each sample was dried after the end of the deposition process in vacuum at 80 ^oC for 2 h. We obtained the samples in Chapter 4 using this process [6].

The hybrid films were formed by first immersing CA nanofibrous mats into the PAH solution for 15 min followed by 2 min of rinsing in three pure water baths. The mats then were immersed into the $H_4SiW_{12}O_{40}$ solution for 15 min followed by identical rinsing steps. The adsorption and rinsing steps were repeated until the desired number of deposition

bilayers was obtained. The hybrid films coated fibrous mats were dried at 80 ^{o}C for 24 h under vacuum to remove the solvent. In chapter 5, we prepared the samples using this procedure [7].

2.3 Characterization

2.3.1 Properties of electrospinning solutions

The viscosity and conductivity of the electrospinning solutions were measured by a viscotester (6L/R, Hakke, USA) and electric conductivity meter (CM-40G, TOA•DKK Co., Japan) at 25 ^{o}C, respectively.

2.3.2 Geometrical characterization of electrospun nanofibers

Geometric properties of nanofibers such as fiber diameter, diameter distribution, fiber orientation, and fiber morphology (e.g. cross-section shape and surface roughness) can be characterized using field emission scanning electron microscopy (FE-SEM), transmission electron microscopy (TEM), and atomic force microscopy (AFM).

The morphology and diameter of nanofibrous mats were determined with FE-SEM (S-4700, Hitachi Ltd., Japan) operated at a voltage of 2.0 kV. Prior to FE-SEM observation, nanofibrous mats were kept on double-sided conductive tape attached to a copper sample holder, and subsequently sputtered with Pt-Pd. The diameters of nanofibers were measured by using image analyzer (Adobe Photoshop 7.0).

The cross-sectional images of the hybrid films coated fibers were observed by TEM (Philips, TECNAI F20). The film coated fibrous mats were embedded in epoxy resin and cut into ultra-thin sections with ultramicrotome equipped with a diamond knife.

Atomic force microscopy (AFM) images were recorded by using contact mode of AFM (nanoscope IIIa, Digital Instruments).

2.3.3 Chemical characterization of electrospun nanofibers

A wide-angle X-ray diffractometer (XRD, RTP300, Rigaku Co., Japan) was used to examine the crystalline phase composition of the nanofibrous mats. The XRD data were collected in 2θ range of 3-60^{o} with the scanning speed of 1-2^{o}/min at room temperature.

The ultra-thin fibrous sheets were separated from the nanofibrous mats. Fourier transform infrared (FT-IR) spectra were recorded using a BIO-RAD spectrometer (FTS-60A/896) in the wave number range of 4000-400 cm^{-1} at 25 ^{o}C.

2.3.4 Physical characterization of electrospun nanofibers

The composition of PVA and CA in blend nanofibrous mats was investigated by immersing the dried blend nanofibrous mats into distilled water to remove the PVA component at 25 ^{o}C. The immersion time was 48 h. Then, the wet nanofibrous mats were dried at 80 ^{o}C in vacuum for 24 h. The content of PVA was calculated with the weight loss during immersion. Each sample for immersion test was checked 10 times.

Surface area measurements were carried out using the BET nitrogen adsorption method with a Micromeritics ASAP 2010 apparatus at 77 K, after pre-treating the samples overnight under vacuum at 100 ^{o}C. For the calculation of BET specific surface area, relative pressures in the range 0.05-0.2 were used.

2.3.5 Mechanical characterization of electrospun nanofibers

The mechanical properties of nanofibrous mats were tested on a tensile tester (AGS-100A, Shimadzu co., Japan) with the extension rate of 10 mm/min. The size of the samples was 100 mm length, 20 mm width, 50 mm distance between two clamps.

2.3.6. Gas sensing properties of electrospun nanofibers

The flow-type experimental setup was built up for measuring the sensing properties of sensors composed of PAA nanofibers and QCM. The sensor was installed in the chamber

which kept with constant temperature and relative humidity. The N_2 was used as carrier gas and controlled the relative humidity at 35, 40, 45, 50, 55, and 60 %, respectively. The flow rates of dry N_2, wet N_2, and NH_3 were kept constant by mass flow controllers (MFCs, Estec, SEC-400 MK3). During the measurement, the concentration of NH_3 was regulated at 130 ppb, 450 ppb, and 1, 2, 5, 50, 100, and 200 ppm, respectively. The temperature in chamber was stabilized at 25 ^{o}C by an external temperature controller. The time for each adsorption was 10 min. The resonance frequencies were measured by a frequency counter (Hewlett Packard 53131 A) which showed in Fig. 2-3. The data from the sensors were recorded by a personal computer.

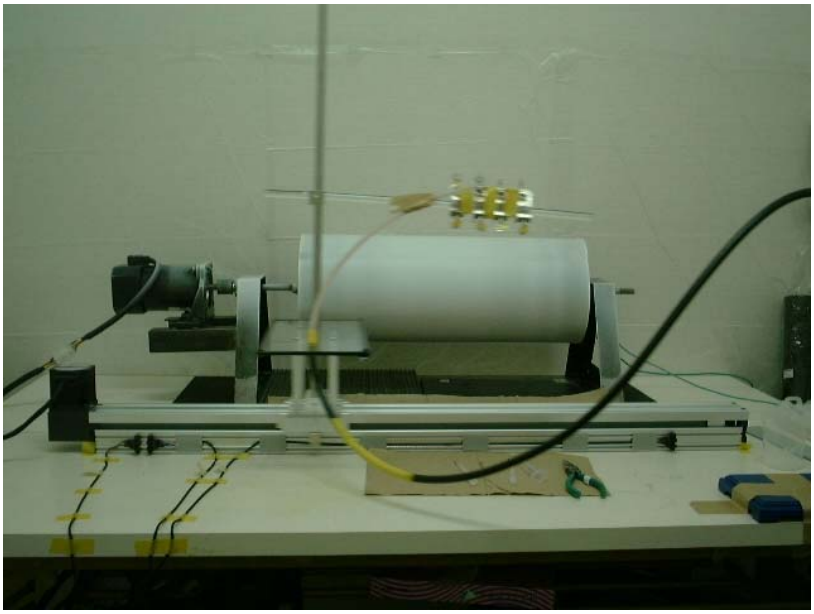

Fig. 2-1. Image of multi-jet electrospinning apparatus.

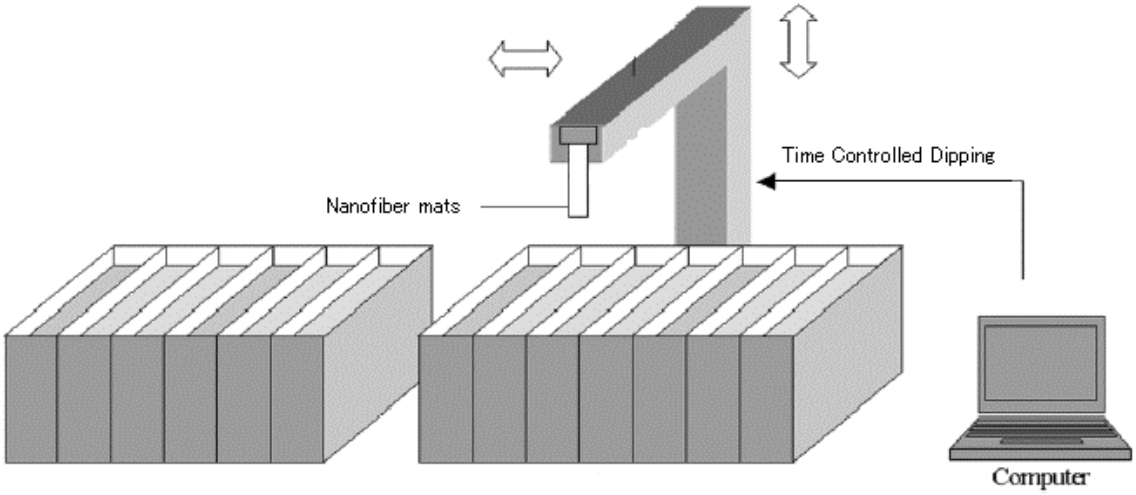

Fig. 2-2. Image of LBL self-assembly apparatus.

Fig. 2-3. Image of the QCM frequency counter.

References

[2-1] B. Ding, E. Kimura, T. Sato, S. Fujita and S. Shiratori, *Polymer* 45 (2004) 1895.

[2-2] B. Ding, J. Kim, Y. Miyazaki and S. Shiratori, *Sens. Actuator B* 101 (2004) 373.

[2-3] B. Ding, M. Yamazaki and S. Shiratori, *Sens. Actuator B* (In press).

[2-4] J. Fei and L. Fu, *Eur. Polym. J.* 38 (2002) 1653.

[2-5] B. Ding, J. Kim, E. Kimura and S. Shiratori, *Nanotechnology* 15 (2004) 913.

[2-6] B. Ding, K. Fujimoto and S. Shiratori, *Thin Solid Films* (Revised).

[2-7] B. Ding, J. Gong, J. Kim and S. Shiratori, Nanotechnology (In review).

[2-8] M.R. Hoffmann, S.T. Martin, W. Choi and D.W. Bahnemann, *Chem. Rev.* 95 (1995) 69.

[2-9] Y. Maehara, S. Takenaka, K. Shimizu, M. Yoshikawa and S. Shiratori, *Thin Solid Films* 438 (2003) 65.

[2-10] Y. Yamagata and S. Shiratori, *Thin Solid Films* 438 (2003) 238.

[2-11] S. Takenaka, Y. Maehara, H. Imai, M. Yoshikawa and S. Shiratori, *Thin Solid Films* 438 (2003) 346.

CHAPTER 3

Fabrication of Blend Biodegradable Nanofibrous Nonwoven Mats via Multi-jet Electrospinning

3.1 Introduction

In past decades, electrospinning technique has attracted great attention because polymer nanofibers with high surface-to-volume ratio can be fabricated by using this technique [1-5]. Polymer nanofibers have a broad range of applications such as tissue engineering [6], sensor [7], protective clothing [8], filter [9], etc. A number of processing techniques are combined with electrospinning to get functional nanofibrous mats such as electrospinning the mixture of polymer with sol-gel solution [10,11], the mixture of blends of polymers in the same solvent [12,13], the mixture of single polymer in co-solvent [14], and the mixture of polymer solution with nanomaterials [15-17]. Additionally, a novel method was reported by Sun et al. to fabricate the compound core/shell polymer nanofibers by co-electrospinning [18].

Recently, Gupta et al. [19] prepared blend nanofibers of bicomponent system by using a side-by-side electrospinning fashion under fixed state. We sought to increase the dispersibility of multi-component in the blend nanofibrous mats in order to get uniform properties of blend nanofibrous mats. Hence, we designed a multi-jet electrospinning device to afford the opportunity for electropinning not only bicomponent but also multi-component. Meanwhile, the movable multi-jet and rotatable grounded tubular layer is adopted to get the uniform thickness of blend nanofibrous mats with good dispersibility of multi-component. This approach can be used to fabricate blend nanofibrous mats with multi-component polymers which can not be dissolved in the same solvent or kept in the same container (polyanion and polycation).

Poly(vinyl alcohol) (PVA), a water-soluble polyhydroxy polymer, has excellent chemical resistance, physical properties, and complete biodegradability which led to broad practical applications. PVA nanofibrous mats are already prepared by electrospinning the aqueous

PVA solution and crosslinked with chemical crosslinking agent [20]. Cellulose acetate (CA) is a particularly useful polymer to prepare hybrid materials because it can be easily molded into different forms such as membranes, fibers, and spheres. The performance of CA may be improved by blending it with appropriate polymers in view of the fact that polymer blends have provided an efficient way to fulfill new requirements for material properties [21]. Preparation and morphology study of CA nanofibrous mats are reported by Liu and Hsieh [14]. Additionally, PVA and CA are both biodegradable polymers which have no pollution to environment. Therefore, the new nanofibrous materials based on PVA and CA are expected to have both advantages of PVA and CA.

However, the blend nanofibrous mats of PVA and CA have not been reported because it is difficult to find a good solvent for preparing the blend solution of PVA and CA. In the current work, we try to fabricate a series of blend nanofibrous nonwoven mats of PVA and CA with multi-jet electrospinning method and study their morphology, dispersibility, and mechanical properties.

3.2 Experimental Procedure

A 10 wt% PVA (M_n 66,000) (Wako Pure Chemical Industries, Ltd., Japan) solution was prepared from PVA powder and distilled water at 80 ^oC with vigorous stirring. CA (M_n 40,000) (Teijin co. Ltd., Japan) solution was produced in acetone and N,N-Dimethylacetamide (DMAc), the weight ratio of acetone to DMAc was 2:1. The concentration of CA solution tested was 10 wt%. The viscosity and conductivity of PVA and CA solutions were measured by a viscotester (6L/R, Hakke, USA) and electric conductivity meter (CM-40G, TOA•DKK Co., Japan), respectively.

The schematic of the electrospinning process was shown in Fig. 1. A grounded stainless tubular layer was covered by a piece of aluminum foil and rotated [22] at 100 rpm. A multi-jet containing four plastic syringes (5 ml) were clamped to a stand which can be moved with the speed of 20 m/min along the track. The distance between two tips was 3 cm. The velocity of the rotatable tubular layer and the movable stand can be controlled by computer. The PVA and CA solutions were placed in different syringes according to the

requirement. The positive electrode of a high voltage power supply (FC30P4, Glassman High Voltage Inc., USA) was connected with copper wires which immersed in polymer solutions. The voltage was 20 kV, and tip-to-collector distance (TCD) was 15 cm. The number ratio of jets of PVA/CA was controlled with 4/0, 3/1, 2/2, and 0/4 to get blend nanofibrous mats with different weight ratio of PVA/CA. The homogenous nanofibrous nonwoven mats were collected on the surface of aluminum foil and dried at 80 ^{o}C in vacuum for 24 h.

The composition of PVA and CA in blend nanofibrous mats was investigated by immersing the dried blend nanofibrous mats into distilled water to remove the PVA component. The immersion time was 48 h. Then, the wet nanofibrous mats were dried at 80 ^{o}C in vacuum for 24 h. The content of PVA was calculated with the weight loss during immersion. Each sample for immersion test was checked 10 times.

The morphology and diameter of nanofibrous mats were determined with field emission scanning electron microscopy (FE-SEM) (S-4700, Hitachi Ltd., Japan). The diameters of nanofibers were measured by using image analyzer (Adobe Photoshop 7.0). FT-IR spectra were recorded using a BIO-RAD FTS-60A/896 FT-IR spectrometer in the range 4000-400 cm^{-1}. The measurement of the crystallinity was carried out at room temperature with a wide-angle X-ray diffractometer (RTP300, Rigaku Co., Japan). The diffraction scans were collected at $2\theta = 5\text{-}40^{o}$ with the speed of 1^{o}/min.

The mechanical properties of nanofibrous mats were tested on a tensile tester (AGS-100A, Shimadzu co., Japan) with the extension rate of 10 mm/min. The size of the samples was 100 mm length, 20 mm width, 50 mm distance between two clamps.

3.3 Results and Discussion

3.3.1 Electrospinning process and determination of composition in blends

Table 1 lists solution properties of PVA and CA. The nanofibrous mats can be fabricated under the given viscosity and conductivity from each polymer solutions. During electrospinning process, a relative high voltage (20 kV) was used to supply the power for

four jets electrospinning. The PVA and CA nanofibers were alternatively and continuously deposited on the collector because of the movable multi-jet and the rotatable collector. The throughput of PVA and CA nanofibers was 1.9 and 2.3 mg/min•jet when all four jets were placed with the same solution during electrospinning, respectively.

The relation between weight ratio of PVA/CA and number ratio of jets of PVA/CA is given in Table 2. The weight ratio of PVA/CA in calculation was deduced from the throughput of each polymer with corresponding amount of jets. Moreover, the real weight ratio of PVA/CA was investigated through the immersion test. Water was a suitable medium for the immersion test because PVA was soluble in water. From the results of the real weight ratio of PVA/CA, it can be observed that the PVA component in blend nanofibrous mats can be dissolved entirely to leave CA in fiber state. And there was no weight loss for CA nanofibrous mats during the immersion test.

However, some differences were found between the calculation and fact in weight ratio of PVA/CA. One reason maybe was due to that the throughput of PVA and CA was measured when all four jets were placed with the same kind of solution. The distribution of current for different jets was changed when four jets were contained with different kinds of polymer solutions because of their different viscosity and conductivity. A linear relation was found between the currents and flow rates by Shin et al [3]. The PVA solution has much higher conductivity (18.6 ms/m) than CA solution (0.3 ms/m). Another reason maybe was due to the throughput in electrospinning couldn't be kept constant for the competition between the mechanical and electric forces. Hence, the real content of PVA in blend nanofibrous mats was different with the arithmetical content which only deduced from the throughput.

3.3.2 Morphology of nanofibrous mats

Fig. 2 shows FE-SEM photographs of PVA, CA, and blend nanofibers. The morphology of the pure PVA nanofibers (Fig. 2(a)) was regular and had an average diameter of 190 nm. In Fig. 2(e), it was observed that the diameters of pure CA nanofibers were broadly distributed with an average diameter of 420 nm. A similar phenomenon of CA nanofibers

morphology was reported by Liu and Hsieh [14]. Fig. 2(b)-(d) provide the morphology of blend nanofibers of PVA and CA. The diameters of blend nanofibers became irregular because of the existence of CA nanofibers. Meanwhile, the average diameters of blend nanofibers were increased from 220 to 290 nm on decreasing the number ratio of jets of PVA/CA from 3/1 to 1/3 (Table 2).

The diameter distributions of nanofibrous mats with different number ratio of jets of PVA/CA are presented in Fig. 3. The region of distribution of pure PVA nanofibers (Fig. 3(a)) was ranged from 100 to 400 nm and the majority was in the range of 100 to 200 nm. However, the diameters of pure CA nanofibers (Fig. 3(e)) were broadly distributed in the range of 100-900 nm with two major regions. The regions of diameter distributions of blend nanofibrous mats were enlarged and the major region was moved to large diameter when the number ratio of jets of PVA/CA was decreased from 3/1 to 1/3 (Fig. 3(b)-(d)). It can be deduced that the percentage of CA component was increased with decreasing the number ratio of jets of PVA/CA.

3.3.3 Fourier transform infrared spectroscopy

Fig. 4 gives the FT-IR spectra of nanofibrous mats with different number ratio of jets of PVA/CA. Both PVA nanofibers (curve a in Fig. 4) and CA nanofibers (curve e in Fig. 4) exhibited a number of FT-IR absorption features below 2000 cm^{-1}. These major absorption features appeared at 1740 cm^{-1} (C=O), 1450 cm^{-1} (O=C–OR), 1340 cm^{-1} ($–CH_2$), and 1110 cm^{-1} (C–O–C) [23,24]. Features above 2000 cm^{-1} are both intense and composition sensitive. They appeared at 2900 cm^{-1} ($–CH_2$) and 3400 cm^{-1} (–OH).

Additionally, PVA nanofiber has a typical band around 860 cm^{-1} and CA nanofiber has typical bands around 1190 and 1150 cm^{-1} [23,24]. These peaks around 3400, 2900 and 1450 cm^{-1} became weaker, two shoulder peaks around 1110 cm^{-1} and the peak around 860 cm^{-1} were disappeared on decreasing the number ratio of jets of PVA/CA from 4/0 to 0/4. Meanwhile, the peaks around 1190 and 1150 cm^{-1} were more evident with decreasing the number ratio of jets of PVA/CA from 4/0 to 0/4. It was also observed that all the blend nanofibers (curves b to d in Fig. 4) have both IR features of PVA and CA without new

peaks. The results demonstrated that there was no chemical reaction between PVA and CA nanofibers, just physical blending. Moreover, the intensities of feature peaks of PVA and CA in blend nanofibrous mats were strongly affected by the weight ratio of PVA/CA. The feature peaks of nanofibrous mats were gradually transformed from PVA to CA with decreasing the number ratio of PVA/CA from 4/0 to 0/4. The regular transforms indicated that PVA and CA nanofibers dispersed into each other very well.

3.3.4 Wide-angle X-ray diffraction

The WAXD patterns of nanofibrous mats with different number ratio of jets of PVA/CA are shown in Fig. 5. As observed in the curve a of Fig. 5, one peak around $2\theta = 20^{o}$ appeared, corresponding to the (101) plane of PVA semicrystalline in pure PVA nanofibers [11]. Pure CA nanofibers (curve e in Fig. 5) also showed a weak amorphous peak [25]. It indicated the amorphous nature of PVA and CA nanofibers. The intensity of amorphous peaks ($2\theta = 20^{o}$) of nanofibrous mats gradually decreased with decreasing the number ratio of jets of PVA/CA. The characteristics of WAXD patterns of nanofibrous mats were gradually transformed from PVA to CA with decreasing the number ratio of PVA/CA from 4/0 to 0/4. It also proved that the weight ratio of PVA/CA in blend nanofibrous mats can be controlled by changing the number ratio of jets of PVA/CA.

3.3.5 Mechanical properties

The mechanical properties of electrospun blend nanofibrous mats were strongly influenced by the properties of each polymer in the blend nanofibrous mats, nanofiber structure, and the interaction between each polymer nanofibers [26]. Stress-strain behavior of nanofibrous mats with different number ratio of jets of PVA/CA is shown in Fig. 6. The nanofibrous mats were broken when the maximum amount of tensile stress (tensile strength) applied to them. After adding with PVA component, the mechanical propertis of CA nanofibrous mats were largely reinforced. The resulting modulus, tensile strength, and yield stress of nanofibrous mats are shown in Fig. 7. CA nanofibrous mats (0/4) showed

much weaker mechanical properties compared with PVA nanofibrous mats (4/0). The modulus of blend nanofibrous mats were increased from 18.1 to 34.0 MPa with increasing the number ratio of jets of PVA/CA from 1/3 to 3/1. Meanwhile, the tensile strength and yield stress also were increased from 7.0 to 9.4 MPa and from 5.9 to 7.2 MPa on increasing the number ratio of jets of PVA/CA from 1/3 to 3/1, respectively.

Fig. 8 presents the elongation of nanofibrous mats as a function of number ratio of jets of PVA/CA. As observed, the elasticity of blend nanofibrous mats was reinforced with addition of PVA component. The breaking elongation of the blend nanofibrous mats gradually increased from 214 to 334 % with increasing the number ratio of jets of PVA/CA from 1/3 to 3/1. As a result, the mechanical properties of blend nanofibrous mats were improved with increasing the content of PVA. Moreover, it also indicated that the blend nanofibrous mats have good dispersibility of PVA and CA nanofibers to lead uniform mechanical properties for each sample.

3.4 Conclusions

Blend biodegradable nanofibrous nonwoven mats with different weight ratio of PVA/CA were successfully fabricated via multi-jet electrospinning. These nanofibrous mats were examined regarding their morphology, dispersibility, and mechanical properties. The results showed the blend nanofibrous mats have good dispersibility because the blend nanofibrous mats have uniform properties for each sample and regular transforms with changing the number ratio of jets of PVA/CA. As a result, the PVA and CA nanofibers were homogenously dispersed into each other. FT-IR results demonstrated that there was no chemical reaction between PVA and CA nanofibers, just physical blending. Additionally, the mechanical properties of CA nanofibrous mats were improved by increasing the content of PVA nanofibers. Furthermore, the multi-component blend nanofibrous mats also can be obtained by increasing the electrospinning jets in this multi-jet electrospinning fashion.

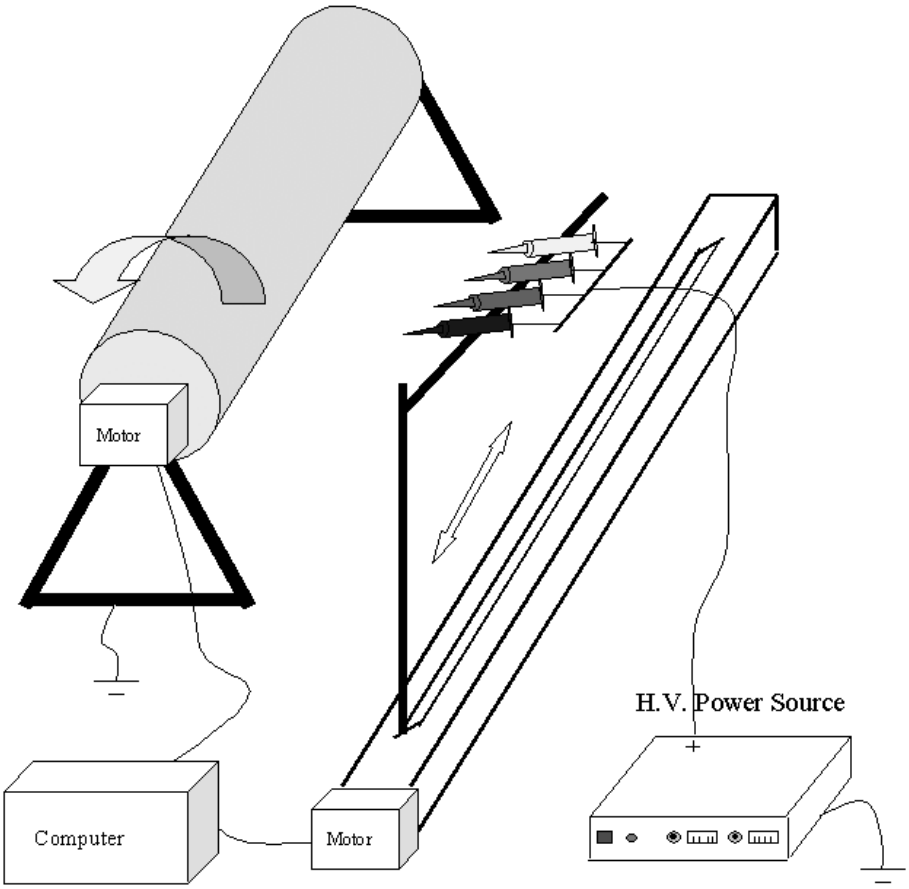

Fig. 3-1. Schematic of the electrospinning process.

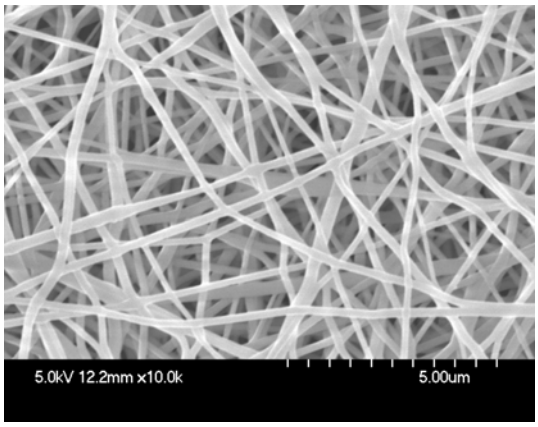

(a)

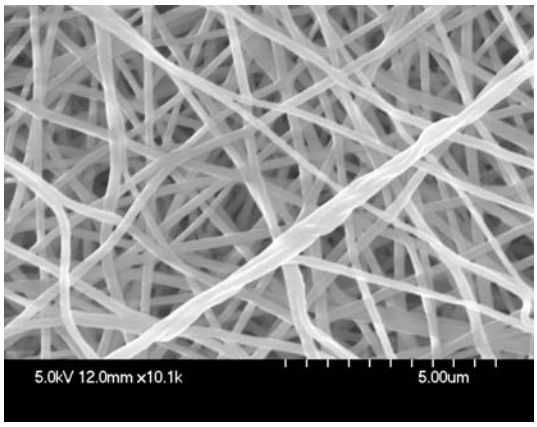

(b)

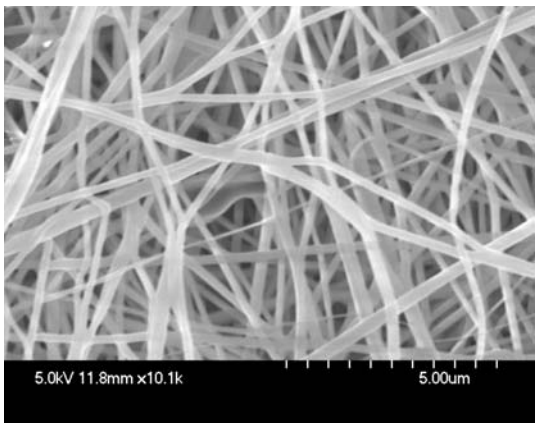

(c)

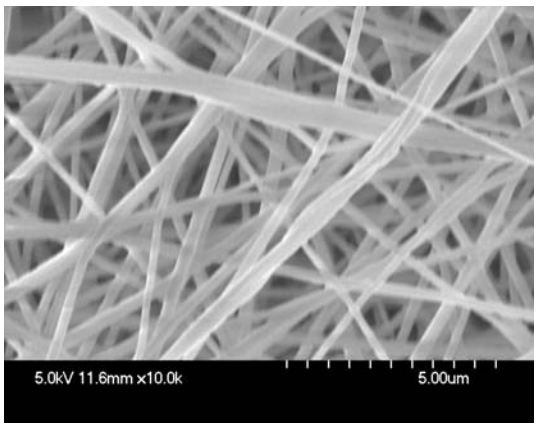

(d)

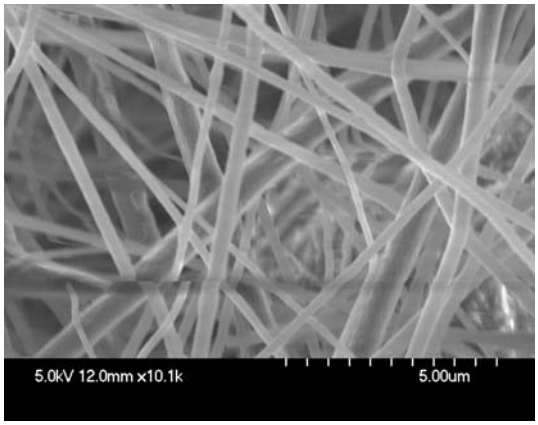

(e)

Fig. 3-2. FE-SEM photographs of nanofibrous mats with different number ratios of jets of PVA/CA. (a) 4/0; (b) 3/1; (c) 2/2; (d) 1/3; (e) 0/4.

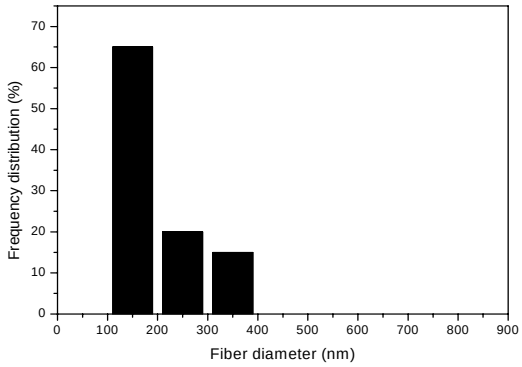

(a)

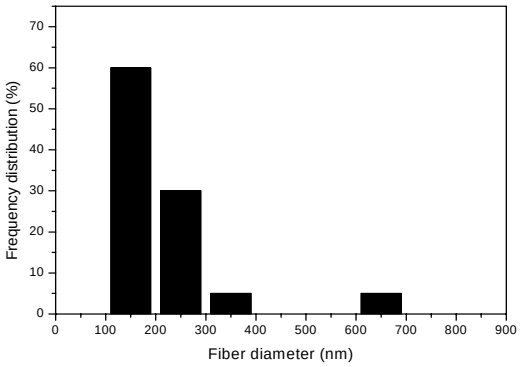

(b)

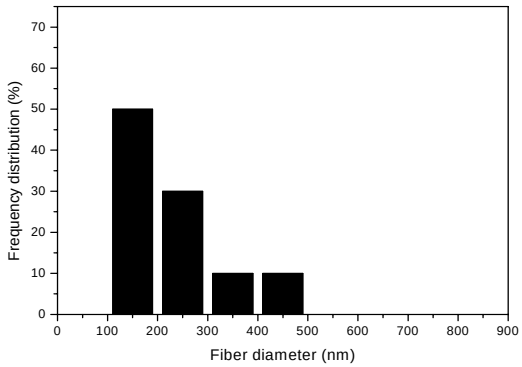

(c)

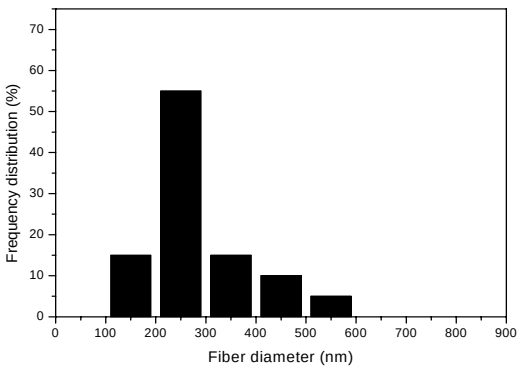

(d)

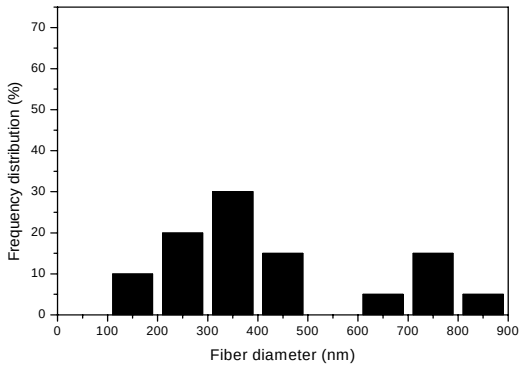

(e)

Fig. 3-3. Nanofiber diameter distributions of nanofibrous mats with different number ratios of jets of PVA/CA. (a) 4/0; (b) 3/1; (c) 2/2; (d) 1/3; (e) 0/4.

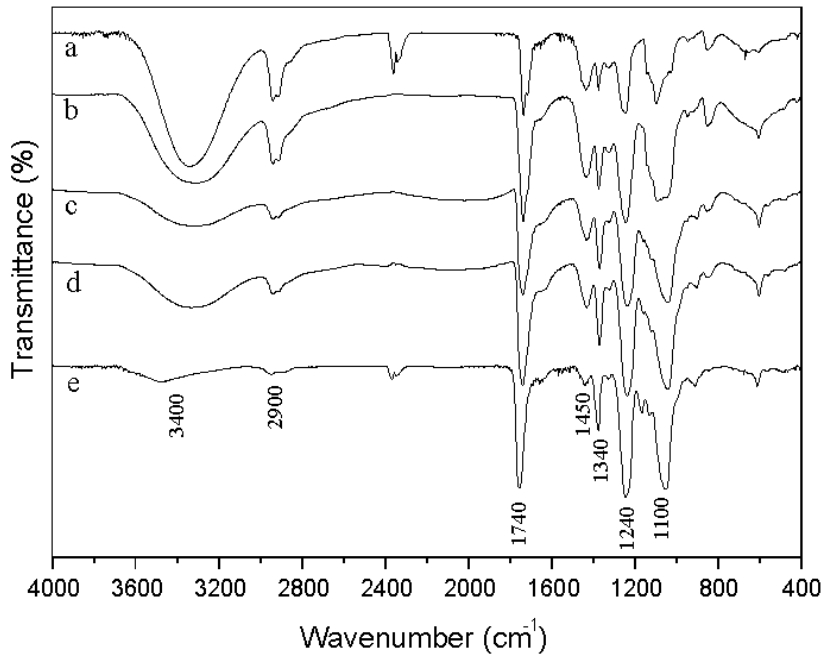

Fig. 3-4. FT-IR spectra of nanofibrous mats with different number ratios of jets of PVA/CA. (a) 4/0; (b) 3/1; (c) 2/2; (d) 1/3; (e) 0/4.

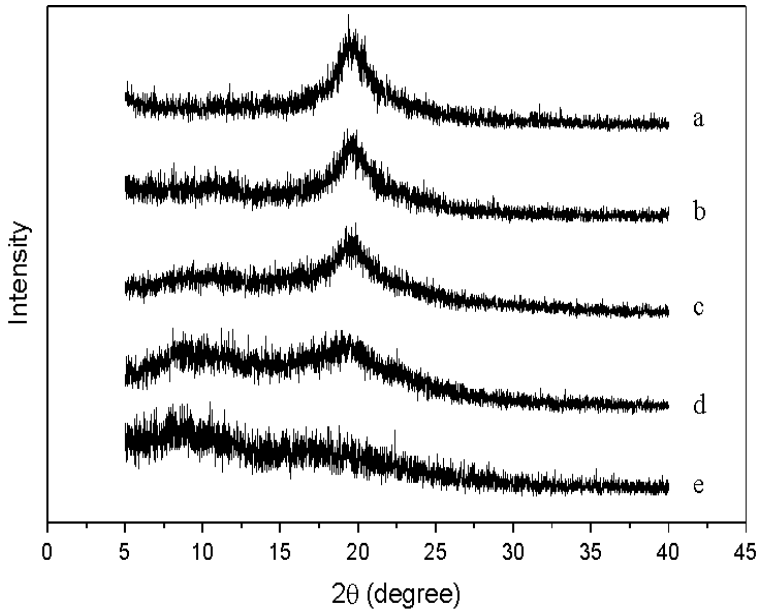

Fig. 3-5. WAXD patterns of nanofibrous mats with different number ratios of jets of PVA/CA. (a) 4/0; (b) 3/1; (c) 2/2; (d) 1/3; (e) 0/4.

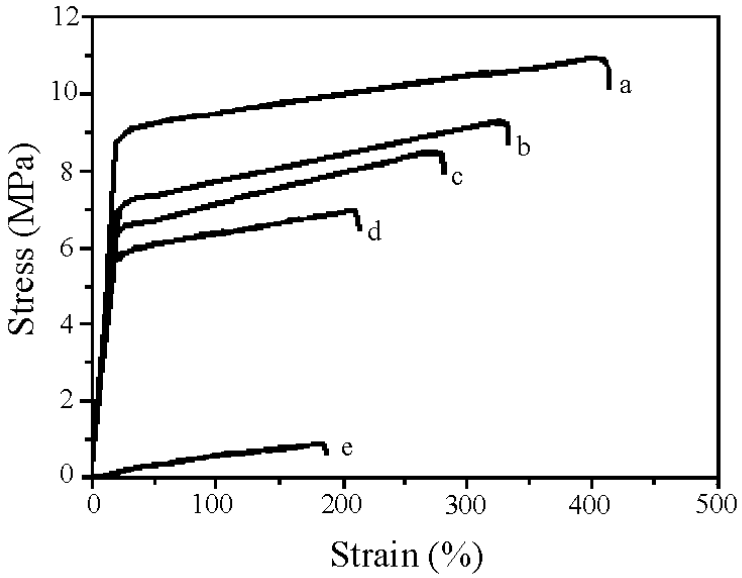

Fig. 3-6. Stress-strain behavior of nanofibrous mats with different number ratios of jets of PVA/CA. (a) 4/0; (b) 3/1; (c) 2/2; (d) 1/3; (e) 0/4.

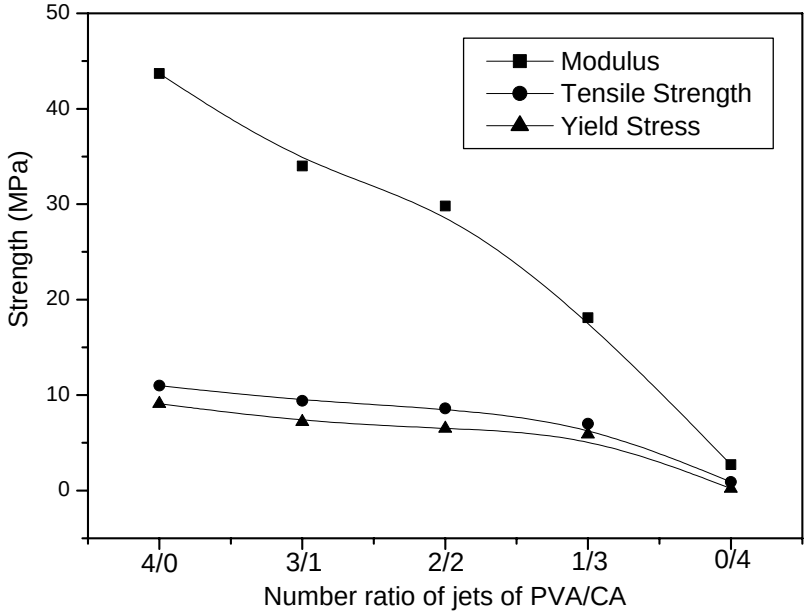

Fig. 3-7. Modulus, tensile strength and yield stress of nanofibrous mats as a function of number ratios of jets of PVA/CA.

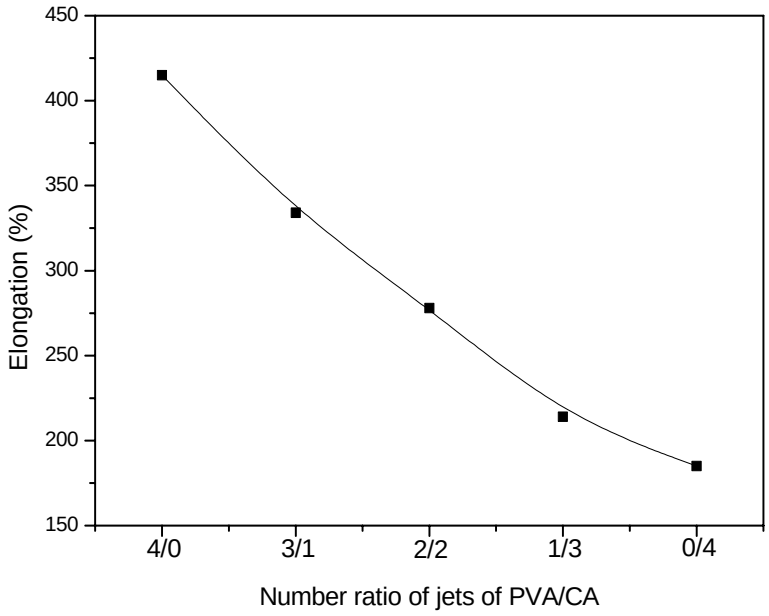

Fig. 3-8. Elongation of nanofibrous mats as a function of number ratios of jets of PVA/CA.

Sample	Concentration (wt%)	Viscosity (centipoise)	Conductivity (ms/m)	Throughput (mg/min•jet)
PVA solution	10	420	18.6	1.9
CA solution	10	360	0.3	2.3

Table 3-1. Properties of PVA and CA solutions.

Sample	No. ratio of jets (PVA/CA)	Arithmetical weight ratio (PVA/CA)	Real weight ratio (PVA/CA)	Average fiber diameter (nm)
A	4/0	100/0	100/0	190
B	3/1	70/30	77/23	220
C	2/2	45/55	51/49	240
D	1/3	20/80	26/74	290
E	0/4	0/100	0/100	420

Table 3-2. Compositions of nanofibrous mats.

References

[3-1] D.H. Reneker and I. Chun, *Nanotechnology* 7 (1996) 216.

[3-2] J.M. Deitzel, J. Kleinmeyer, D. Harris and T.N.C. Beck, *Polymer* 42 (2001) 261.

[3-3] Y.M. Shin, M.M. Hohman, M.P. Brenner and G.C. Rutledge, *Polymer* 42 (2001) 9955.

[3-4] D.H. Reneker, A.L. Yarin, H. Fong and S. Koombhongse, *J. Appl. Phys.* 87 (2000) 4531.

[3-5] A.L. Yarin, S. Koombhongse and D.H. Reneker, *J. Appl. Phys.* 89 (2001) 3018.

[3-6] J.A. Matthews, G.E. Wnek, D.G. Simpson and G.L. Bowlin, *Biomacromolecules* 3 (2002) 232.

[3-7] X.Y. Wang, C. Drew, S.H. Lee, K.J. Senecal, J. Kumar and L.A. Samuelson, *Nano Lett.* 2 (2002) 1273.

[3-8] H.L. Schreuder-Gibson, P. Gibson, K. Senecal, M. Sennett, J. Walker and W. Yeomans, *J. Adv. Mater.* 34 (2002) 44.

[3-9] P.P. Tsaia, H. Schreuder-Gibson and P. Gibson, *J. Electrostat.* 54 (2002) 333.

[3-10] B. Ding, H.Y. Kim, C.K. Kim, M.S. Khil and S.J. Park, *Nanotechnology* 14 (2003) 532.

[3-11] C.L. Shao, H.Y. Kim, J. Gong, B. Ding, D.R. Lee and S.J. Park, *Mater. Lett.* 57 (2003) 1579.

[3-12] I.D. Norris, M.M. Shaker, F.K. Ko and A.G. MacDiarmid, *Synthetic Met.* 114 (2000) 109.

[3-13] E.R. Kenawy, G.L. Bowlin, K. Mansfieled, J. Laman, D.G. Simpson, E.H. Sanders and G.E. Wnek, *J. Control. Release* 81 (2002) 57.

[3-14] H.Q. Liu and Y.L. Hsieh, *J. Polym. Sci., Polym. Phys.* 40 (2002) 2119.

[3-15] C.H. He and J. Gong, *Polym. Degrad. Stabil.* 81 (2003) 117.

[3-16] F. Ko, Y. Gogotsi, A. Ali, N. Naguib, H. Ye, G.L. Yang, C. Li and P. Willis, *Adv. Mater.* 15 (2003) 1161.

[3-17] Y. Dror, W. Salalha, R.L. Khalfin, Y. Cohen, A.L. Yarin and E. Zussman, *Langmuir* 19 (2003) 7012.

[3-18] Z. Sun, E. Zussman, A.L. Yarin, J.H. Wendorff and A. Greiner, *Adv. Mater.* 15 (2003) 1929.

[3-19] P. Gupta and G.L. Wilkes, *Polymer* 44 (2003) 6353.

[3-20] B. Ding, H.Y. Kim, S.C. Lee, C.L. Shao, D.R. Lee, S.J. Park, G.B. Kwag and K.J. Choi, *J. Polym. Sci., Polym. Phys.* 40 (2002) 1261.

[3-21] C.J. Sajitha and D. Mohan, *Polym. Int.* 52 (2003) 138.

[3-22] A. Theron, E. Zussman and A.L. Yarin, *Nanotechnology* 12 (2001) 384.

[3-23] J.H. Ryu, H.J. Lee, Y.J. Kim, Y.S. Kang and H.S. Kim, *Chem. Eur. J.* 7 (2001) 525.

[3-24] Y.H. Yu, C.Y. Lin, J.M. Yeh and W.H. Lin, *Polymer* 44 (2003) 3553.

[3-25] Q. Zhou, L.N. Zhang, M. Zhang, B. Wang and S.J. Wang, *Polymer* 44 (2003) 1733.

[3-26] K.H. Lee, H.Y. Kim, Y.J. Ryu, K.W. Kim and S.W. Choi, *J. Polym. Sci., Polym. Phys.* 41 (2003) 1256.

CHAPTER 4

Layer-by-layer Structured Films of TiO_2 Nanoparticles and Poly(acrylic acid) on Electrospun Nanofibers

4.1 Introduction

In recent years, growing attention has been paid to the design and fabrication of fine structured metal oxides on nano- and microscales because of their unique promising properties and application. Among fine structured metal oxides, TiO_2 has been extensively studied as a ceramic microporous membrane [1], as a dye-sensitized solar cell [2], as a catalyst [3], and as a humidity chemical sensor [4]. Various approaches for the preparation of nano- and microstructures of TiO_2 have been reported, such as sol-gel process [5], pyrolysis [6], electron beam evaporation [7], chemical vapor deposition [8], atomic-layer deposition [9], and hydrothermal process [10].

Electrospinning is a simple and efficient method to produce polymeric nanofibrous mats with high surface-to-volume ratio under the driving force of an external electric field on polymer solutions or melts [11-13]. The electrospun nanofibers has a typical length > 100 μm and diameters in the range of 30-2000 nm [14]. Recently, a number of processing techniques combined with electrospinning have been employed to prepare different forms of nanostructured TiO_2. Li et al. prepared the pure anatase TiO_2 nanofibers by sintering the electrospun hybrid nanofibers comprising poly(vinyl pyrrolidone) and titanium tetraisopropoxide [15]. Additionally, Caruso and his co-workers reported to fabricate TiO_2 tubes by sol-gel coating and thermal degradation of the electrospun poly(L-lactide) fibers [16]. Drew et al obtained TiO_2 coated with polyacrylonitrile nanofibers prepared by immersing the electrospun nanofibers into an aqueous solution of titanium halide salts and halogen scavengers [17].

These above processes prepared fiberlike TiO_2 by hydrolysis of titanium alkoxide and adjusted the crystalline phase of TiO_2 by sintering at elevated temperature. We sought to avoid the irregular transformations of crystalline phase, the growths of crystal size, and the

damages to other functional materials in the precursor during the sintering process. Hence, we designed to deposit the anatase TiO_2 nanoparticles directly on the electrospun nanofibers using the electrostatic LBL self-assembly technique. The technique, based on alternate adsorption of oppositely charged polyelectrolytes, shows the advantage of allowing stable films to be produced in air with the use of a simple and inexpensive apparatus and many different substrates [18]. The method of electrostatic LBL self-assembly is ideally suited for growing thin nanoparticle films with controllable thickness on the 3D structured nanofibrous mats.

It is critical to select the suitable core polymer as the fiber template. The polymer fibers with negative or positive charges, low fiber density, and good water insolubility can be regarded as ideal fiber templates, such as poly(ethylene-co-vinyl alcohol) (EVAL), CA, and chitosan. In this study, the CA nanofibers were employed as the fiber template for the electrostatic LBL deposition of TiO_2 particles and PAA.

4.2 Experimental Procedure

The starting materials included cellulose acetate (CA) (M_n 40,000, Teijin Co., Ltd., Japan), acetone and N,N-Dimethylacetamide (DMAc) (Junsei Chemical Co., Ltd.), poly(acrylic acid) (PAA) (M_w 90,000, Polysciences Co., Ltd.) aqueous solution of 25 wt%, and TiO_2 (anatase) colloid solution of 30 wt% with a pH of 1.5 (Ishihara Co., Ltd., Japan). The diameter of TiO_2 particles was 7 nm. Pure water with a resistance of 18.2 MΩ was used as solvent.

CA nanofibrous mats were fabricated by electrospinning a 10 wt% CA solution, which were prepared from acetone and DMAc with the acetone/DMAc weight ratio of 2:1. The positive electrode of a high voltage power supply was connected with a copper wire, was immersed into a pipette containing CA solution. The pipette was fixed to a stand which was above a grounded metal collector, and the distance between the tip of pipette to collector was 15 cm. The applied voltage was kept as 20 kV. The nanofibrous mats were obtained on the surface of the metallic collector. The details concerning the preparation of CA nanofibrous mats and the electrospinning process were described elsewhere [19]. The

zeta potential of CA had a negative value in the range pH 2-10 [20].

PAA, a weak anionic polyelectrolyte, was dissolved in pure water under vigorous stirring. The concentration of the PAA solution tested was set as 10^{-2} M (based on the repeat unit molecular weight) and its pH value was adjusted to be 2.5 with either HCl or NaOH solution. The concentration of $–COO^-$ was estimated in the range of 5.6×10^{-5}-9.9×10^{-5} M (pK_a of PAA 4.5-4.75). The TiO_2 colloid solution, having positively charged $–TiOH_2^+$ surface [21], was diluted into 0.1 wt% with a pH of 2.5 and a zeta potential of 35.5 mV.

In the deposition process, the negatively charged CA nanofibrous mats were immersed into the following solutions separately for different time periods: (a) the cationic TiO_2 colloid solution for 15 min, (b) the pure water three times, 1.5 min for each time, (c) the anionic PAA solution for 15 min, (d) the pure water three times, 1.5 min for each time. Steps (a) to (d) were repeated until 5 bilayers of TiO_2/PAA films were deposited. These processes were performed on an automatic dipping machine with the controlled dipping time in each bath by a personal computer. The schematic illustration of the experiment setup and detailed processes for preparation of LBL films were reported in our previous work [22]. The LBL films coated fibrous mats were dried 24 h at 80 ^oC under vacuum for prior to the subsequent characterizations.

A wide-angle X-ray diffractometer (XRD, RTP300, Rigaku Co., Japan) was used to examine the crystalline phase composition of the uncoated and the films coated fibrous mats. The XRD data were collected in 2θ range of 5-60^o with a scanning speed of 1^o/min at room temperature. The ultra-thin fibrous sheets were separated from the uncoated and films coated fibrous mats. Fourier transform infrared (FT-IR) spectra were recorded using a BIO-RAD spectrometer (FTS-60A/896) in the wave number range of 4000-400 cm^{-1} at room condition.

The morphologies of the uncoated and the films coated fibrous mats were examined by scanning electron microscopy (SEM) (S-4700, Hitachi Ltd., Japan). The diameters of fibers were measured using image analyzer (Adobe Photoshop 7.0). The films coated fibrous mats were embedded in epoxy resin and cut into ultra-thin sections with ultramicrotome equipped with a diamond knife. The cross-sectional images of the films coated fibers were

observed by a transmission electron microscope (TEM, Philips, TECNAI F20).

Surface area measurements were carried out using the BET nitrogen adsorption method with a Micromeritics ASAP 2010 apparatus at 77 K, after pre-treating the samples overnight under vacuum at 100 ^{o}C. For the calculation of BET specific surface area, relative pressures in the range 0.05-0.2 were used.

4.3 Results and Discussion

4.3.1 Wide-angle X-ray diffraction

Fig. 1 shows the WAXD patterns of the uncoated and the films coated fibrous mats. As seen in Fig. 1, the broad peaks appeared below $2\theta = 20^{o}$ in the uncoated and the films coated fibrous mats, corresponding to the semicrystalline phase of CA nanofibrous mats [23]. The WAXD pattern of the films coated fibrous mats (Fig. 1b) exhibited new reflection peaks at 2θ: 25°, 37°, 48°, and 54°, which showed that this sample possessed anatase TiO_2 phase with tetragonal anatase structure [24]. As a result, the TiO_2 particles were coated on the fibrous mats and the crystalline phase of anatase TiO_2 was not altered during the coating process. Additionally, the peak intensities of the crystalline anatase TiO_2 were lower than those of the semicrystalline CA, due to the small amount of TiO_2 in the films coated fibrous mats.

4.3.2 Fourier transform infrared spectroscopy

The FT-IR spectra of the uncoated and the films coated fibrous mats are shown in Fig. 2. The uncoated CA nanofibrous mats (Fig. 2a) exhibited a number of FT-IR absorption features [23]. It can be seen that the films coated fibrous mats (Fig. 2b) maintained the FT-IR features of CA nanofibrous mats. After the deposition of LBL films, the band of CA around 1748 cm^{-1} became broader and shifted to 1731 cm^{-1}. This absorption peak was most likely attributed to the carboxylic acid groups of PAA in LBL films that was detected around 1724 cm^{-1} in most of the cases. The new band at 1634 cm^{-1} (Fig. 2b) indicated the

presence of the intramolecular hydrogen bonding between TiO_2 particles and PAA molecules [25,26]. The bands at 1432 and 1043 cm^{-1} of CA observed in the case of C-O stretching were broaden and appeared at 1436 and 1038 cm^{-1}. And the CA band at 1235 cm^{-1} due to CH_2 deformation tended to be broader and moved to lower wave number of 1228 cm^{-1} after coating with the LBL films. Moreover, the peak at 1368 cm^{-1} was assigned to symmetrical CO_2^- stretching of PAA [25]. We also noticed a strong absorption peak around 450 cm^{-1}, attributed to TiO_2 [27]. A very broad absorption band in the region of 1800-4000 cm^{-1} indicated the presence of large amount of water molecules because the LBL films were easy to absorb the moisture in air [28]. The FT-IR spectra together with the above WAXD patterns supported the fact that the anatase TiO_2 particles and PAA were successfully coated on the CA nanofibrous mats.

4.3.3 Morphology of fibrous mats

The SEM images and diameter distributions of the uncoated and the TiO_2/PAA films coated CA fibrous mats are shown in Fig. 3. As was typical for electrospun nanofibrous mats, there was a distribution of fiber diameters, and the fibers were randomly oriented as a porous mat. The uncoated CA nanofibrous mats (Fig. 3a) showed a relatively regular morphology compared with the films coated fibrous mats (Fig. 3c). Some beads were found in the uncoated CA nanofibrous mats. The contraction of the radius of electrospinning jet, which was driven by surface tension, caused the remaining solution to form beads [29]. The diameter distribution of the uncoated CA nanofibrous mats (Fig. 3b) ranged from 100 to 600 nm and the majority was in the range of 300-400 nm. Their average diameter was 344 nm with a standard deviation of 98 nm.

We observed from Fig. 3c that the diameters of the films coated fibers were larger than the uncoated CA nanofibers due to the coating of the additional TiO_2/PAA films. The diameter distribution of the films coated fibers is shown in Fig. 3d. The diameter of the films coated fibers was distributed in the broad range of 200 to 1700 nm. The region of diameter distribution of the films coated fibers was enlarged and the major region was moved to large diameter. The average diameter of the films coated fibers was 584 nm and

the standard deviation was 192 nm. The calculated average thickness of 5 bilayers of TiO_2/PAA films coated on CA nanofibers was approximately 120 nm, and thus the average thickness of one bilayer of TiO_2/PAA film was estimated to be about 24 nm.

Fig. 4 shows the SEM image of 5 bilayers of TiO_2/PAA films coated fibers under a higher magnification. The coating appeared to have covered the fiber completely. Grainlike TiO_2 particles (called the secondary structure of fibers), were formed on the fiber surface and in the region among adjacent fibers. The size of grainlike TiO_2 particles was much larger than that of the original TiO_2 nanoparticles (7 nm), possibly ascribed to the aggregation of TiO_2 nanoparticles in colloid solution.

4.3.4 Transmission electron microscopy

The cross-sectional TEM image of TiO_2/PAA films coated fibers under low magnification is shown in Fig. 5a. Due to the fuzzy characteristics of the LBL structure associated with the interpenetration between the layers [30], it was difficult to identify the layered structure in the TEM observations. It can be seen that the TiO_2 particles were uniformly dispersed in the films without layered structure formed and the thickness of TiO_2/PAA films coated on CA nanofibers was irregular. Meanwhile, some junctions were found among the adjacent fibers that were randomly distributed. These findings differ from those observed in LBL films with flat substrates used [22]. The possible reason was that the electrospun nanofibers serving as substrates were not distributed in the same plane, but existed in 3D structure. Therefore, the thickness of films deposited on nanofibers was irregular when the fibers were located in different positions in 3D structured nanofibrous mats.

Fig. 5b displays the TEM image of the films coated fibers under a higher magnification. The outer diameter of the films coated fibers was dependent on the thickness of the TiO_2/PAA wall. The thickness of the wall was closely related to the deposition conditions, i.e., molecular weight of PAA, concentration, pH value and zeta potential of the dipping solution, the deposition time, and the amount of bilayers. The inner diameter of the TiO_2/PAA wall was controlled by the size of the electrospun template CA nanofibers.

However, the average thickness of TiO_2/PAA wall cannot be estimated from Fig. 5 since the shape of the films coated fibers was considered to deform during the sample preparation.

4.3.5 BET surface area

The BET surface area and average pore radius of fibrous mats are listed in Table 1. The BET surface area of the uncoated nanofibrous mats (2.5 m^2/g) was lower than that of other nanoparticles. However, it was much higher than the currently available textile fibers [31]. The polymer nanofibers with a pore structure can be found with the use of volatile solvents such as acetone. The reason was due to the rapid phase separation during the electrospinning process. The solvent rich regions were apparently transformed into pores [32]. The average pore radius of the uncoated CA nanofibers was 1.9 nm which was much smaller than that found in [32], ascribed to the use of blend solvents of acetone with a higher vapor pressure and DMAc with a lower vapor pressure. After the deposition of TiO_2/PAA films on CA nanofibers, the pores on nanofibers were closed by the additional films. However, the new pores with an average pore radius of 5.0 nm were formed on the rough surface of TiO_2/PAA films. The BET surface area of fibrous mats increased from 2.5 to 6 m^2/g after being coated with 5 bilayers of TiO_2/PAA films. Usually, the BET surface area decreased with increasing the fiber diameter [33]. However, the present results were inverse here. The experiment showed that the BET surface area of fibrous mats increased with an increasing diameter of fibers. We deduce that the inverse result comes from the rough surface of the films coated fibers. The BET surface area of hybrid films coated fibrous mats was expected to be increase by decreasing the diameter of CA fibers and increasing the amount of TiO_2 nanoparticles which deposited on the fiber surface.

4.4 Conclusions

Self-assembled LBL ultrathin hybrid TiO_2/PAA films coated CA nanofibrous mats were successfully fabricated by combination of electrospinning and electrostatic LBL

self-assembly techniques. The crystalline phase of anatase TiO_2 was kept in the resultant films coated fibrous mats. Additionally, the average diameter of the films coated fibers and the BET surface area of the films coated fibrous mats increased in comparison with the uncoated ones. And such LBL films coated fibrous mats would show great potential to be used as catalysts, filters and sensors. Furthermore, the LBL structured tubes might be made by thermal degradation or solvent extraction of the template nanofibers.

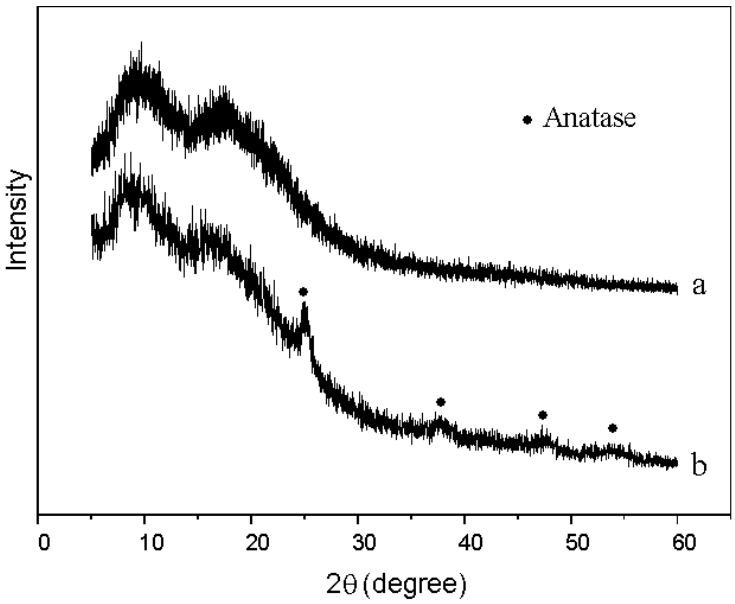

Fig. 4-1. WAXD patterns of (a) the uncoated and (b) the films coated fibrous mats.

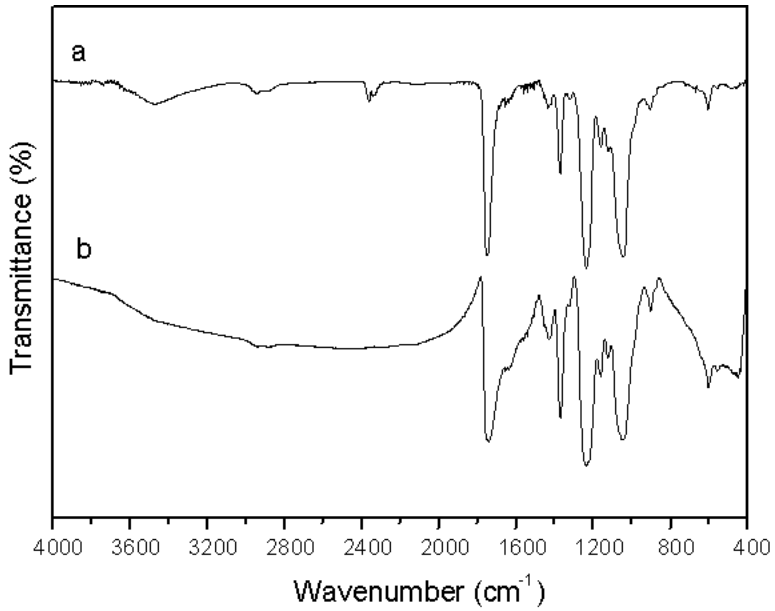

Fig. 4-2. FT-IR spectra of (a) the uncoated and (b) the films coated fibrous mats.

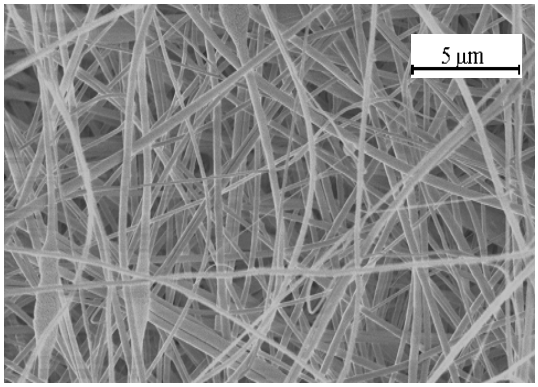

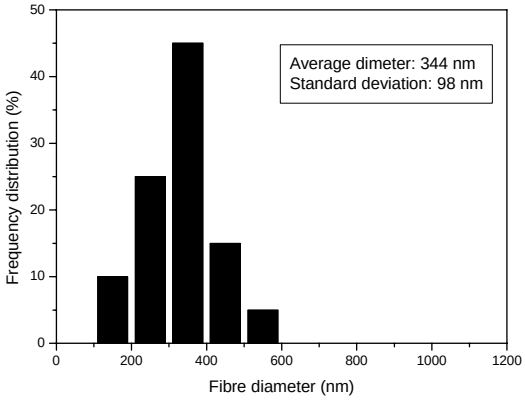

(a) (b)

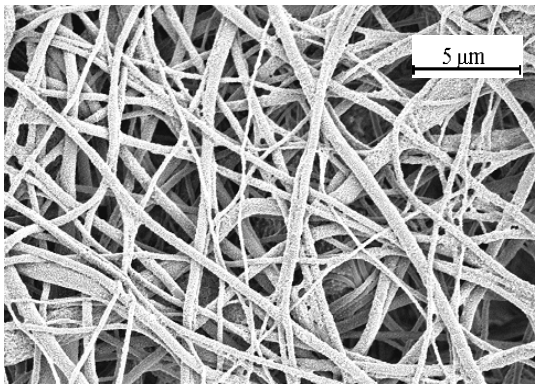

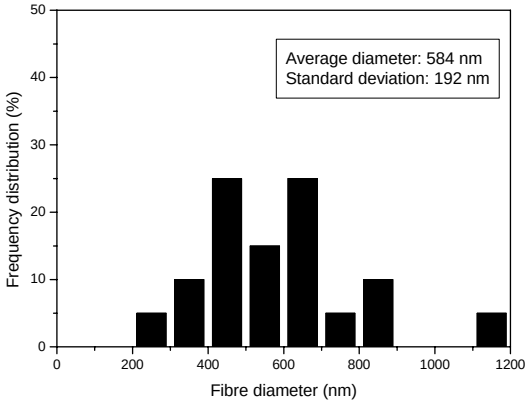

(c) (d)

Fig. 4-3. SEM images and diameter distributions of various fibrous mats: (a) SEM image and (b) diameter distribution of the uncoated CA nanofibers; (c) SEM image and (d) diameter distribution of the films coated fibrous mats.

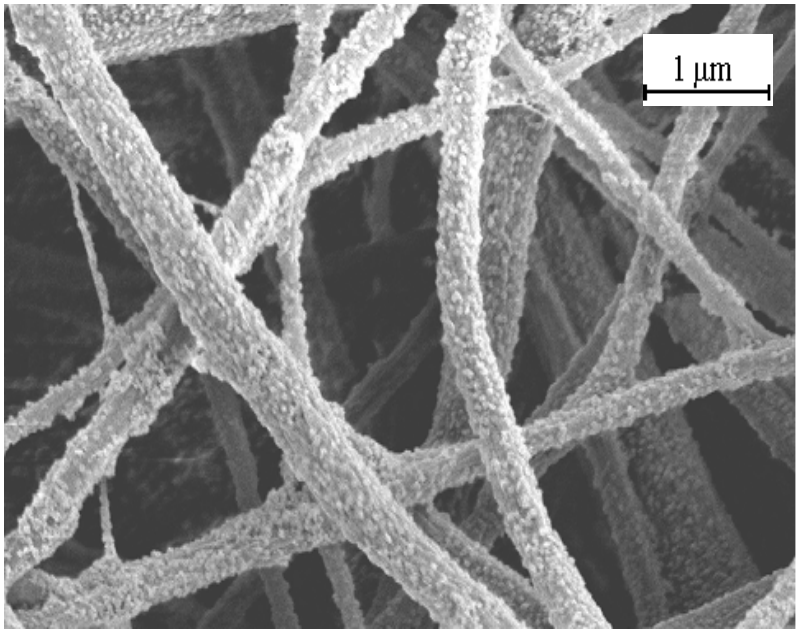

Fig. 4-4. SEM image of higher magnification showing the films coated fibrous mats.

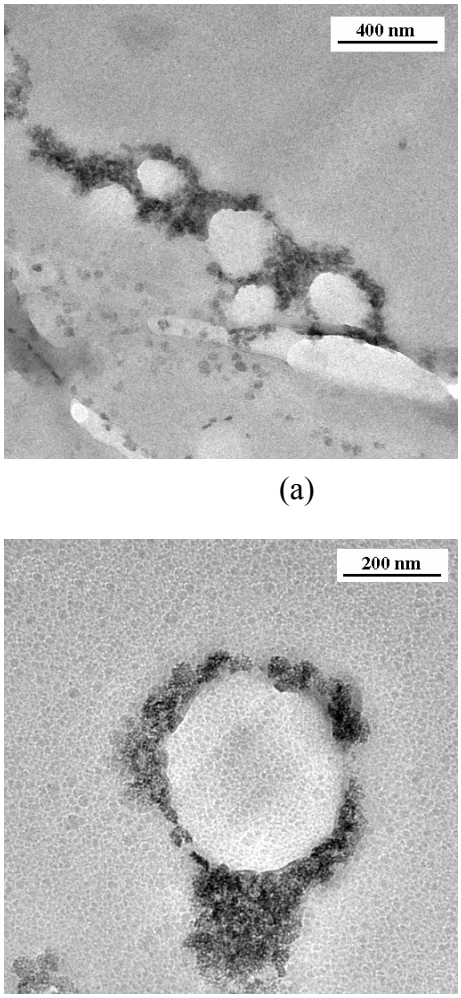

Fig. 4-5. TEM images of (a) cross-sectional films coated fibers embedded in epoxy resin and (b) detail of the coated fibers at higher magnification.

Sample	BET surface area (m^2/g)	Average pore radius (nm)
Uncoated	2.5	1.9
Coated	6.0	5.0

Table 4-1. BET surface area and average pore radius of fibrous mats.

References

[4-1] W.P. Chen, Y. Wang, X.X. Wang, J. Wang and H.L.W. Chan, *Mater. Chem. Phys.* 77 (1994) 1939.

[4-2] C.T. Kresge, M.E. Leonowicz, W.J. Roth, J.C. Vartulli and J.S. Beck, *Nature* 359 (1992) 710.

[4-3] P. Ball, *Nature* 377 (1995) 290.

[4-4] L.Y. Zheng, M.X. Xu and T.X. Xu, *Sensor. Actuat. B* 66 (2000) 28.

[4-5] H. Lin, H. Hozuka and T. Yoko, *Thin Solid Films* 315 (1998) 111.

[4-6] P. Murugavel, M. Kalaiselvam, A.R. Raju and C.N.R. Rao, *J. Mater. Chem.* 7 (1997) 1433.

[4-7] T.S. Yang, C.B. Shiu and M.S. Wong, *Surf. Sci.* 548 (2004) 75.

[4-8] S.K. Pradhan, P.J. Reucroft, F.Q. Yang and A. Dozier, *J. Cryst. Growth* 256 **(**2003) 83.

[4-9] J. Aarik, A. Aidla, V. Sammelseg and T. Vustare, *J. Cryst. Growth* 181 (1997) 259.

[4-10] M. Tan, G. Wang and L. Zhang, *J. Appl. Phys.* 80 (1996) 1186.

[4-11] D.H. Reneker, A.L. Yarin, H. Fong and S. Koombhongse, *J. Appl. Phys.* 87 (2000) 4531.

[4-12] J.M. Deitzel, J. Kleinmeyer, D. Harris and T.N.C. Beck, *Polymer* 42 (2001) 261.

[4-13] Y.M. Shin, M.M. Hohman, M.P. Brenner and G.C. Rutledge, *Polymer* 42 (2001) 9955.

[4-14] D.H. Reneker and I. Chun, *Nanotechnology* 7 (1996) 216.

[4-15] D. Li and Y. Xia, *Nano lett.* 3 (2003) 555.

[4-16] R.A. Caruso, J.H. Schattka and A. Greiner, *Adv. Mater.* 13 (2001) 1577.

[4-17] C. Drew, X. Liu, D. Ziegler, X. Wang, F.F. Bruno, J. Whitten, L.A. Samuelson and J. Kumar, *Nano Lett.* 3 (2003) 143.

[4-18] M.T. Crisp and N.A. Kotov, *Nano lett.* 3 (2003) 173.

[4-19] H.Q. Liu and Y.L. Hsieh, *J. Polym. Sci., Polym. Phys.* 40 (2002) 2119.

[4-20] H. Matsumoto, Y. Koyama and A. Tanioka, *J. Colloid Interf. Sci.* 239 (2001) 467.

[4-21] M.R. Hoffmann, S.T. Martin, W. Choi and D.W. Bahnemann, *Chem. Rev.* 95 (1995)

69.

[4-22] S.S. Shiratori, T. Ito and T. Yamada, *Colloid surf. A* 198 (2002) 415.

[4-23] B. Ding, E. Kimura, T. Sato, S. Fujita and S. Shiratori, *Polymer* 45 (2004) 1895.

[4-24] T. Trung and C.S. Ha, *Mater. Sci. Eng. C* 24 (2004) 19.

[4-25] D. Santhiya, S. Subramanian, K.A. Natarajan and S.G. Malghan, *J. Colloid Interf. Sci.* 216 (1999) 143.

[4-26] H. Tokuhisa and P.T. Hammond, *Langmuir* 20 (2004) 1436.

[4-27] H. Joe, A.K. Vasudevan, G. Aruldhas, A.D. Damodaran and K.G.K. Warrier, *J. Solid State Chem.* 131 (1997) 181.

[4-28] E. Hao and T. Lian, *Langmuir* 16 (2000) 7879.

[4-29] H. Fong, I. Chun and D.H. Reneker, *Polymer* 40 (19994) 585.

[4-30] G. Decher, *Science* 277 (1997) 1232.

[4-31] H. Fong, W. Liu, C.S. Wang and R.A. Vaia, *Polymer* 43 (2002) 775.

[4-32] M. Bognitzki, W. Czado, T. Frese, A. Schaper, M. Hellwig, M. Steinhart, A. Greiner and J.H. Wendorff, *Adv. Mater.* 13 (2001) 70.

[4-33] B. Ding, H.Y. Kim, C.K. Kim, M.S. Khil and S.J. Park, *Nanotechnology* 14 (2003) 532.

CHAPTER 5

Preparation and Characterization of Self-assembled Polyelectrolyte Multilayered Films on Electrospun Nanofibers

5.1 Introduction

Since the introduction of the electrostatic layer-by-layer (LBL) technique in 1991 by Decher et al [1], this self-assembly technique, based on alternating adsorption of oppositely charged polyelectrolytes or particles, has been one of the most frequently utilized process for preparation of functional ultra-thin films. By using the LBL technique, the multilayered films with well-defined thickness, composition, and structures can be prepared on the solid supports [2-4]. The thickness of the multilayered films can be controlled with nanoscale precision [2]. The LBL thin films have a broad range of applications such as light-emitting diodes [5-6], electrochromic devices [7], nonlinear optical devices [8], optical sensors [9], and bioinert coatings [10].

The versatility of the LBL technique involves not only the wide range of suitable layer components that can be used, but also the applicability of a wide range of substrates that can be used as supports to deposit the ultra-thin multilayered films [11,12]. A number of substrates with various shapes and sizes have been successfully employed to use as supports for deposition of multilayered films such as metal nanorods [13], short inorganic fibers [14], metal nanoparticles [15], polymer microspheres [16], etc.

On the other hand, the polymer nanofibers with diameters in the range of 30-2000 nm can be obtained from polymer solutions or melts by using electrospinning technique [17]. The morphology and properties of the polymer nanofibers depend on the properties of polymers and the process parameters, including the average molecular weight of the polymers, kinds of solvents, solution viscosity and conductivity, applied electric field strength, and deposition distance [18,19]. The nanofibrous mats composed of electrospun nanofibers has surface area approximately 1-2 orders of the magnitude larger than the flat substrates [20].

In the present work, the electrospun CA nanofibrous mats with high surface area are selected as support because their negative charges, low fiber density, and good water insolubility. The LBL self-assembly technique is applied to coat CA nanofibers with oppositely charged PAH and PAA. The influence of pH value of polyelectrolyte solutions and the number of PEM bilayers on the formation of PAH/PAA multilayered films deposited onto nanofibers is investigated to determine the suitable parameters that permit the uniform deposition on nanofibers.

5.2 Experimental Procedure

CA (M_n 40,000, Teijin co. Ltd., Japan), acetone and N,N-Dimethylacetamide (DMAc) (Junsei Chemical Co., Ltd), PAH (M_w 70,000, Aldrich), PAA (M_w 90,000, Polysciences Co., Ltd) auqueous solution of 25 % and pure water (18.2 Ω) were used as received.

A 10 wt% CA solution was prepared in acetone and DMAc, the weight ratio of acetone to DMAc was 2:1. The CA solution was placed in a syringe which was above a grounded metallic collector. The positive electrode of a high voltage power supply (FC30P4, Glassman High Voltage Inc., USA) was connected with a copper wire which immersed in CA solution. The applied voltage was 20 kV, and the distance from the tip of syringe to collector was 15 cm. The CA nanofibrous mats were obtained on the metallic collector and dried at 80 ^{o}C for 24 h under vacuum to remove the trace solvent. Liu and Hsieh [21] reported the details concerning the preparation of CA nanofibrous mats and the electrospinning process. And the zeta potential of CA had a negative value [22] in the range pH 2-10.

PAH and PAA were dissolved in pure water with vigorous stirring, respectively. The concentration of PAH and PAA was fixed as 10^{-2} M (based on repeat unit) and their pH values were adjusted to the desired value with either HCl or NaOH solution. The chemical structures of the PAA and PAH are shown in Fig. 1. PEM films were formed by first immersing CA nanofibrous mats into the PAH solution for 15 min followed by 1.5 min of rinsing in three pure water baths. The mats then were immersed into the PAA solution for 15 min followed by identical rinsing steps. The adsorption and rinsing steps were repeated

until the desired number of bilayers was obtained. The PEM films coated fibrous mats were dried at 80 ^{o}C for 24 h under vacuum to remove the solvent. Five bilayers of PEM films fabricated from a PAH solution of pH 7.5 and a PAA solution of pH 3.5 denoted as $(PAH7.5/PAA3.5)_5$. Meanwhile, PEM films of PAH and PAA adsorbed at pH 5 referred to as PAH5/PAA5.

The ultra-thin fibrous sheets were separated from the uncoated CA and PEM films coated fibrous mats. Fourier transform infrared (FT-IR) spectra were recorded using a BIO-RAD spectrometer (FTS-60A/896) in the wave number range of 4000-400 cm^{-1} with a resolution of 1 cm^{-1} at room condition. The morphologies of the uncoated CA and PEM films coated fibrous mats were examined by field emission scanning electron microscopy (FE-SEM) (S-4700, Hitachi Ltd., Japan). The diameters of fibers were measured using image analyzer (Adobe Photoshop 7.0). Atomic force microscopy (AFM) images were recorded by using tapping mode of AFM (nanoscope IIIa, Digital Instruments).

5.3 Results and Discussion

5.3.1 Influence of pH on the formation of PEM films on nanofibers

The typically electrospun nanofibrous mats composed of polymer nanofibers have a three-dimensional (3D) structure with pores in micro and sub-micro size. Different from the other supports, the deposition spaces among the adjacent nanofibers in CA nanofibrous mats were limited. It was necessary to determine the suitable deposition parameters for the fabrication of uniform PEM films on the surface of nanofibers.

In order to investigate the pH influence on the formation of PEM films on nanofibers, two types of pH combinations for the polyelectrolyte adsorption solutions were used. Fig. 2 shows the FT-IR spectra of uncoated CA nanofibers, $(PAH5/PAA5)_5$ and $(PAH7.5/PAA3.5)_5$ coated fibers. As shown in Fig. 2a, the CA nanofibers exhibited an absorption peak at 1748 cm^{-1} which was attributed to carbonyl group (C=O) [23]. After the deposition of $(PAH5/PAA5)_5$ on nanofibers (Fig. 2b), the band of CA around 1748 cm^{-1} became broader, which was most likely attributable to the vibrational mode of carboxylic

acid groups (-COOH) of PAA in PEM films that was detected around 1724 cm^{-1} in most of the cases [24]. The most notable peak was due to the carboxylate peak ($-COO^-$) [24] appeared around 1540 cm^{-1}, indicating the coexistence of both –COOH and $–COO^-$ groups in PEM films. The CA nanofibers coated with $(PAH7.5/PAA3.5)_5$ (Fig. 2c) showed the similar absorption peaks as found in the $(PAH5/PAA5)_5$ coated fibers (Fig. 2b). However, the coabsorption peak (around 1730 cm^{-1}) in $(PAH7.5/PAA3.5)_5$ coated fibers was much broader than that in $(PAH5/PAA5)_5$ coated fibers. Moreover, the relative ratio of carboxylate peak to coabsorption peak of the carboxylic acid group of PAA and the carbonyl group of CA in $(PAH7.5/PAA3.5)_5$ coated fibers was much higher than that in $(PAH5/PAA5)_5$ coated fibers. The broadened coabsorption peak and the increased relative ratio of carboxylate peak to coabsorption peak indicated that content of PAA in $(PAH7.5/PAA3.5)_5$ coated fibers was much higher than that in $(PAH5/PAA5)_5$ coated fibers. As a result, the PEM films were successfully deposited on nanofibers and the content of PEM films in fibrous mats was increased by changing the pH combinations from PAH5/PAA5 to PAH7.5/PAA3.5.

The morphology of uncoated CA nanofibers, $(PAH5/PAA5)_5$ and $(PAH7.5/PAA3.5)_5$ coated fibers are shown in Fig.3. The CA nanofibers (Fig. 3a) showed a relatively regular morphology compared with PEM films coated fibers. The characteristics of fibers and PEM films are shown in Table 1. The CA nanofibers have an average diameter of 344 nm with a standard deviation of 98 nm. After deposition of $(PAH5/PAA5)_5$ on nanofibers (Fig. 3b), the region of the diameter distribution of PEM films coated fibers was enlarged and the average diameter was increased from 344 to 486 nm due to the additional coating of PEM films. Meanwhile, the standard deviation was increased from 98 to 148 nm because of the imperfect coating led by the 3D structure of fibrous mats. Some beads were found in PEM films coated fibers which also existed in uncoated CA nanofibers (Fig. 3a). The contraction of the radius of electrospinning jet, which was driven by surface tension, caused the remaining solution to form beads [19]. The calculated average film thickness of $(PAH5/PAA5)_5$ coated on CA nanofibers was approximately 71 nm, and thus the average bilayer thickness was estimated to be about 14 nm. A similar average bilayer thickness (ca. 12.5 nm) in the same pH condition using flat supports was reported by Rubner et al. [25] to

study the pH-dependent thickness behavior.

The $(PAH7.5/PAA3.5)_5$ coated fibers (Fig. 3c) did not keep the perfect fiber shape. The PEM films formed not only on the surface of nanofibers, but also in the region among adjacent fibers. The CA nanofibers were embedded in PAH7.5/PAA3.5 films. The reason maybe was due to the fast growth of PAH/PAA films in this pH condition. The fast growth of PEM films was explained that the PAH7.5/PAA3.5 films have surfaces enriched almost completely in PAH and PAA depending on the last polyelectrolyte adsorbed [26]. This type of architecture resulted from the multilayered films fabrication process in which an adsorbing polyelectrolyte was in a partially ionized state and the previously adsorbed polyelectrolyte was in a highly ionized state. When PAA was adsorbed at pH 3.5, it was only partially ionized in solution and hence a relatively large amount (thick layer) of PAA was adsorbed to pair with the highly ionized, previously adsorbed PAH. When PAH was adsorbed at pH 7.5, all of the remaining carboxylic acid groups on the previously adsorbed PAA were ionized. In turn, a relatively large amount of PAH was required for charge compensation [26]. Therefore, the thick PEM films were formed in the 3D structure and blocked some spaces among the adjacent CA nanofibers.

The results illustrated that the morphology of PEM films coated fibers and the content of PEM films in fibrous mats were strongly affected by the pH value of polyelectrolyte solutions. The PEM films with thin bilayer thickness (PAH5/PAA5) were preferred to form a relatively uniform coating on nanofibers.

5.3.2 Influence of the number of PEM films on nanofibers

To investigate the influence of the number of PEM films on nanofibers, the CA nanofibers were deposited with 10, 15, 20, and 25 bilayers of PAA5/PAH5, respectively. Fig. 4 shows the FT-IR spectra of CA nanofibers coated with various bilayers of PAH5/PAA5. It was observed that the coadsorption peak (around 1730 cm^{-1}) composed of the carboxylic acid groups of PAA and carbonyl groups of CA was gradually broadened with increasing the number of PEM bilayers coated on nanofibers. Meanwhile, the relative ratio of the carboxylate peak (around 1540 cm^{-1}) to the coadsorption peak was gradually

increased on increasing the number of PEM bilayers on nanofibers. It can be concluded that the content of PAA in the large number of PEM bilayers coated fibers was higher than that in few number of PEM bilayers coated fibers. As a result, the content of PEM films in fibrous mats was gradually increased corresponding to the increased number of PEM bilayers coated on nanofibers.

FE-SEM images of CA nanofibers coated with various bilayers of PAH5/PAA5 are shown in Fig. 5. The related characteristics of fibers and PEM films are listed in Table 1. The average diameter of PEM films coated fibers was gradually increased from 788 to 1052 nm, and the average film thickness was gradually increased from 222 to 354 nm with increasing the number of PAH5/PAA5 bilayers from 10 to 25. The standard deviation of each PEM films coated fibers was still higher than that of uncoated CA nanofibers. The increased diameter and film thickness illustrated that the content of PEM films was increased with increasing the deposition bilayers. This was also supported by FT-IR results in Fig. 4. Moreover, some junctions which were randomly distributed among the adjacent fibers were found after deposition of 10 bilayers of PEM films. The reason was due to the limited space among the adjacent fibers and the 3D growth of PEM films along the CA nanofibers.

5.3.3 Surface roughness of PEM films coated fibers

It was reported that the electrospun nanofibers showed cylindrical-like geometries by Viswanathamurthi et al [27] using AFM in a large scan range (10 μm × 10 μm). In order to investigate the surface roughness of electrospun nanofibers, a narrow AFM scan range (2 μm × 2 μm) was adopted in this study. AFM top view images and cross section profiles of uncoated CA nanofibers and $(PAH5/PAA5)_{25}$ coated fibers are shown in Fig. 6. The folded fibers can be seen from the AFM images. The cross section profiles were shown which corresponding to the marked direction in top view. Compared with the smooth surface of uncoated CA nanofibers (Fig. 6a), the PEM films coated fibers (Fig. 6b) showed a relatively high surface roughness. The same phenomenon was reported after LBL deposition by using other flat substrates as supports [28]. The surface roughness of

$(PAH5/PAA5)_{25}$ coated fibers was estimated to be below 20 nm.

5.4 Conclusions

LBL structured ultra-thin PAH/PAA films coated CA fibrous mats were successfully produced by a combination of electrospinning and electrostatic LBL self-assembly techniques. The results showed that the formation of PEM films on CA nanofibers was strongly influenced by the pH value of polyelectrolyte solutions. The growing speed of PAH7.5/PAA3.5 films was much higher than that of PAH5/PAA5 films. Therefore, the spaces among the adjacent fibers in fibrous mats were blocked by the quickly growing PAH7.5/PAA3.5 films. However, a relatively regular deposition was found in PAH5/PAA5 coated fibers, and the PEM films coated fibers kept the fiber shape. Moreover, it was observed that the thickness of PAH5/PAA5 films coated on CA nanofibers was controllable by regulating the number of PEM bilayers. The results of AFM indicated that the PEM films coated fibers have a rougher surface than the uncoated CA nanofibers.

Poly(acrylic acid), PAA Poly(allylamine hydrochloride), PAH

Fig. 5-1. Chemical structures of PAA and PAH.

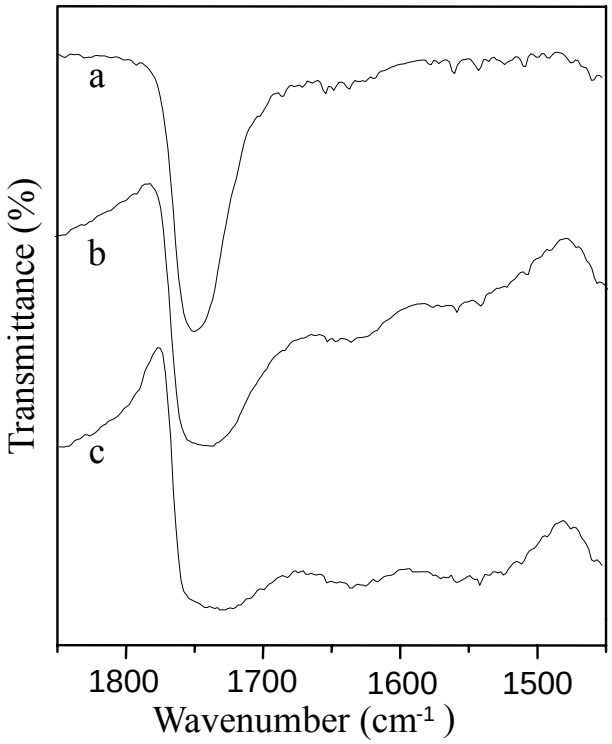

Fig. 5-2. FT-IR spectra of uncoated CA nanofibers (a), $(PAH5/PAA5)_5$ coated fibers (b) and $(PAH7.5/PAA3.5)_5$ coated fibers (c).

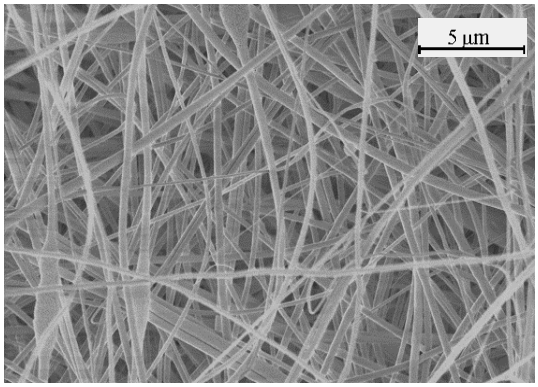

(a)

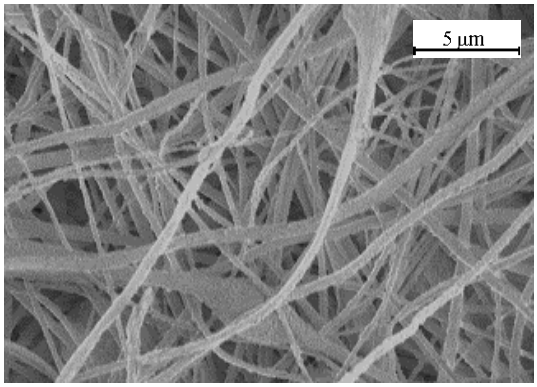

(b)

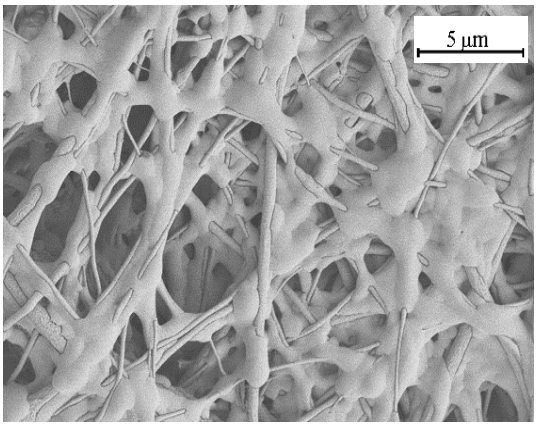

(c)

Fig. 5-3. FE-SEM images of uncoated CA nanofibers (a), $(PAH5/PAA5)_5$ coated fibers (b) and $(PAH7.5/PAA3.5)_5$ coated fibers (c).

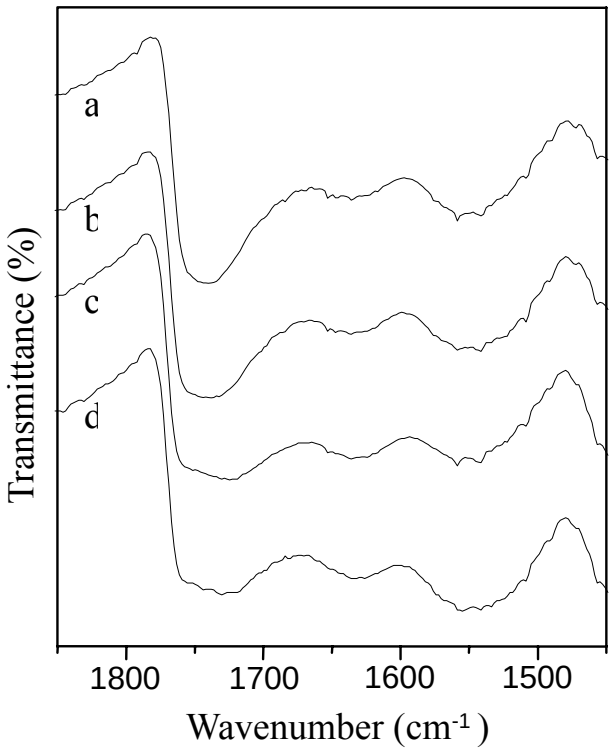

Fig. 5-4. FT-IR spectra of CA nanofibers coated with various bilayers of PAH5/PAA5. (a) 10, (b) 15, (c) 20, and (d) 25 bilayers.

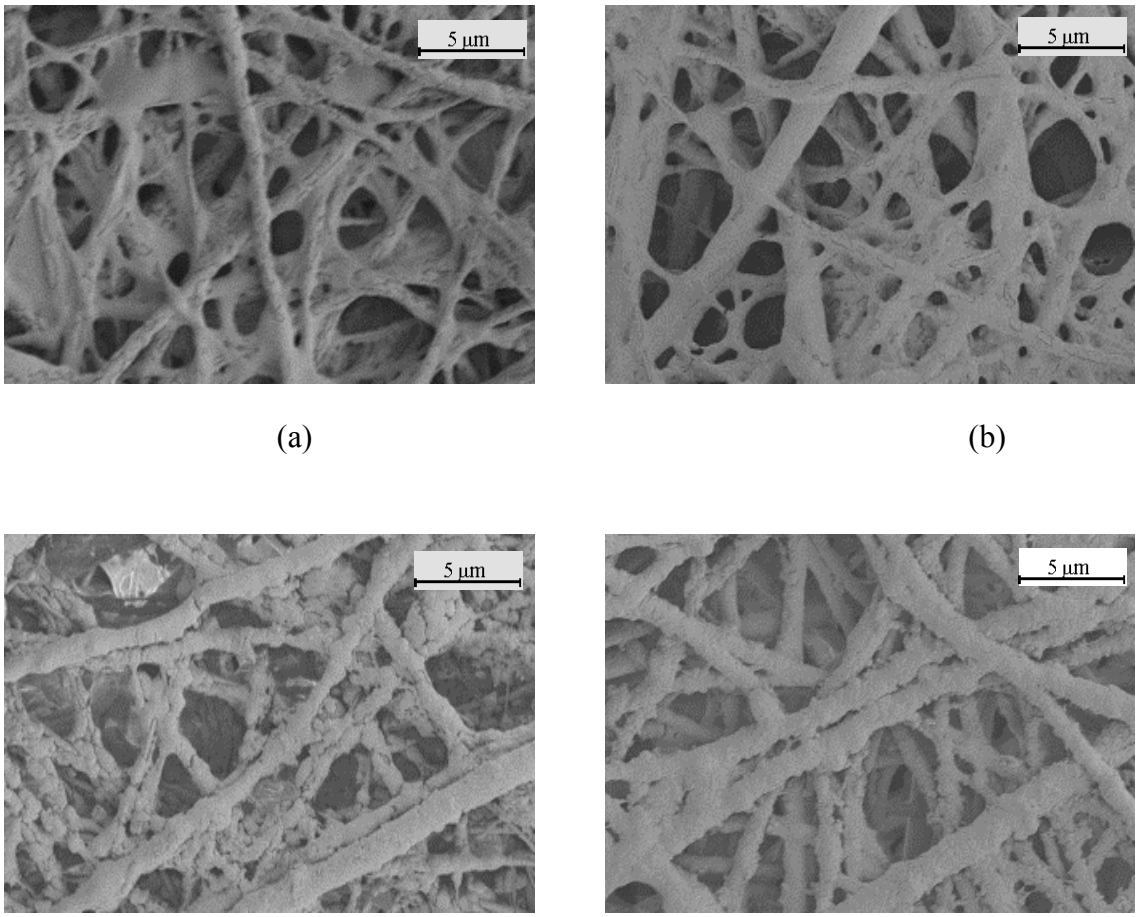

Fig. 5-5. FE-SEM images of CA nanofibers coated with various bilayers of PAH5/PAA5. (a) 10, (b) 15, (c) 20, and (d) 25 bilayers.

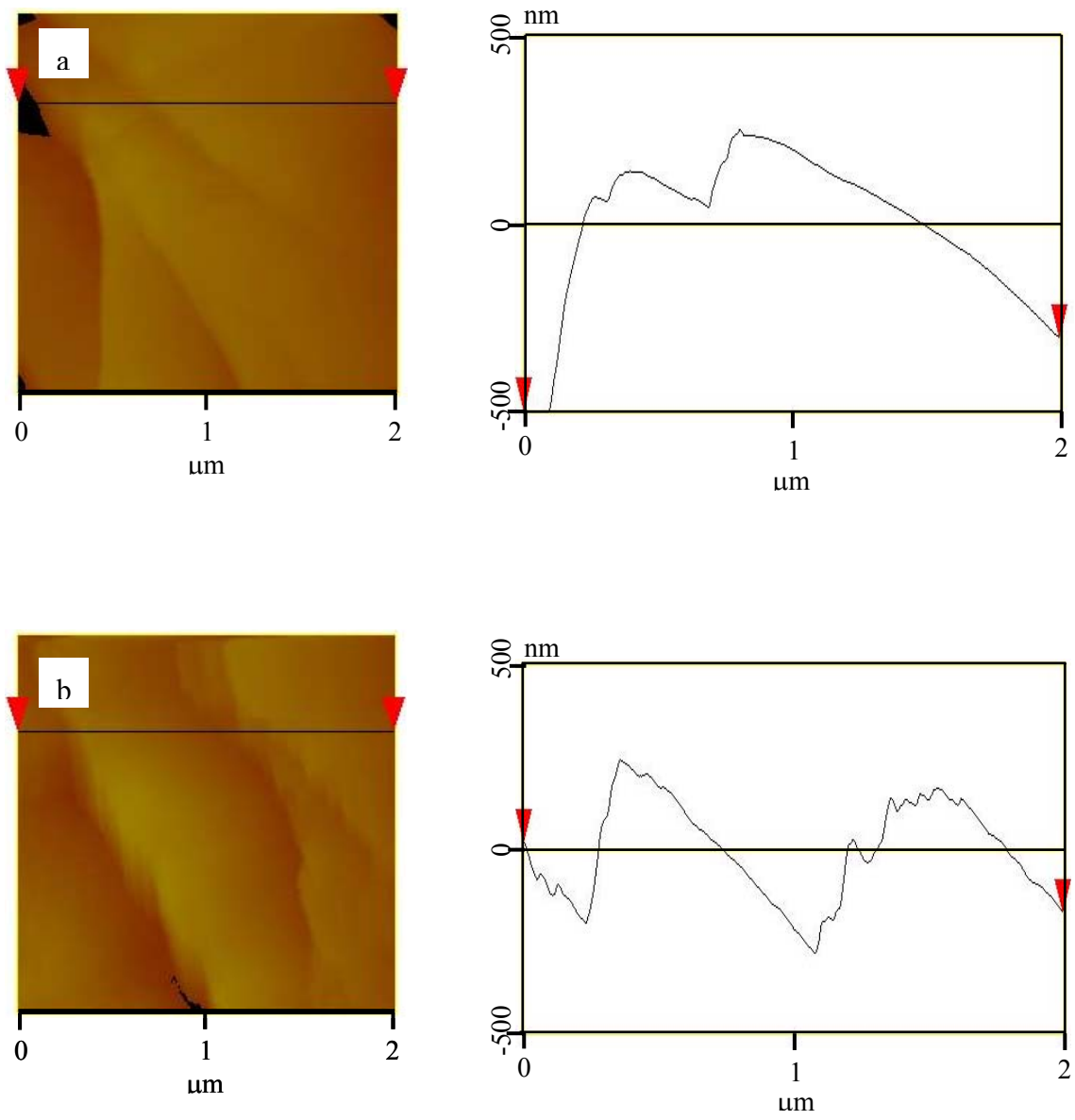

Fig. 5-6. AFM top view images and cross section profiles along the marked direction of uncoated CA nanofibers (a) and $(PAH5/PAA5)_{25}$ coated fibers (b).

Number of bilayers	Average fiber diameter (nm)	Standard deviation (nm)	Average film thickness (nm)	Average bilayer thickness (nm)
0	344	98	0	0
5	486	148	71	14
10	788	193	222	22
15	810	375	233	16
20	934	324	295	15
25	1052	256	354	14

Table 5-1. The characteristics of fibers and PEM films.

References

[5-1] G. Decher, J.D. Hong and J. Schmitt, *Macromol. Chem., Macromol. Symp.* 46 (1991) 321.

[5-2] G. Decher, *Science* 277 (1997) 1232.

[5-3] Y. Lvov, K. Ariga, M. Onda, I. Ichinose and T. Kunitake, *Colloid Surface A* 146 (1999) 337.

[5-4] L.I. Shabarchina, M.M. Montrel, G.B. Sukhorukov and B.I. Sukhorukov, *Thin Solid Films* 440 (2003) 217.

[5-5] P.K. Ho, M. Granstrom, R.H. Friend and N.C. Greenham, *Adv. Mater.* 10 (1998) 769.

[5-6] A.C. Hou, O. Onitsuka, M. Ferreira, M.F. Rubner and B.R. Hsieh, *J. Appl. Phys.* 79 (1996) 7501.

[5-7] D. Laurent and J.B. Schlenoff, *Langmuir* 13 (1997)1552.

[5-8] A. Laschewsky, E. Wischerhoff, M. Kauranen and A. Persoons, *Macromolecules* 30 (1997) 8304.

[5-9] S.H. Lee, J. Kumar and S.K. Tripathy, *Langmuir* 16 (2000) 10482.

[5-10] D.L. Elbert, C.B. Herbert and J.A. Hubbell, *Langmuir* 15 (1999) 5355.

[5-11] M.T. Crisp and N.A. Kotov, *Nano lett.* 3 (2003) 173.

[5-12] F. Caruso, *Adv. Mater.* 13 (2001) 5.

[5-13] K.S. Mayya, D.I. Gittins, A.M. Dibaj and F. Caruso, *Nano lett.* 1 (2001) 727.

[5-14] B. Li, L. Shen, X. Liu, S. Zhang, C. Wu and W. Liu, Mater. *Sci. Eng. A* 364 (2004) 324.

[5-15] D.I. Gittins and F. Caruso, *Adv. Mater.* 12 (2000) 1947.

[5-16] F. Caruso, R.A. Caruso and H. Mohwald, *Science* 282 (1998) 1111.

[5-17] D.H. Reneker and I. Chun, *Nanotechnology* 7 (1996) 216.

[5-18] A. Theron, E. Zussman and A.L. Yarin, *Nanotechnology* 12 (2001) 384.

[5-19] H. Fong, I. Chun and D. Reneker, *Polymer* 40 (1999) 4585.

[5-20] J. Huang, S. Virji, B. Weiller and R. Kaner, *J. Am. Chem. Soc.* 125 (2003) 314.

[5-21] H.Q. Liu and Y.L. Hsieh, *J. Polym. Sci. B* 40 (2002) 2119.

[5-22] H. Matsumoto, Y. Koyama and A. Tanioka, *J. Colloid Interface Sci.* 239 (2001) 467.

[5-23] B. Ding , E. Kimura , T. Sato , S. Fujita and S. Shiratori, *Polymer* 45 (2004) 1895.

[5-24] D. Yoo, S. Shiratori and M.F. Rubner, *Macromolecules* 31 (1998) 4309.

[5-25] S. Shiratori and M.F. Rubner, *Macromolecules* 33 (2000) 4213.

[5-26] T.C. Wang, B. Chen, M.F. Rubner and R.E. Cohen, *Langmuir* 17 (2001) 6610.

[5-27] P. Viswanathamurthi, N. Bhattarai, H.Y. Kim, D.R. Lee, S.R. Kim and M.A. Morris, *Chem. Phys. Lett.* 374 (2003) 79.

[5-28] N. Sarkar, M.K. Ram, A. Aarkar, R. Narizzano, S. Paddeu and C. Nicolini, *Nanotechnology* 11 (2000) 30.

CHAPTER 6

Polyoxometalate Nanotubes from Layer-by-layer Coating and Thermal Removal of Electrospun Nanofibers

6.1 Introduction

One-dimensional nanostructured materials, such as nanofibers and nanotubes, have attracted great attention because of their potential application in electronics [1], optical device [2], sensor [3], catalysis [4], medicine [5], and controlled release technology [6]. A rich variety of methods have been adopted to fabricate nanotubes from various kinds of materials. For example, Lou et al [7] prepared Pt nanoshell tubes by annealing the poly(D,L-lactide)/$Pt(acac)_2$ mixture which formed in a porous alumina membrane template. Xia and co-workers [8] reported fabricating the metal nanostructures with hollow interiors by a replacement reaction between the surface of a nanoscale template and the solution of an appropriate salt precursor. Additionally, Liang et al [9] and Hou et al [10] prepared nanotubes by layer-by-layer (LBL) coating and removal of the porous polycarbonate and alumina membranes, respectively.

On the other hand, the nanofibers with the diameter in the range of 30-2000 nm, prepared by electrospinning technique [11-14], are selected as a suitable template for the fabrication of nanotubes. The mats composed of electrospun nanofibers have surface area approximately 1-2 orders of the magnitude larger than continuous films [15]. Caruso, Greiner and their co-workers [16-18] reported fabricating polymer, metal, and hybrid nano- and mesotubes by chemical vapor deposition and sol-gel coating degradable polymer template electrospun fibers. Dong et al [19] obtained the conducting polyaniline tubes by the “in situ polymerization” coating and removal of electrospun nanofibers template. Additionally, Li et al [20] fabricated the composite and ceramic hollow nanofibers by co-electrospinning method.

Polyoxometalates (POMs) are currently attracting much attention as building blocks for functional composite materials because of their particularly interesting nanosized structure

and their potential application in catalysis, conductivity, photo- and electrochromic devices [21,22]. The pure POM ultra-fine fiber mats [23] have been prepared via electrospinning. However, to our best knowledge, there are no reports for the fabrication of the pure POM nanotubes.

Encouraged by our recent success in the fabrication of LBL structured hybrid films of TiO_2 nanoparticles and poly(acrylic acid) on electrospun nanofibers using the electrostatic LBL self-assembly technique [24], we have developed a straightforward and highly versatile template method for the production of nanotubes. The concept (Fig. 1) is to coat the electrospun negatively charged CA nanofibers with oppositely charged PAH and POM using electrostatic LBL self-assembly technique. POM nanotubes are subsequently formed via selective removal of the core fiber template and PAH by thermal degradation.

In the current work, we want to fabricate the pure $H_4SiW_{12}O_{40}$ nanotubes by a combination of electrospinning and electrostatic LBL self-assembly techniques. Meanwhile, the influence of the number of deposition bilayers and pH of dipping solutions on the formation of PAH/$H_4SiW_{12}O_{40}$ films deposited on nanofibers is investigated.

6.2 Experimental Procedure

The starting materials included cellulose acetate (CA) (M_n 40 000, Teijin Co., Ltd., Japan), acetone and N,N-Dimethylacetamide (DMAc) (Junsei Chemical Co., Ltd.), poly(allylamine hydrochloride) (PAH) (M_w 70 000, Aldrich) and $H_4SiW_{12}O_{40}\cdot 25\text{-}26H_2O$ (Aldrich). Pure water with a resistance of 18.2 MΩ was used as the solvent.

The CA nanofibrous mats were fabricated by electrospinning a 10 wt% CA solution, which were prepared from acetone and DMAc with the acetone/DMAc weight ratio of 2:1, between two electrodes bearing electrical charges of opposite polarity. The distance between two electrodes was 15 cm and the applied voltage was 25 kV. Liu and Hsieh [25] reported the details concerning the preparation of CA nanofibrous mats and the electrospinning process. The zeta potential of CA had a negative value in the range pH 2-10 [26].

The concentration of the aqueous PAH solution tested was fixed as 10^{-2} M (based on

repeat unit) and its pH was adjusted to be 2.5 and 7.5 with either HCl or NaOH solution. The concentration of the aqueous $H_4SiW_{12}O_{40}$ solution was 10^{-3} M and its pH was controlled at 2.5.

The hybrid films were formed by first immersing CA nanofibrous mats into the PAH solution for 15 min followed by 2 min of rinsing in three pure water baths. The mats then were immersed into the $H_4SiW_{12}O_{40}$ solution for 15 min followed by identical rinsing steps. The adsorption and rinsing steps were repeated until the desired number of deposition bilayers was obtained. The hybrid films coated fibrous mats were dried at 80 ^oC for 24 h under vacuum to remove the solvent. Five bilayers of hybrid films fabricated from a PAH solution of pH 2.5 and a $H_4SiW_{12}O_{40}$ solution of pH 2.5 denoted as (PAH2.5/ $H_4SiW_{12}O_{40}$2.5)$_5$. Meanwhile, the hybrid films deposited from a PAH solution of pH 7.5 and a $H_4SiW_{12}O_{40}$ solution of pH 2.5 referred to as PAH7.5/ $H_4SiW_{12}O_{40}$2.5.

The hybrid LBL films coated fibrous mats were calcined at 380 ^oC for 5 h in air to get the $H_4SiW_{12}O_{40}$ nanotubes. The heating rate is 5 ^oC min^{-1}. All the samples were dried at 80 ^oC for 24 h under vacuum prior to the subsequent characterizations. The concept for preparation of $H_4SiW_{12}O_{40}$ nanotubes is shown in Fig. 1.

The morphologies of the fibrous mats and nanotubes were examined by scanning electron microscopy (SEM) (S-4700, Hitachi Ltd., Japan). The diameters of fibers were measured using image analyzer (Adobe Photoshop 7.0). The hybrid films coated fibrous mats were embedded in epoxy resin and cut into ultra-thin sections with the thickness of 80 nm using ultramicrotome equipped with a diamond knife. The cross-sectional images of the hybrid films coated fibers were observed by a transmission electron microscope (TEM, Philips, TECNAI F20).

Fourier transform infrared (FT-IR) spectra were recorded using a BIO-RAD spectrometer (FTS-60A/896) in the wave number range of 4000-400 cm^{-1} at room condition. The measurement of crystallinity was carried out by using a wide-angle X-ray diffractometer (XRD, RTP300, Rigaku Co., Japan). The XRD data were collected in 2θ range of 3-40^o with a scanning speed of 2^o min^{-1} at room temperature.

6.3 Results and Discussion

6.3.1 Morphology of the films coated fibrous mats

The typically electrospun nanofibrous mats composed of polymer nanofibers have a three-dimensional (3D) structure with pores in micro and sub-micro size [12]. Different from the other flat supports, the deposition spaces among the adjacent nanofibers in CA nanofibrous mats are limited. It is necessary to determine the suitable deposition parameters for the fabrication of uniform LBL films on the surface of nanofibers.

In order to investigate the influence of the number of deposition bilayers on the formation of hybrid films on nanofibers, the CA nanofibers were deposited with 5, 10, and 15 bilayers of PAH2.5/$H_4SiW_{12}O_{40}$2.5, respectively. SEM images of CA nanofibers coated with various bilayers of PAH2.5/$H_4SiW_{12}O_{40}$2.5 are shown in Fig. 2. The pure CA nanofibers (Fig. 2a) showed a relatively regular morphology and a smaller diameter compared with PAH/$H_4SiW_{12}O_{40}$ films coated fibers. It has an average diameter of 275 nm with a standard deviation of 136 nm.

After deposition of hybrid PAH2.5/$H_4SiW_{12}O_{40}$2.5 films on nanofibers, the fiber ship was maintained with 5 and 10 bilayers deposited on nanofibers (Fig. 2b and c). The average diameter of hybrid nanofibers with 5 and 10 bilayers deposition were 432 and 582 nm. Moreover, the standard deviation of diameters of hybrid nanofibers with 5 and 10 bilayers coating were calculated to be 149 and 250 nm. It can be seen that the average diameter of fibers was increased with increasing the deposition bilayers. Meanwhile, the standard deviation of fiber diameters was increased after LBL deposition because of the imperfect deposition led by the 3D structure of fibrous mats. The average thickness of hybrid films, which deduced from the average diameter of hybrid films coated nanofibers, was 79 and 154 nm with 5 and 10 bilayers deposition. Furthermore, the average thickness of each PAH2.5/$H_4SiW_{12}O_{40}$2.5 bilayer can be estimated to be 16 nm.

The (PAH2.5/$H_4SiW_{12}O_{40}$2.5)$_{15}$ films coated fibers (Fig. 2d) did not keep the perfect fiber shape. The hybrid films formed not only on the surface of nanofibers, but also in the region among adjacent fibers. The CA nanofibers were embedded in

PAH2.5/$H_4SiW_{12}O_{40}$2.5 films. It was considered that the reason was due to the limited space among the adjacent fibers and the 3D growth of hybrid films along the CA nanofibers.

To investigate the pH influence on the formation of hybrid films on nanofibers, two types of pH combinations for the dipping solutions were used. The morphology of (PAH2.5/$H_4SiW_{12}O_{40}$2.5)$_5$ and (PAH7.5/$H_4SiW_{12}O_{40}$2.5)$_5$ films coated fibers are shown in figure 3. The hybrid films of PAH2.5/$H_4SiW_{12}O_{40}$2.5 coated on nanofibers (Fig. 3a) showed homogenous depositon on CA nanofibers. Some beads were found in hybrid films coated fibers which also existed in pure CA nanofibers. The contraction of the radius of electrospinning jet, which was driven by surface tension, caused the remaining solution to form beads [27]. However, the (PAH7.5/$H_4SiW_{12}O_{40}$2.5)$_5$ films coated fibers (Fig. 3b) did not keep the perfect fiber shape. The hybrid films formed on the surface of nanofibers and in the region among adjacent fibers. The reason was due to the fast growth of PAH7.5/$H_4SiW_{12}O_{40}$2.5 films in the limited spaces of fibrous mats when PAH deposited at pH 7.5 [28]. Therefore, the thick hybrid films were formed in the 3D structure and blocked some spaces among the adjacent CA nanofibers. The results illustrated that the morphology of hybrid films coated fibers was strongly affected by the pH of dipping solutions. The low growth speed of PAH2.5/$H_4SiW_{12}O_{40}$2.5 films was preferred to form a relatively uniform coating on nanofibers.

Fig. 4 shows the cross-sectional TEM image of (PAH2.5/$H_4SiW_{12}O_{40}$2.5)$_5$ films coated fibers. The hybrid films were found as connected rings which resulted in a tubular network. It was difficult to identify the layered structure in the TEM image because of the fuzzy characteristics of the LBL structure associated with the interpenetration between the layers [29]. The $H_4SiW_{12}O_{40}$ was uniformly dispersed in the hybrid films without layered structure formed and the thickness of (PAH2.5/$H_4SiW_{12}O_{40}$2.5)$_5$ films coated on CA nanofibers was irregular. Meanwhile, some randomly distributed junctions were found among the adjacent fibers. These observations were different from those observed in LBL films with flat substrates used [30]. The reason was that the electrospun nanofibers serving as substrates were not distributed in the same plane, but existed in 3D structure [24]. Hence, the thickness of films deposited on nanofibers was irregular when the fibers were located

in different positions in 3D structured nanofibrous mats.

The outer diameter of the hybrid films coated fibers was dependent on the thickness of the PAH2.5/$H_4SiW_{12}O_{40}$2.5 wall. The thickness of the wall was closely related to the deposition conditions, i.e., molecular weight of PAH, concentration and pH of the dipping solutions, the deposition time, and the number of deposition bilayers. The inner diameter of the PAH2.5/$H_4SiW_{12}O_{40}$2.5 wall was controlled by the size of the electrospun template CA nanofibers. The size of the template CA fibers can be adjusted by changing the average molecular weight of CA, solution viscosity, kinds of solvents, applied electric field strength, and deposition distance during the electrospinning process.

6.3.2 Morphology of nanotubes

Fig. 5a shows that the hybrid (PAH2.5/$H_4SiW_{12}O_{40}$2.5)$_5$ films coated fibers has a rough surface due to the LBL deposition [24]. In order to get pure $H_4SiW_{12}O_{40}$ nanotubes, the hybrid films coated fibers were subjected to calination in air. After calcination at 380 ^oC for 5 h, the fibrous mats (Fig. 5b) were contracted with the fiber shape. Moreover, the diameter of calcined fibers was largely reduced due to the decomposition of the core fiber template and PAH.

SEM image of cross-sectional calcined fibers is shown in Fig. 6. It can be seen the tubular shape of the calined fibers were obtained. And the outer and inner diameter of $H_4SiW_{12}O_{40}$ nanotubes was largely reduced compared with those of hybrid films coated fibers (Fig. 4). As seen in the high magnified image of Fig. 6, the $H_4SiW_{12}O_{40}$ nanotube has an outer diameter about 200 nm and an inner diameter about 100 nm. The wall thickness was estimated to be 50 nm which thinner than the corresponded wall thickness of hybrid films. This allowed the preparation of macroscopic mats consisting of $H_4SiW_{12}O_{40}$ nanotubes.

6.3.3 Fourier transform infrared spectroscopy

Fig. 7 shows the FT-IR spectra of CA nanofibers, (PAH2.5/$H_4SiW_{12}O_{40}$2.5)$_5$ films

coated CA nanofibers, and $H_4SiW_{12}O_{40}$ nanotubes. The pure CA nanofibrous mats (Fig. 7a) exhibited a number of FT-IR absorption features below 2000 cm^{-1} [31]. After the LBL deposition, the hybrid films coated fibrous mats (Fig. 7b) still maintained the FT-IR features of CA nanofibrous mats. Moreover, the feature bands of $H_4SiW_{12}O_{40}$ appeared at 976, 919, and 786 cm^{-1} corresponding to the stretching vibrations of Si-O, W-O_d, and W-O_c-W, respectively, indicating that the identity of the Keggin anions was preserved in the hybrid films [23,32]. However, the bands associated with the $H_4SiW_{12}O_{40}$ in the hybrid films were generally slightly shifted compared with the pure $H_4SiW_{12}O_{40}$. The new band at 1518 cm^{-1} indicated the possible presence of the intramolecular hydrogen bonding between $H_4SiW_{12}O_{40}$ and PAH molecules. Meanwhile, a very broad absorption band in the region of 1800-4000 cm^{-1} indicated the presence of large amount of water molecules because the LBL films were easy to absorb the moisture in air [33]. The spectra of $H_4SiW_{12}O_{40}$ nanotubes (Fig. 7c) exhibited the complete Keggin structure [23] without the feature bands of CA fibrous mats. This indicated that the CA decomposed. As a result, the Keggin structure of $H_4SiW_{12}O_{40}$ was kept in hybrid films coated fibers and inorganic nanotubes. Moreover, the pure $H_4SiW_{12}O_{40}$ nanotubes were obtained after the calcination of PAH/$H_4SiW_{12}O_{40}$ films coated CA nanofibers.

6.3.4 Wide-angle X-ray diffraction

Fig. 8 provides the WAXD patterns of the various fibrous mats. As seen in Fig. 8a and b, the broad peaks appeared around $2\theta = 20^o$ in the CA and the hybrid films coated fibrous mats, corresponding to the semicrystalline phase of CA nanofibrous mats [31]. Moreover, the hybrid films coated fibrous mats (Fig. 8b) exhibited a new peak at $2\theta < 10^o$ indicated that the molecules of the fibrous mats were ordered in short distance [34]. For the pure $H_4SiW_{12}O_{40}$ nanotubes (Fig. 8c), there were four groups' peaks in the ranges of 2θ, 5-10^o, 17-22^o, 25-30^o, and 31-37^o, corresponding to the characteristic peaks of Keggin structure [23]. This result also illustrated that the pure $H_4SiW_{12}O_{40}$ nanotubes still kept the Keggin structure.

6.4 Conclusions

LBL structured hybrid PAH/$H_4SiW_{12}O_{40}$ films coated CA nanofibrous mats were successfully fabricated by the combination of electrospinning and electrostatic LBL self-assembly techniques. The various morphologies of hybrid films coated fibers were obtained by adjusting the number of deposition bilayers and pH of dipping solutions. And the Keggin structure of $H_4SiW_{12}O_{40}$ was kept in the hybrid films. The pure $H_4SiW_{12}O_{40}$ nanotubes with Keggin structure have been prepared by the calcination of the hybrid films coated fibers. Additionally, the outer and inner diameter of the $H_4SiW_{12}O_{40}$ nanotubes was much smaller than those of the corresponded hybrid fibers.

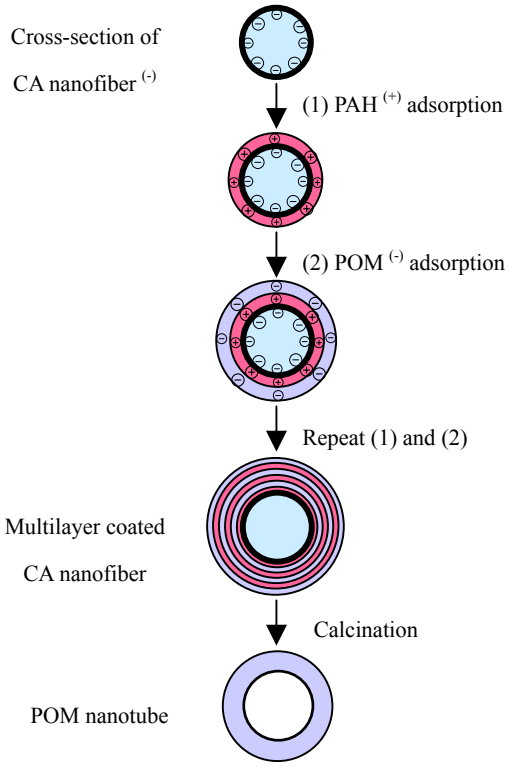

Fig. 6-1. Schematic diagram illustrating the fabrication of POM nanotube via LBL coating and thermal removal of the electrospun nanofiber.

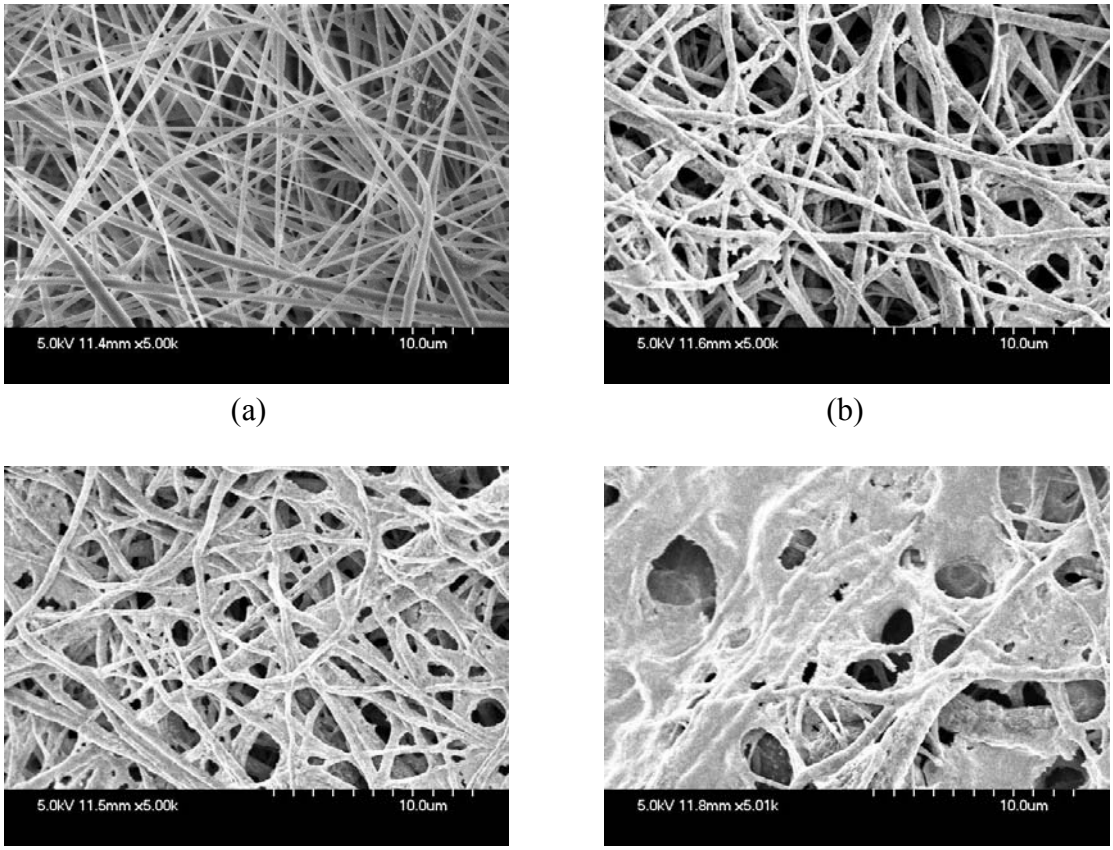

Fig. 6-2. SEM images of CA nanofibers deposited with various bilayers of PAH2.5/ $H_4SiW_{12}O_{40}$2.5. (a) 0, (b) 5, (c) 10, and (d) 15 bilayers.

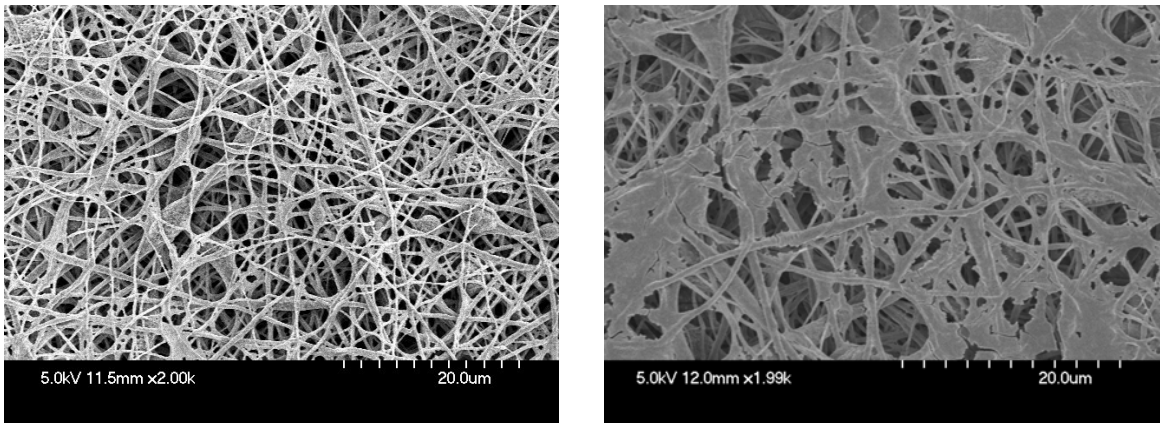

(a) (b)

Fig. 6-3. SEM images of $(PAH2.5/H_4SiW_{12}O_{40}2.5)_5$ films coated fibers (a) and $(PAH7.5/H_4SiW_{12}O_{40}2.5)_5$ films coated fibers (b).

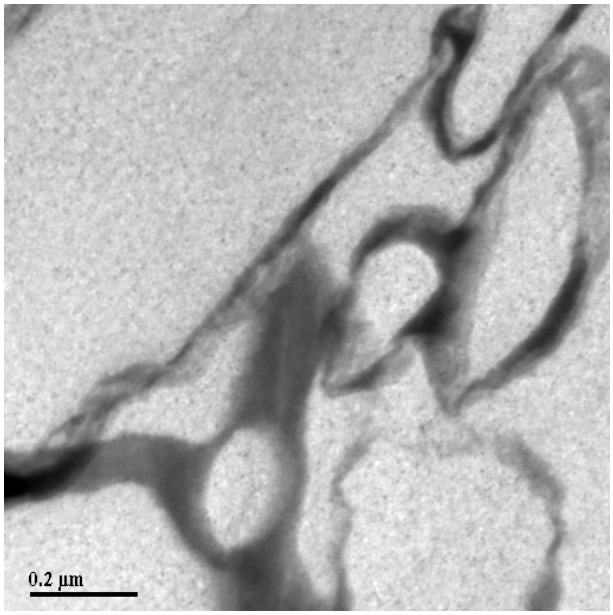

Fig. 6-4. TEM image of cross-sectional (PAH2.5/$H_4SiW_{12}O_{40}$2.5)$_5$ films coated fibers embedded in epoxy resin.

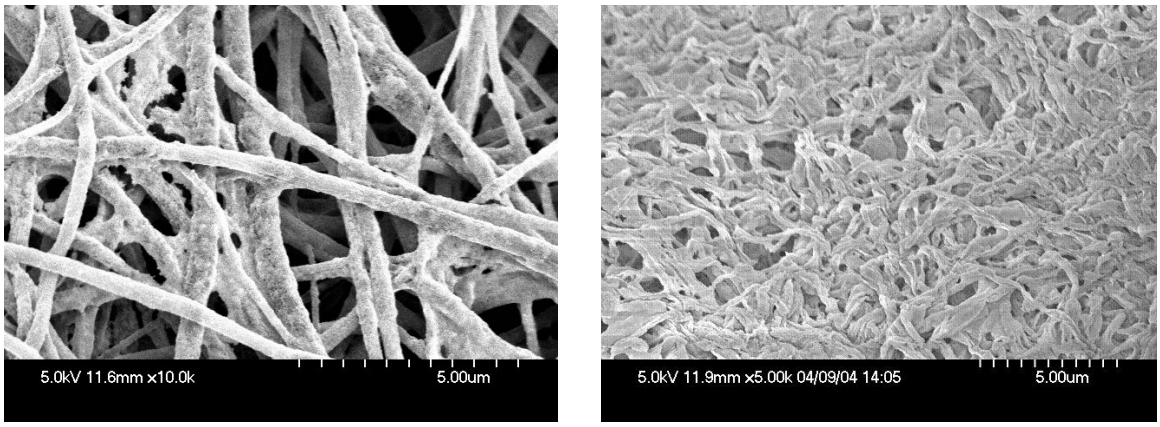

(a) (b)

Fig. 6-5. SEM images of (PAH2.5/$H_4SiW_{12}O_{40}$2.5)$_5$ films coated fibers (a) and fibers calcined at 380 ^oC (b).

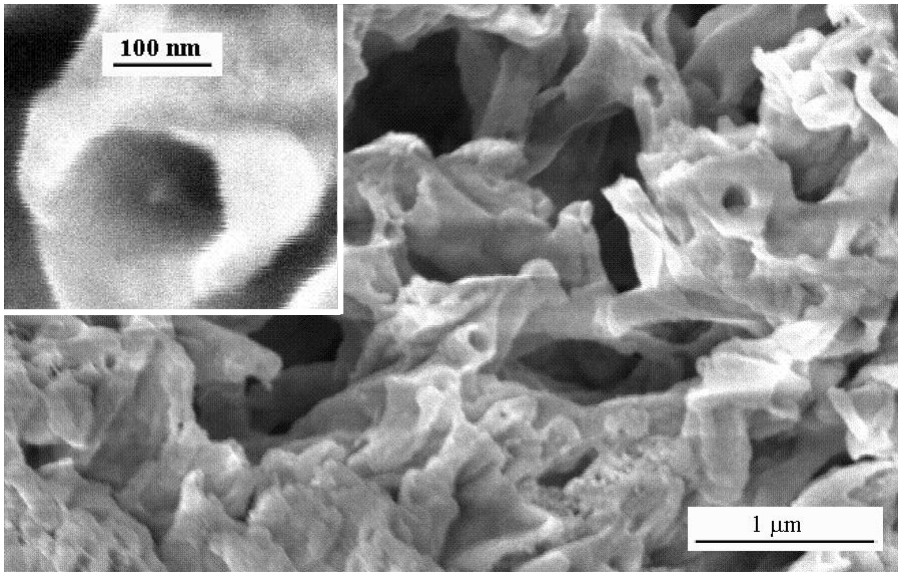

Fig. 6-6. SEM image of cross-sectional fibers calcined at 380 ^{o}C.

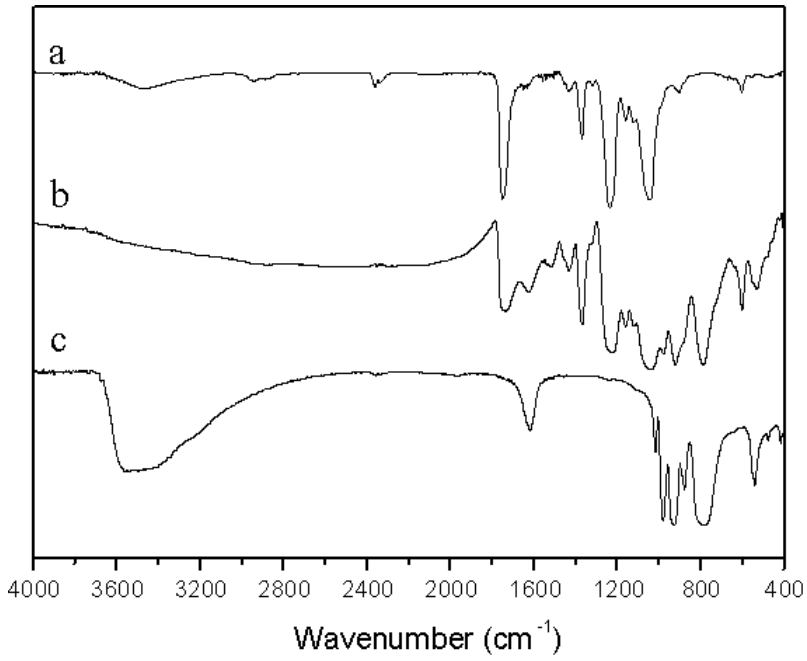

Fig. 6-7. FT-IR spectra of (a) CA nanofibers, (b) $(PAH2.5/H_4SiW_{12}O_{40}2.5)_5$ films coated nanofibers, and (c) $H_4SiW_{12}O_{40}$ nanotubes.

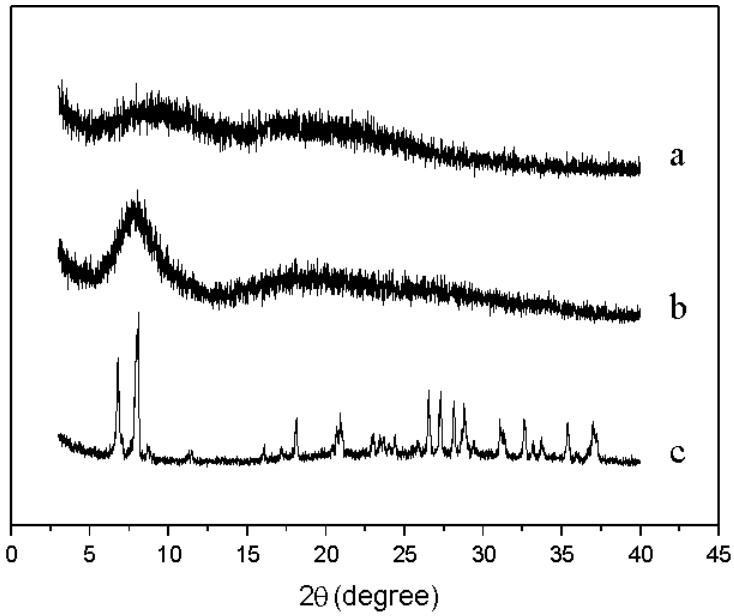

Fig. 6-8. WAXD patterns of (a) CA nanofibers, (b) $(PAH2.5/H_4SiW_{12}O_{40}2.5)_5$ films coated nanofibers, and (c) $H_4SiW_{12}O_{40}$ nanotubes.

References

[6-1] K. Bradley, J.C.P Gabriel and G. Gruner, *Nano Lett.* 3 (2003) 1353.

[6-2] E. Kymakis and G.A.J. Amaratunga, *Synth. Met.* 142 (2004) 161.

[6-3] B. Ding, J. Kim, Y. Miyazaki and S. Shiratori, *Sens. Actuator B* 101 (2004) 373.

[6-4] S. Delpeux, K. Szostak, E. Frackowiak, S. Bonnamy and F. Beguin, *J. Nanosci. Nanotechnol.* 2 (2002) 481.

[6-5] W.M. Tolles and B.B. Rath, *Curr. Sci.* 85 (2003) 1746.

[6-6] N.H. Leeuw, Z.M. Du, J. Li, S. Yip and T. Zhu, *Nano Lett.* 3 (2003) 1347.

[6-7] Y. Luo, S.K. Lee, H. Hofmeister, M. Steinhart and U. Gosele, *Nano Lett.* 4 (2004) 143.

[6-8] Y.G. Sun, B. Mayers and Y.N. Xia, *Adv. Mater.* 15 (2003) 641.

[6-9] Z.J. Liang, A.S. Susha, A. Yu and F. Caruso, *Adv. Mater.* 15 (2003) 1849.

[6-10] S.F. Hou, C.C. Harrell, L. Trofin, P. Kohli and C.R. Martin, *J. Am. Chem. Soc.* 126 (2004) 5674.

[6-11] D.H. Reneker, A.L. Yarin, H. Fong and S. Koombhongse, *J. Appl. Phys.* 87 (2000) 4531.

[6-12] J.M. Deitzel, J. Kleinmeyer, D. Harris and T.N.C. Beck, *Polymer* 42 (2001) 261.

[6-13] Y.M. Shin, M.M. Hohman, M.P. Brenner and G.C. Rutledge, *Polymer* 42 (2001) 9955.

[6-14] D.H. Reneker and I. Chun, *Nanotechnology* 7 (1996) 216.

[6-15] J. Huang, S. Virji, B. Weiller and R. Kaner, *J. Am. Chem. Soc.* 125 (2003) 314.

[6-16] H.Q. Hou, Z. Jun, A. Reuning, A. Schaper, J.H. Wendorff and A. Greiner, *Macromolecules* 35 (2002) 2429.

[6-17] R.A. Caruso, J.H. Schattka and A. Greiner, *Adv. Mater.* 13 (2001) 1577.

[6-18] M. Bognitzki, H.Q. Hou, M. Ishaque, T. Frese, M. Hellwing, C. Schwarte, A. Schaper, J.H. Wendorff and A. Greiner, *Adv. Mater.* 12 (2000) 637.

[6-19] H. Dong, S. Prasad, V. Nyame and W.E.J. Jr, *Chem. Mater.* 16 (2004) 371.

[6-20] D. Li and Y.N. Xia, *Nano Lett.* 4 (2004) 933.

[6-21] Y. Guo, Y. Wang, C. Hu. Y. Wang, E. Wang, Y. Zhou and S. Feng, *Chem. Mater.* 12

(2000) 3501.

[6-22] Y. Guo, D. Li, C. Hu. Y. Wang. E. Wang, Y. Zhou and S. Feng, *Appl. Catal. B* 30 (2001) 337.

[6-23] J. Gong, C. Shao, G. Yang, Y. Pan and L. Qu, *Inorg. Chem. Commun.* 6 (2003) 916.

[6-24] B. Ding, J. Kim, E. Kimura and S. Shiratori, *Nanotechnology* 15 (2004) 913.

[6-25] H. Liu and Y. Hsieh, *J. Polym. Sci., Polym. Phys.* 40 (2002) 2119.

[6-26] H. Matsumoto, Y. Koyama and A. Tanioka, *J. Colloid Interf. Sci.* 239 (2001) 467.

[6-27] H. Fong, I. Chun and D.H. Reneker, *Polymer* 40 (1999) 4585.

[6-28] T.C. Wang, B. Chen, M.F. Rubner and R.E. Cohen, *Langmuir* 17 (2001) 6610.

[6-29] G. Decher, *Science* 277 (1997) 1232.

[6-30] S.S. Shiratori, T. Ito and T. Yamada, *Colloid surf. A* 198 (2002) 415.

[6-31] B. Ding, E. Kimura, T. Sato, S. Fujita and S. Shiratori, *Polymer* 45 (2004) 1895.

[6-32] Y. Wang, C. Guo, Y. Chen, C. Hu and W. Yu, *J. Colloid Interface Sci.* 264 (2003) 176.

[6-33] E. Hao and T. Lian, *Langmuir* 16 (2000) 7879.

[6-34] J. Gong, R. Hua, Z. Xie, S. Wang and L. Qu, *Polym. J.* 33 (2001) 377.

CHAPTER 7

Electrospun Nanofibrous Membranes Coated Quartz Crystal Microbalance as Gas Sensor for NH_3 Detection

7.1 Introduction

Quartz crystal microbalances (QCMs) are one of a broad class of acoustic wave (AW) techniques that have been applied to detect small mass uptake when used as chemical-vapor-deposition thickness probes and chemical microsensors [1]. Other examples include surface acoustic waves (SAWs), shear horizontally polarized SAWs (SH-SAWs) and acoustic plate modes [2]. QCM sensors are widely used for the characterization of thin layers, fluids, and gases due to their high mass sensitivity and durability [3].

It is well known that the sensor performance such as sensitivity, selectivity, and time response is largely influenced by the properties of the sensing films. QCM is highly sensitive to mass changes in the presence of a coating that interacts with the target gas [4]. The characteristics of QCM gas sensors depend on the kinds of sensing films coated on their electrodes. A number of materials have been successfully employed in the coating of QCM sensors such as zeolites [5], fullerene C_{60} [6], chiral materials [7], polypyrrole [3], carbon graphites [8], ITO films [9], and oligonucleotides [10].

On the other hand, electrospinning of polymer solutions or melts produces polymer fibers with nanoscale diameters through the action of an external electric field [11,12]. The morphology and properties of the nanofibers depend on the properties of polymer and the process parameters, including the average molecular weight of the polymer, solution viscosity, kinds of solvents, applied electric field strength, and deposition distance [13,14]. The thin membrane composed of electrospun nanofibers, which obtained from electrospinning technique, has the strong potential application for sensor because the nanofibers have surface area approximately one to two orders of the magnitude larger than continuous films [15].

PAA, a weak anionic polyelectrolyte, shows the interaction with basic gas such as NH_3 [16]. However, according to our experiments, it is difficult to get nanofibers on the collector by electrospinning the pure PAA solution because of the formation of strong hydrogen bond [17] between water and the large amount of carboxyl groups of PAA. After the PAA fibers formed from the splitting of the droplet in electrospinning process, it can't evaporate the water completely during the distance between the tip and QCM due to the strong hydrogen bond. Therefore, the water-soluble PVA can be introduced as template material [18] to blend with PAA for preparing the sensing nanofibrous membranes. Additionally, the heat treatment may be employed to lead the crosslinking between PAA and PVA [19] for reinforcing the antiwater solubility of the blend nanofibrous membranes. In the current work, we try to fabricate nanofibrous membranes coated QCM sensors (NMC-QCMS) by electrospinning the viscous blend solutions of PAA and PVA on the QCM surface and investigate their morphology and sensitivity to NH_3.

7.2 Experimental Procedure

PAA (M_w 90,000) purchased from Aldrich was dissolved in distilled water at 12.5 wt%. A 10 wt% PVA (M_n 66,000) (Wako Pure Chemical Industries, Ltd., Japan) solution was prepared from PVA powder and distilled water at 80 ^oC with vigorous stirring. The electrospinning solutions were obtained by blending the PVA and PAA solutions at room temperature. The weight percentage of PAA to PVA in blend solutions was 0, 11, 18, 25, and 33 wt%, respectively. The viscosity and conductivity of blend solutions were measured by a viscotester (6L/R, Hakke, USA) and electric conductivity meter (CM-40G, TOA•DKK Co., Japan), respectively.

Fig. 1 shows the schematic of electrospinning process. The transparent solution was placed in a plastic capillary. The plastic capillary was then clamped to a stand which was above a grounded QCM (10 MHz, AT-cut quartz crystal with Ag electrodes). The positive electrode of a high voltage power supply (FC30P4, Glassman High Voltage Inc., USA) was connected with a copper wire which immersed in solution. The applied voltage was 15 kV, and the tip-to-QCM distance was 10 cm. The droplet instantly disintegrated into nanofibers

that were drawn to the QCM. Nanofibrous membranes were incontinuously collected on the surface of QCM until about 10,000 Hz frequency shift was got. The resonance frequencies were measured by a frequency counter (Hewlett Packard 53131 A). Then, the NMC-QCMS were dried at 80 ^{o}C in vacuum for 2 h to remove the trace solvent and crosslink the PVA and PAA [19].

The morphology of nanofibers on QCM was determined with field emission scanning electron microscopy (FE-SEM) (S-4700, Hitachi Ltd., Japan). The diameters of nanofibers were measured by using image analyzer (Adobe Photoshop 7.0).

For comparison the sensitivity of the NMC-QCMS and continuous films coated QCM sensor (CFC-QCMS), a gas sensor was prepared by the deposition of continuous layer-by-layer (LBL) films of poly(allylamine hydrochloride) (PAH) and PAA on QCM using the electrostatic LBL self-assembly technique. Details concerning preparation of the multi-layer thin films on QCM can be found in a previous paper [20]. The pH of the PAA and PAH solutions was 2.5. The deposition process was performed until about 10,000 Hz frequency shift was got. Then, the CFC-QCMS were dried at 80 ^{o}C in vacuum for 2 h to remove the solvent.

The sensing properties of NMC-QCMS and CFC-QCMS to NH_3 were measured by the resonance frequency shift response. The flow-type experimental setup for measuring the sensing properties of sensors is shown in Fig. 2. The sensor was installed in the chamber which kept with constant temperature and relative humidity. The N_2 was used as carrier gas and controlled the relative humidity at 50, 55, and 60 %, respectively. The flow rates of dry N_2, wet N_2, and NH_3 were kept constant by mass flow controllers (MFCs, Estec, SEC-400 MK3). During the measurement, the concentration of NH_3 was regulated at 50, 100, and 200 ppm, respectively. The temperature in chamber was stabilized at 25 ^{o}C by an external temperature controller. The time for each absorption and desorption was 10 min. Each sample was tested for 4 cycles. The resonance frequencies were measured by the frequency counter. The data from the sensors were recorded by a personal computer.

7.3 Results and Discussion

7.3.1 Properties of polymer solution

It is well known that the morphology and properties of electrospun nanofibers are strongly influenced by the solution properties such as viscosity and conductivity [14]. The viscosity of solutions as a function of weight percentage of PAA to PVA is shown in Fig. 3. The viscosity of pure PVA and PAA solutions was 420 and 180 cPs, respectively. The viscosity of blend solutions was gradually increased from 670 to 1180 cPs with increasing the weight percentage of PAA to PVA from 11 to 33 wt%. The increased viscosity was caused by the partial crosslinking of PVA and PAA due to the formation of hydrogen bond between the carboxyl groups of PAA and hydroxyl groups of PVA [19].

The uniform properties of blend PVA and PAA nanofibrous membranes can be fabricated due to the reinforced interaction between PVA and PAA which caused by the crosslinking. On the other hand, the difficulty was increased for electrospinning the high viscous blend solution which led by crosslinking to form some three-dimensional netted structures. It was different from another report [21] which increased the viscosity by increasing the molecular weight of linear polymer.

Fig. 4 shows the conductivity of solutions as a function of weight percentage of PAA to PVA. The pure PVA solution has a low conductivity (18.6 mS/m) compared with the pure PAA solution (240 mS/m). After blending, the conductivity of bend solutions was gradually increased from 74.9 to 102.2 mS/m with increasing the weight percentage of PAA to PVA from 11 to 33 wt%.

7.3.2 Morphology of electrospun nanofibrous membranes

Fig. 5 and 6 show FE-SEM photographs and fiber diameter distributions of nanofibrous membranes with various content of PAA deposited on QCM. All the images of nanofibrous membranes showed 3D structures of nanofibers and nanofibrous networks with random fiber orientation. The electrospun nanofibrous membranes with porous structures have 1 to 2 orders of magnitude more surface area than that found in continuous films [15]. The pure PVA nanofibers (Fig. 5a) showed many overlaps among the fibers which caused by the

relative low viscosity [14] of PVA solution. The region of distribution of pure PVA nanofibers (Fig. 6a) was broadly distributed in the range of 100 to 400 nm and the majority was in the range of 100 to 200 nm. The average diameter of pure PVA nanofibers was 190 nm.

Fig. 5b-e provide the morphology of blend PAA and PVA nanofibers. It can be observed that the diameter of blend nanofibers became regular and the rigidity of nanofibers was increased. The regions of diameter distributions of blend nanofibers (Fig. 6b-e) were shifted to large diameter with increasing the content of PAA. Meanwhile, the average nanofiber diameters were increased from 200 to 330 nm on increasing the weight percentage of PAA to PVA from 11 to 33 wt%. The reason was due to the increased viscosity and conductivity of electrospinning solutions [14] with adding the PAA component. According to the diameter changes of nanofiber with the various content of PAA, the surface area of nanofibrous membranes was estimated to be a little decrease with increasing the content of PAA [22].

7.3.3 Gas sensing properties of sensors for NH_3

In order to investigate the influence of the content of PAA in nanofibrous membranes to the gas sensing properties of NMC-QCMS, a series of NMC-QCMS with various content of PAA were examined. Fig. 7 shows the time-dependent responses of NMC-QCMS with various content of PAA exposed to 50 ppm of NH_3. The pure PVA NMC-QCMS (Fig. 7a) has no response to NH_3. It indicated that the PVA was not the sensing material for NH_3.

The NMC-QCMS showed fast responses to NH_3 after adding the PAA component in nanofibrous membranes (Fig. 7b-e). The average resonance frequency shifts of NMC-QCMS with 11, 18, 25, and 33 wt% of PAA to PVA were 40, 150, 240, and 380 Hz, respectively. It can be observed that the average resonance frequency shifts were gradually increased on increasing the content of PAA component in nanofibrous membranes because there were more absorption sites in the NMC-QCMS with high content of PAA. The fact showed an opposite result from the consideration of the surface area of nanofibrous membranes. It was considered that the sensitivity of NMC-QCMS with relatively high

surface area should be higher than that of NMC-QCMS with low surface area. As a result, the content of PAA in nanofibrous membranes was the key parameter to affect the gas sensing properties of NMC-QCMS when the nanofibrous membranes have a little difference in surface area.

It also can be found that the response of NMC-QCMS for the first exposure was markedly different from the subsequent exposures, which were similar to each other. Additionally, it was obvious that the base line of the frequency shift was gradually decreased with increasing the testing time. These facts suggested that there was an irreversible absorption process during the first exposure, which originated from some strong interactions between NH_3 molecules and carboxyl groups of PAA. As a result of the slow desorption, the sensor signal couldn't return to its base line and whole sequence showed a corresponding drift. A similar phenomenon was reported by Ding et al. to fabricate sensor using LB films with various layers [23]. It was concluded that the sensitivity of NMC-QCMS to NH_3 was strongly affected by the content of PAA in nanofibrous membranes.

The responses of NMC-QCMS with 18 wt% of PAA to PVA exposed to various concentration of NH_3 are shown in Fig. 8. As the NMC-QCMS exposed to 50 and 100 ppm of NH_3 (Fig. 8a and 8b), the responses showed relatively regular curves of absorption and desorption compared with the NMC-QCMS exposed to 200 ppm of NH_3. However, all the frequencies of NMC-QCMS couldn't return to the original position after absorption and desorption processes due to the excessive NH_3 was kept inside the 3D structures of nanofibrous membranes which led to the desorption lag [23]. The base lines of frequency shifts were gradually decreased with increasing the concentration of NH_3. Meanwhile, the maximum frequency shift was gradually increased with increasing the exposure cycles. The average frequency shifts were 150, 410, and 730 Hz for them, respectively. The responses of NMC-QCMS were reinforced with increasing the concentration of NH_3.

The influence of the relative humidity to the sensing properties of NMC-QCMS is shown in Fig. 9. The frequency shifts of NMC-QCMS were examined during the stabilization of the relative humidity in sensor chamber. Under a constant relative humidity before introducing NH_3, H_2O molecules were pre-sorbed [24] in the nanofibrous

membranes, resulting in a decrease of frequency. Fig. 9a shows the frequency shifts of NMC-QCMS with 18 wt% of PAA to PVA after stabilization at various relative humidity. The frequency shifts were increased from 12 to 46 Hz on increasing the relative humidity from 50 to 60 % because H_2O molecules were absorbed by the large amount of hydrophilic carboxyl groups of PAA and hydroxyl groups of PVA. As a result, the NMC-QCMS has the possibility to use as a humidity sensor.

The responses of NMC-QCMS with 18 wt% of PAA to PVA exposed to 50 ppm of NH_3 at various relative humidity are shown in Fig. 9b. The frequency shifts of NMC-QCMS stabilized at the relative humidity of 50, 55, and 60 % were 65, 150, and 330 Hz, respectively. It can be observed that the responses of NMC-QCMS were sharply increased with increasing the relative humidity after introducing NH_3. One reason maybe was due to the conductivity of carboxyl groups of anionic PAA was reinforced with increasing the relative humidity [25]. The capacity of interaction between nanofirous membranes and NH_3 molecules was enlarged by the high conductivity of carboxyl groups. Another reason was due to the amount of H_2O molecules absorbed on hydrophilic groups in nanofibrous membranes were increased by increasing the relative humidity. And NH_3 molecules were easy to be absorbed by H_2O molecules. The formation of hydrogen bond between NH_3 and H_2O molecules was confirmed by the coadsorption study of NH_3 and H_2O [26]. Therefore, the more NH_3 molecules can be absorbed by increasing the amount of H_2O molecules in nanofibrous membranes to lead large frequency shift.

Fig. 10 shows the responses of CFC-QCMS exposed to various concentration of NH_3 at the relatively humidity of 55 %. The sensing properties of CFC-QCMS were found to be similar to that of NMC-QCMS. The frequency of CFC-QCMS also couldn't return to the original position after absorption and desorption processes. Moreover, the base line of frequency shifts was also gradually decreased with increasing the concentration of NH_3. The average frequency shifts were 70, 90, and 120 Hz when the CFC-QCMS exposed to 50, 100, and 200 ppm of NH_3. Compared with the NMC-QCMS, the sensing properties of CFC-QCMS were much lower than that of NMC-QCMS. The reason was due to the nanofibrous membranes have approximately one to two orders of the magnitude larger surface area than that of the continuous films.

7.4 Conclusions

Nanofibrous membranes contained PVA and PAA components were successfully deposited on the surface of QCM by using electrospinning technique. The average diameter and rigidity of nanofibers was increased due to the increasing of viscosity and conductivity of the blend solutions by increasing the content of PAA component. The sensing properties of NMC-QCMS indicated the content of PAA component, concentration of NH_3, and relative humidity were important parameters to influence the sensitivity of NMC-QCMS for NH_3. Additionally, the NMC-QCMS has the potential application to use as a humidity sensor. Compared with the CFC-QCMS, the NMC-QCMS showed much higher sensitivity.

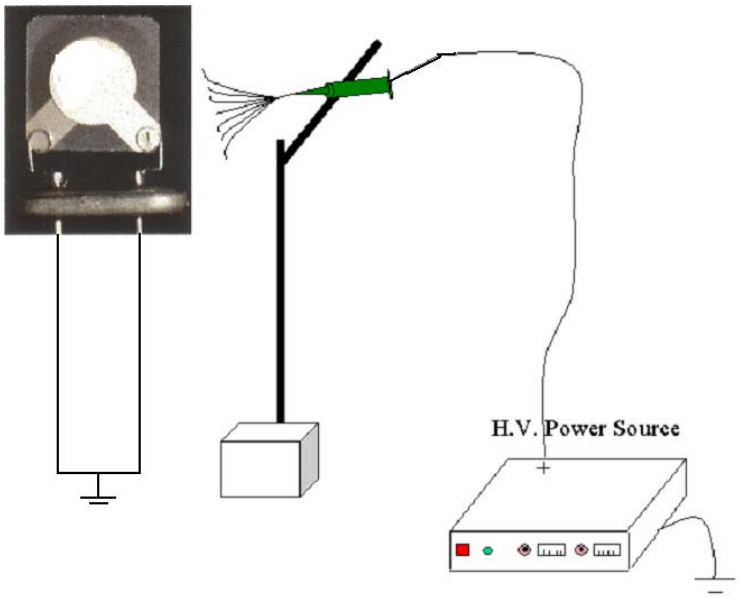

Fig. 7-1. Schematic of the electrospinning process.

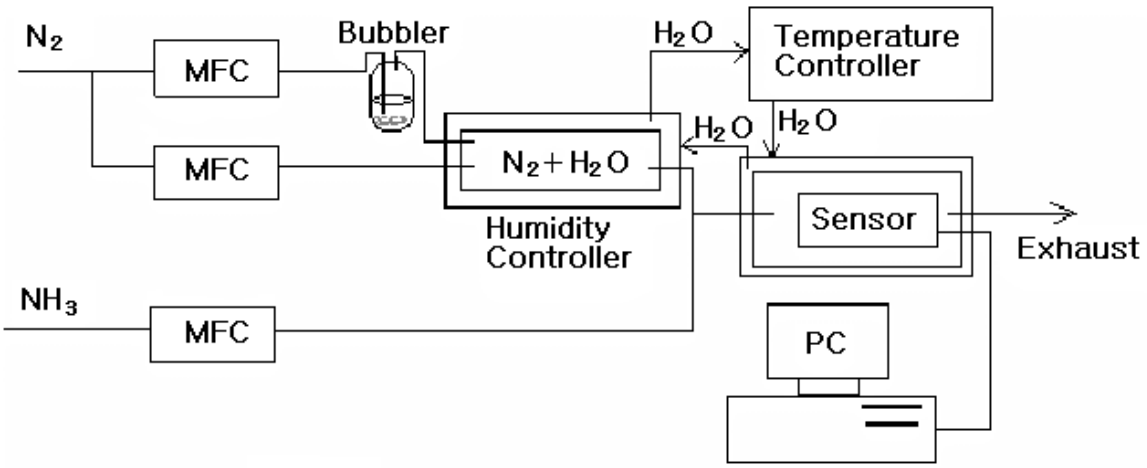

Fig. 7-2. Schematic of a gas testing system for NH_3 detection.

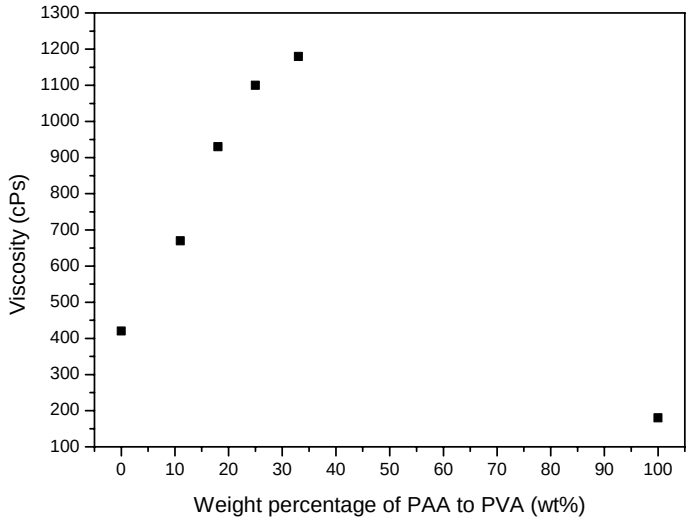

Fig. 7-3. Viscosity of solutions as a function of weight percentage of PAA to PVA.

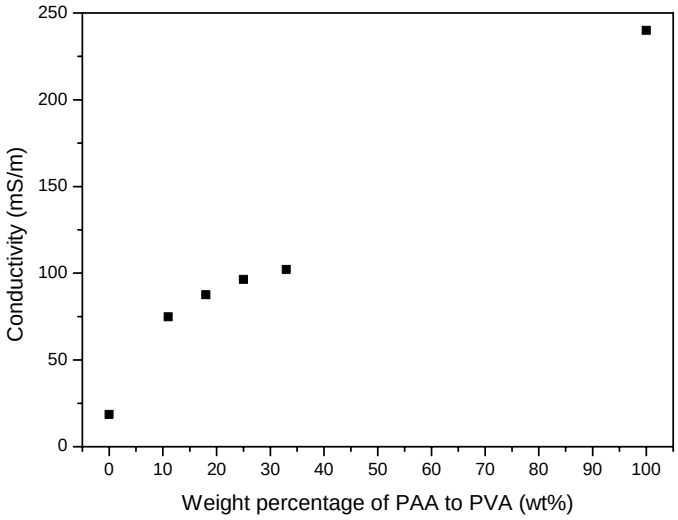

Fig. 7-4. Conductivity of solutions as a function of weight percentage of PAA to PVA.

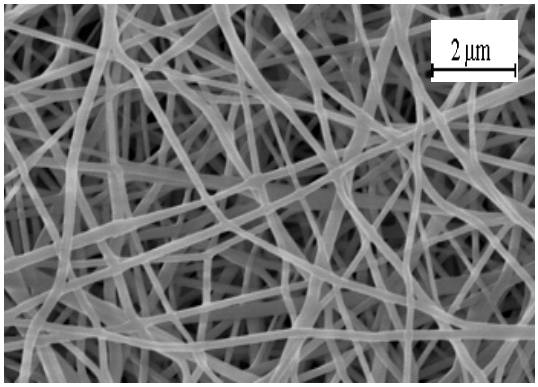

(a)

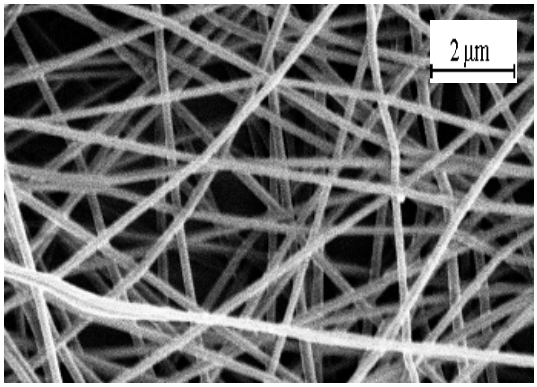

(b)

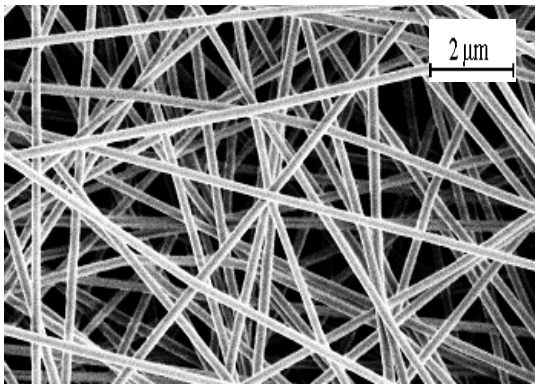

(c)

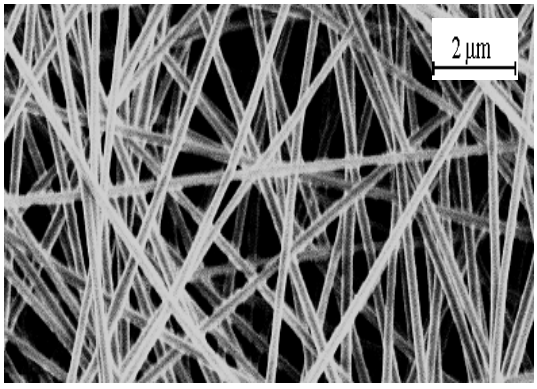

(d)

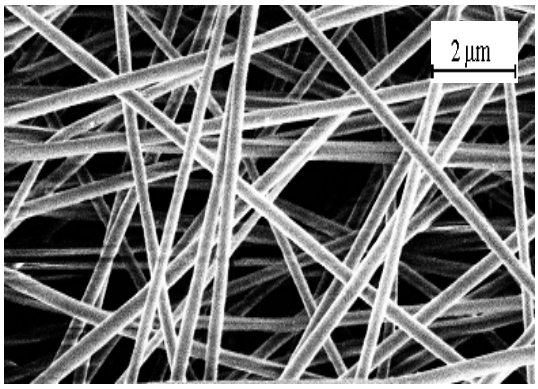

(e)

Fig. 7-5. FE-SEM photographs of nanofibrous membranes deposited on QCM with various weight percentage of PAA to PVA. (a) 0 wt%; (b) 11 wt%; (c) 18 wt%; (d) 25 wt%; (e) 33 wt%.

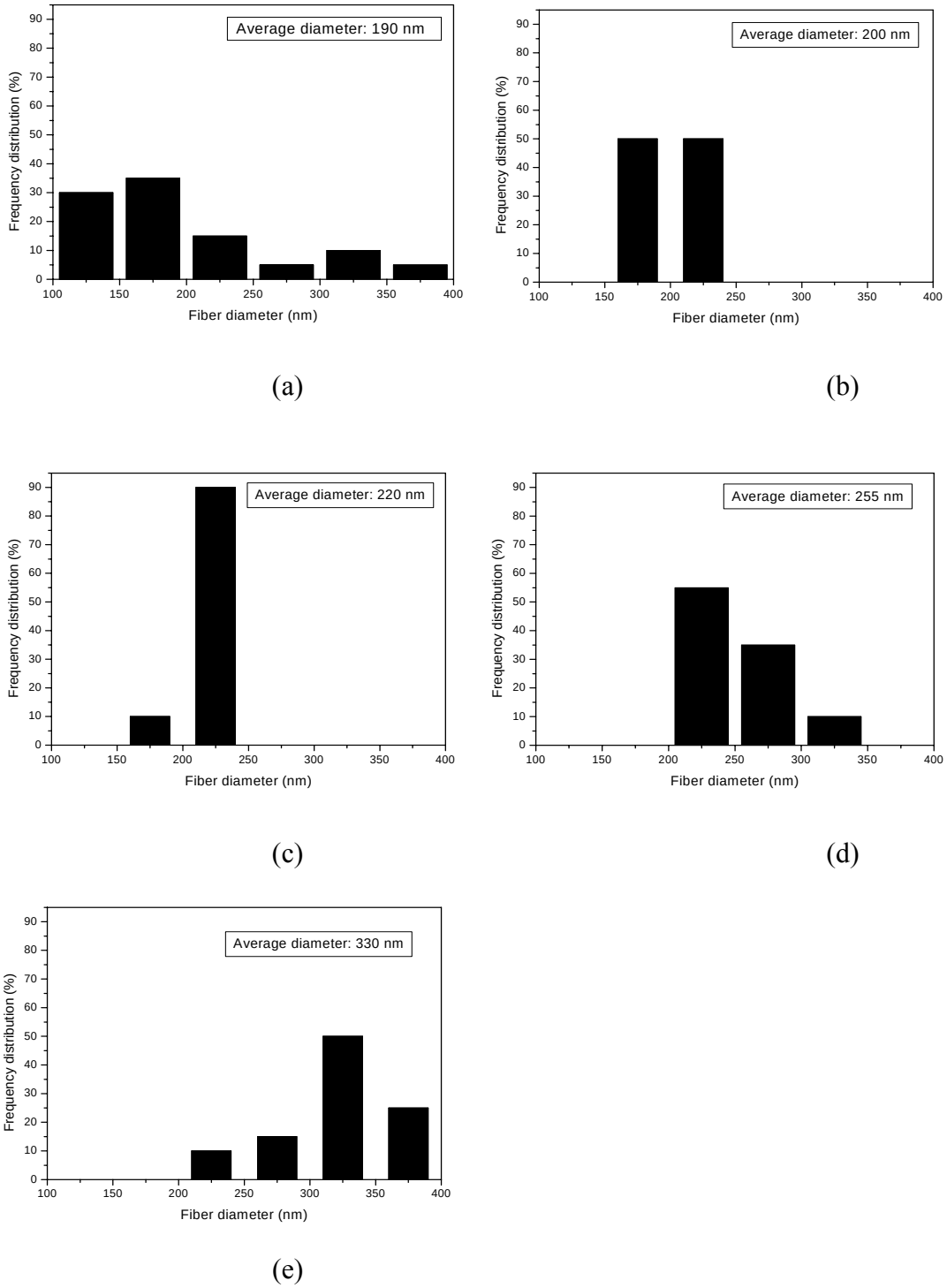

Fig. 7-6. Frequency distributions of nanofibrous membranes deposited on QCM with various weight percentage of PAA to PVA. (a) 0 wt%; (b) 11 wt%; (c) 18 wt%; (d) 25 wt%; (e) 33 wt%.

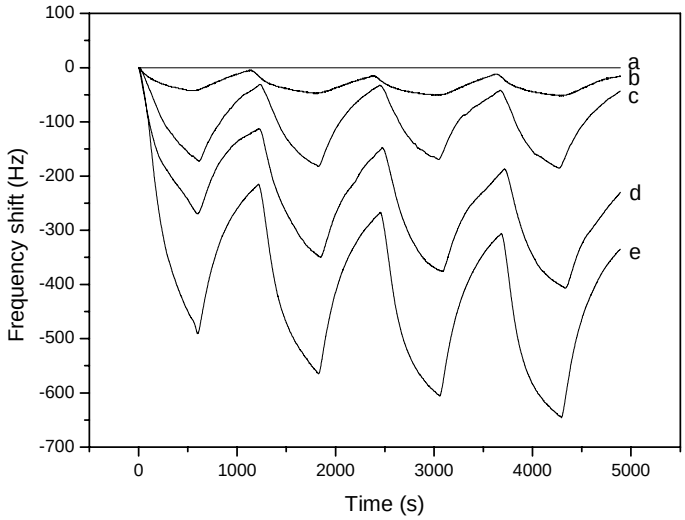

Fig. 7-7. Response of NMC-QCMS with various weight percentage of PAA to PVA exposed to 50 ppm of NH_3 at the relative humidity of 55 %. (a) 0 wt%; (b) 11 wt%; (c) 18 wt%; (d) 25 wt%; (e) 33 wt%.

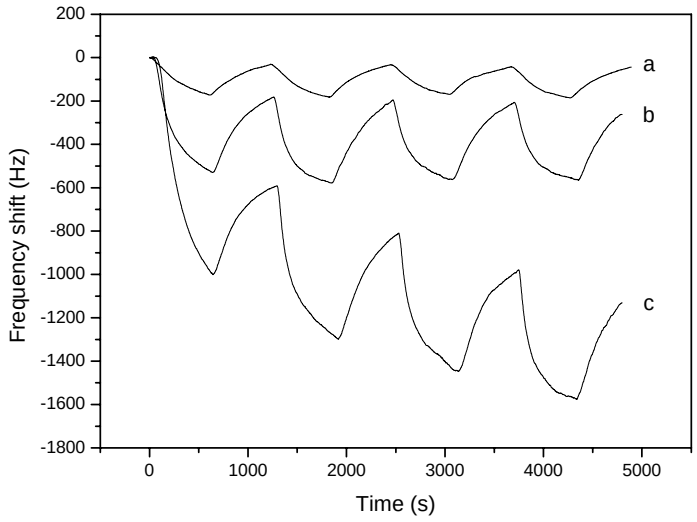

Fig. 7-8. Response of NMC-QCMS with 18 wt% of PAA to PVA exposed to various concentration of NH_3 at the relative humidity of 55 %. (a) 50 ppm; (b) 100 ppm; (c) 200 ppm.

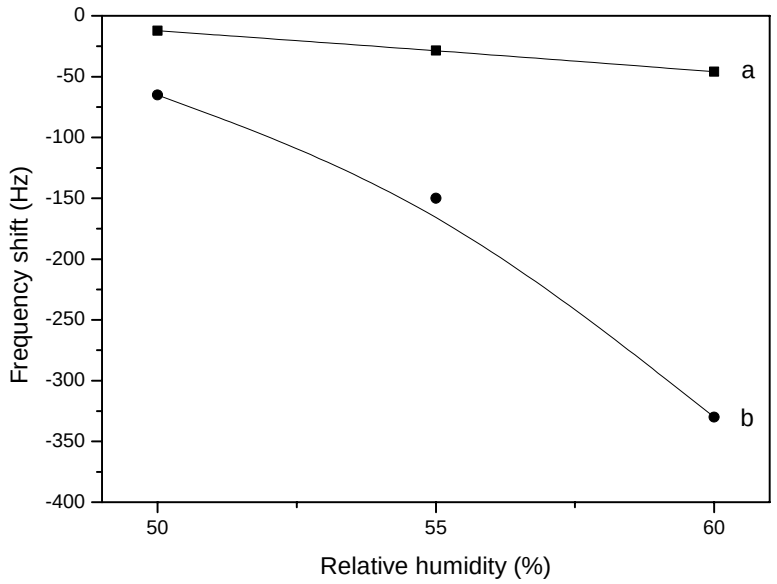

Fig. 7-9. Response of NMC-QCMS with 18 wt% of PAA to PVA (a) stabilized at various relative humidity; (b) exposed to 50 ppm of NH_3 at various relative humidity.

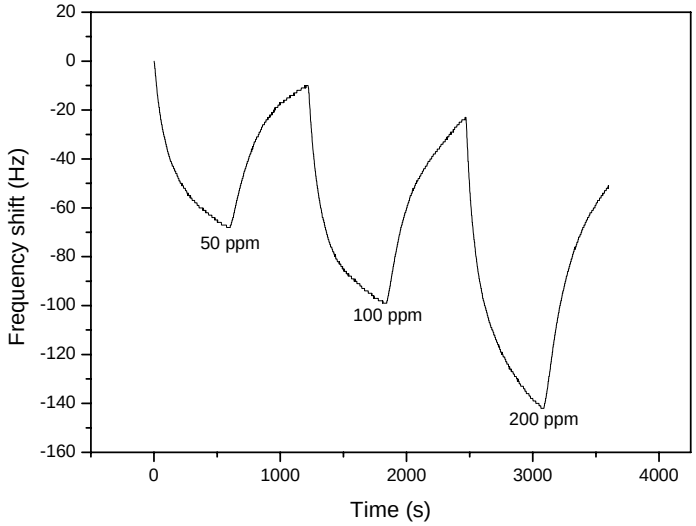

Fig. 7-10. Response of CFC-QCMS exposed to various concentration of NH_3 at the relative humidity of 55 %.

References

[7-1] C. Zhang, B.P. Cappleman, M. Defibaugh-Chavez and D.H. Weinkauf, *J. Polym. Sci., Polym. Phys.* 41 (2003) 2109.

[7-2] G. Mchale, M.I. Newton, M.K. Banerjee and J.A. Cowen, *Mater. Sci. Eng. C* 12 (2000) 17.

[7-3] V. Syritski, J. Reut, A. Opik and K. Idla, *Synth. Met.* 102 (1999) 1326.

[7-4] M. Gomes, P. Nogueira and J. Oliveira, *Sens. Actuator B* 68 (2000) 218.

[7-5] I. Sasaki, H. Tsuchiya, M. Nishioka, M. Sadakata and T. Okubo, *Sens. Actuator B* 86 (2002) 26.

[7-6] H.B. Lin and J.S. Shih, *Sens. Actuator B* 92 (2003) 243.

[7-7] W. Guo, J. Wang, C. Wang, J.Q. He, X.W. He and J.P. Cheng, *Tetrahedron Lett.* 43 (2002) 5665.

[7-8] J.M. Kim, S.M. Chang, Y. Suda and H. Muramatsu, *Sens. Actuator A* 72 (1999) 140.

[7-9] J. Zhang, J.Q. Hu, F.R. Zhu, H. Gong and S.J. Shea, *Sens. Actuator B* 87 (2002) 159.

[7-10] M. Duman, R. Saber and E. Piskin, *Biosens. Bioelectron.* 18 (2003) 1355.

[7-11] D.H. Reneker and I. Chun, *Nanotechnology* 7 (1996) 216.

[7-12] A.G. MacDiarmid, W.E. Jones, I.D. Norris, J. Gao, A.T. Johnson, N.J. Pinto, J. Hone, B. Han, F.K. Ko, H. Okuzaki and M. Llaguno, *Synth. Met.* 119 (2001) 27.

[7-13] A. Theron, E. Zussman and A.L. Yarin, *Nanotechnology* 12 (2001) 384.

[7-14] H. Fong, I. Chun and D. Reneker, *Polymer* 40 (1999) 4585.

[7-15] J. Huang, S. Virji, B. Weiller and R. Kaner, *J. Am. Chem. Soc.* 125 (2003) 314.

[7-16] S. Shiratoi, Y. Inami and M. Kikuchi, *Thin Solid Films* 393 (2001) 243.

[7-17] D. Santhiya, S. Subramanian, K.A. Natarajan and S.G. Malghan, *J. Colloid Interface Sci.* 216 (1999) 143.

[7-18] B. Ding, H. Kim, S. Lee, C. Shao, D. Lee, S. Park, G. Kwag and K. Choi, *J. Polym. Sci., Part B: Polym. Phys.* 40 (2002) 1261.

[7-19] J. Fei and L. Fu, *Eur. Polym. J.* 38 (2002) 1653-1658.

[7-20] S.S. Shiratori and M.F. Rubner, *Macromolecules* 33 (2000) 4213.

[7-21] A. Koski, K. Yim and S. Shivkumar, *Mater. Lett.* 58 (2004) 493.

[7-22] B. Ding, H.Y. Kim, C.K. Kim, M.S. Khil and S.J. Park, *Nanotechnology* 14 (2003) 532.

[7-23] H. Ding, V. Erokhin, M.K. Ram, S. Paddeu, L. Valkova and C. Nicolini, *Thin Solid Films* 379 (2000) 279.

[7-24] M. Matsuguchi, A. Okamoto and Y. Sakai, *Sens. Actuator B* 94 (2003) 46.

[7-25] A. Bozkurt, W. H. Meyer and G. Wegner, *J. Power Sources* 123 (2003) 126.

[7-26] Y. Shingaya, H. Kubo and M. Ito, *Surf. Sci.* 427 (1999) 173.

CHAPTER 8

Electrospun Fibrous Polyacrylic Acid Membrane-based Gas Sensors

8.1 Introduction

Ammonia (NH_3) is an important industrial gas with high toxicity. The maximum value allowed at the working place for 8 h exposure is only 25 ppm and the olfactory limit of detection of ammonia gas is 55 ppm [1]. Therefore, ammonia sensors are required to monitor its concentration in chemical, food processing and power plants where this gas is used or generated. Various sensing materials have been reported for the detection of ammonia, such as tellurium thin films [2], nanoporous anodized alumina [3], thin films of CuBr [1], acrylic acid doped polyaniline [4], solid-state Cu_xS films [5], and Langmuir-Blodgett polypyrrole films [6]. However, the sensors prepared with these above sensing materials have the limitation for ammonia detection at ppb level.

On the other hand, quartz crystal microbalances (QCMs) are established as reliable technique to detect small mass uptake when used as chemical-vapor-deposition thickness probes and chemical microsensors [7]. The ultrahigh sensitivity of QCM sensors can accurately detect mass uptake on the order of nanograms. The QCM technology has been enormously applied to the area of environment monitoring, gas sensor, pressure sensor, and chemical sensor [8]. The sensitivity of QCM gas sensors is highly increased in the presence of a coating that interacts with the target gas [9]. The characteristics of QCM gas sensors depend on the kinds of sensing films coated on their electrodes.

The fibrous membranes, which obtained from electrospinning technique [10-12], have the strong potential application for sensor because the fibrous membranes have surface area approximately one to two orders of the magnitude larger than continuous films [13]. The mechanism of acrylic acid used as sensing materials for ammonia has been reported by Chabukswar et al [4]. Here, polyacrylic acid (PAA), a weak anionic polyelectrolyte, is regarded as ideal sensing materials for coating on QCM because of the interaction between ammonia molecules and carboxyl groups of PAA. In our previous study [14], a gas sensor

was prepared with composite nanofibrous membranes. However, its sensitivity is still not high enough to detect ammonia at ppb level.

In this research, we try to fabricate the fibrous PAA membranes coated QCM sensors to detect the low concentration of ammonia (130 ppb-5 ppm) and investigate the parameters which influenced the sensor performance of the FM-QCM sensors.

8.2 Experimental Procedure

The starting materials included polyacrylic acid (PAA) (M_w 250000, Wako Pure Chemical Industries, Ltd, Japan), ethanol (99.5 vol%, Junsei Chemical Co., Ltd) and distilled water. Various polymer solutions were prepared with H_2O/ethanol weight ratios of 100/0, 50/50, and 0/100. The concentration of PAA solution was 6 wt.%. The viscosity and conductivity of PAA solutions were measured by a viscotester (6L/R, Hakke, USA) and electric conductivity meter (CM-40G, TOA•DKK Co., Japan), respectively.

The positive electrode of a high voltage power supply (FC30P4, Glassman High Voltage Inc., USA) was connected with a copper wire and was immersed into a syringe containing PAA solution. The syringe was fixed to a stand which was above a grounded QCM (10 MHz, AT-cut quartz crystal with Ag electrodes), and the distance from the tip of syringe to the electrode of QCM was 5 cm. The applied voltage was kept at 20 kV. To minimize falling drops at the tip of syringe, the syringe was tilted at 15^o from the horizontal. Fibrous PAA membranes were in continuously collected on the electrode of QCM until the required frequency shift was got. The resonance frequencies were measured by a frequency counter (Hewlett Packard 53131 A). The coating load of the fibrous PAA membranes on QCM were about 5000, 10000, 15000, and 20000 Hz, respectively. Then, the FM-QCMs were dried for 2 h at 80 ^{o}C under vacuum prior to the subsequent characterizations.

In order to compare the sensitivity of the FM-QCM and CF-QCM sensors, a gas sensor was prepared by the casting method. A 10^{-2} M of PAA solution was prepared in distillated water to use as casting solution. The electrode of QCM was coated with 25 μl of PAA solution. The casting film coated QCM was dried for 2 h at 80 ^{o}C under vacuum. The frequency shift of the casting film coated QCM was about 10000 Hz.

The morphology of the fibrous membrane and casting film coated on QCM was determined with field emission scanning electron microscopy (FE-SEM) (S-4700, Hitachi Ltd., Japan). The diameter of electrospun PAA fibers was measured by using image analyzer (Adobe Photoshop 7.0).

Fig. 1 shows the flow-type experimental setup for measuring the sensing properties of the sensors. The N_2 was used as carrier gas and controlled the relative humidity at 25, 35, 40, and 45 %, respectively. The flow rates of dry N_2, wet N_2 and ammonia were kept constant by the mass flow controllers (MFCs, Estec, SEC-400 MK3). The temperature in chamber was stabilized at 25 ^oC by an external temperature controller. The sensor was installed in the chamber with constant temperature and relative humidity. During the measurement, the ammonia concentration was regulated at 130 ppb, 450 ppb, 1 ppm, 2 ppm, and 5 ppm, respectively. The time for each adsorption was 10 min, and desorption was 60 min. The sensing properties of the sensors to ammonia were examined by measuring the resonance frequency shifts of QCM which due to the additional mass loading. The resonance frequencies were measured by the frequency counter. The data from the sensors were recorded by a personal computer. The stability of FM-QCM sensors was tested at the constant temperature and relative humidity for 10 days. A cycle of adsorption and desorption of 450 ppb of ammonia gas was examined for each day.

8.3 Results and Discussion

8.3.1 Morphology of fibrous membranes

The morphology of the fibrous PAA membranes, the solution properties and the average diameter of PAA fibers as a function of solvent composition are shown in Figs. 2-4, respectively. As was typical for electrospun fibrous membranes, there was a distribution of fiber diameters, and the fibers were randomly oriented as a porous membrane. It is well known that the morphology and properties of electrospun fibers are strongly influenced by the solution properties such as viscosity and conductivity [15]. For a PAA solution dissolved only in H_2O, the beaded PAA fibers (Fig. 2a) were formed with an average

diameter of 1.1 μm (Fig. 4) due to its low viscosity (40 cPs) and high conductivity (149.2 mS/m) (Fig. 3). Meanwhile, the beaded fibers showed a poor morphology which differ from that generally showed by other electrospun fibers. The reason may be due to the formation of the strong hydrogen bond [16] between water and the large amount of carboxyl groups of PAA. After the PAA fibers formed from the splitting of the droplet in electrospinning process, it can not evaporate the water completely during the distance from the tip of syringe to the electrode of QCM.

For electrospun fibers from a mixed solvent of H_2O and ethanol (Fig. 2b), it can be observed that the fibers showed a dramatically increased diameter without beads which corresponded to the sharply increased viscosity (420 cPs) and decreased conductivity (9.3 mS/m) [15]. Their average diameter was 6.7 μm. In ethanol only (Fig. 2c), the PAA fibers were formed with an improved rigidity. The average diameter was 2 μm, lower than that formed from the mixed solvent of H_2O and ethanol, but higher than that formed from the solvent of H_2O, which corresponded to its medium viscosity (110 cPs) of PAA solution in ethanol. In general, the rigidity of electrospun fibers was improved with the increasing of polymer solution viscosity [14] or adding the volatile solvent with a low boiling point [17]. Here, it can be observed that the rigidity of PAA fibers was gradually increased with increasing the content of ethanol because the hydrogen bond between PAA and ethanol was weaker than that between PAA and H_2O. The solvent became easily to evaporate with increasing the content of ethanol. As a result, the morphology of PAA fibers was strongly related with the solution properties.

8.3.2 Effect of morphology of fibrous membranes

Fig. 4 shows the average PAA fiber diameter and the response of FM-QCM sensors exposed to 1 ppm of ammonia as a function of solvent composition. The sensor with fibrous PAA membranes, which obtained from the solvent of H_2O, showed the largest response compared with those obtained from the mixed solvent and pure ethanol. The maximum frequency shifts of FM-QCM sensors were 113, 60, and 94 Hz when they formed from the H_2O/ethanol with the weight ratios of 100/0, 50/50, and 0/100,

respectively. It can be seen that the frequency shifts have an opposite trend with the average fiber diameter. In general, the sensitivity of sensors increases with increasing the surface area [18]. And the surface area increases with decreasing the average fiber diameter [19]. Hence, the FM-QCM sensors with small average fiber diameter had a higher sensitivity.

8.3.3 Comparison between FM-QCM and CF-QCM sensors

It is well known that the sensitivity of QCM sensors is strongly related with the morphology of coating materials [8]. The comparison between the FM-QCM and CF-QCM sensors for detection of ammonia was made. Fig. 5 shows the SEM image of the casting PAA film on QCM. The casting film showed a relatively flat plane without complicated 3D structures compared with the fibrous membrane. The response of FM-QCM and CF-QCM sensors with same coating load exposed to 1 ppm of ammonia at the relative humidity of 40 % are shown in Fig. 6. The maximum frequency shift of the FM-QCM sensors was 4 times larger than that of the CF-QCM sensors. The electrospun fibrous membranes with porous structures have 1 to 2 orders of magnitude more surface area than that found in continuous films [13]. The coating material with high surface area has more adsorption sites to lead the high sensitivity.

8.3.4 Effect of ammonia concentration

Fig. 7 shows the response of the FM-QCM sensors exposed to various concentration of ammonia. As the FM-QCM sensors exposed to 130 and 450 ppb of ammonia, the frequency returned to the original position after 10 min adsorption and 60 min desorption process. However, the FM-QCM sensors exposed to 1, 2, and 5 ppm of ammonia, their frequency can not return to the original position within 70 min. We considered that the extra time was needed for the desorption process. The time for desorption of ammonia was gradually increased with increasing the concentration of ammonia due to the excessive ammonia was kept inside the 3D structures of fibrous membranes which led to the

desorption lag [20]. The desorption time was much longer than the adsorption time, which originated from some strong interactions between ammonia molecules and carboxyl groups of PAA.

The maximum frequency shifts of the FM-QCM sensors exposed to 130 ppb, 450 ppb, 1 ppm, 2 ppm, and 5 ppm of ammonia were 12, 37, 60, 111, and 232 Hz, respectively. We can found that the response of the FM-QCM sensors to ammonia was gradually increased with increasing the concentration of ammonia.

8.3.5 Effect of coating load

The effect of the coating load of fibrous PAA membranes on the frequency response of the FM-QCM sensors was investigated for ammonia, as shown in Fig. 8. The maximum frequency shift of the FM-QCM sensors increased on increasing the coating load from 5000 to 20000 Hz. The FM-QCM sensors with a larger coating load of fibrous PAA membranes exhibited a larger frequency response for the same concentration of ammonia because there were more absorption sites in the FM-QCM sensors with large coating load. A similar phenomenon was reported by Lin et al. to fabricate sensor using fullerene C_{60}-crystand coating [21].

8.3.6 Effect of humidity

The influence of the relative humidity to the sensing properties of the FM-QCM sensors is shown in Fig. 9. Fig. 9a shows the frequency shifts of the FM-QCM sensors after stabilization at various relative humidity. The frequency shifts were increased from 32 to 225 Hz on increasing the relative humidity from 25 to 45 % because H_2O molecules were pre-sorbed by the large amount of hydrophilic carboxyl groups of PAA in the fibrous membranes to lead a decrease of frequency.

The responses of the FM-QCM sensors exposed to 450 ppb of ammonia at various relative humidity are shown in Fig. 9b. The frequency shifts of the FM-QCM sensors stabilized at the relative humidity of 25, 35, 40, and 45 % were 0, 18, 39, and 65 Hz,

respectively. The FM-QCM sensors have no response to 450 ppb of ammonia at the relative humidity of 25 %. Meanwhile, it can be seen that the responses of the FM-QCM sensors were increased with increasing the relative humidity. The sensitivity of FM-QCM sensors was strongly affected by the relative humidity. One reason was due to the amount of H_2O molecules absorbed on hydrophilic groups in the fibrous membranes were increased with increasing the relative humidity. And ammonia molecules were easy to be adsorbed by H_2O molecules. The formation of hydrogen bond between ammonia and H_2O molecules was confirmed by the coadsorption study of ammonia and H_2O [22]. Therefore, the more ammonia molecules can be adsorbed by increasing the amount of H_2O molecules in the fibrous membranes to lead large frequency shift. Another reason maybe was due to the conductivity of carboxyl groups of anionic PAA was reinforced with increasing the relative humidity [23]. The capacity of interaction between the fibrous membranes and ammonia molecules was enlarged by the high conductivity of carboxyl groups.

It can be found that the FM-QCM sensors have cross-sensitivity to ammonia and H_2O. Moreover, the response of FM-QCM sensors to humidity was much larger than to ammonia when ammonia was in low concentration. As a result, the FM-QCM sensors have the potential application to use as a humidity sensor.

8.3.7 The stability of FM-QCM sensors

In order to investigate the stability of FM-QCM sensors for ammonia detection in humid atmosphere, a series of examinations were carried out for 10 days at the relative humidity of 40%. Fig. 10 displays the response of FM-QCM sensors to 450 ppb ammonia for 10 days. It can be seen that the average frequency shift of FM-QCM sensors was 38 Hz with a low standard deviation of 3.2 Hz. This phenomenon indicated that the FM-QCM sensors exhibited good stability for detection of ammonia in humid atmosphere within 10 days.

8.4 Conclusions

As a new sensing material, the fibrous PAA membranes were successfully deposited on

the electrode of QCM by using electrospinning technique. The morphology of PAA membranes was found to be strongly related with the solvent composition. The FM-QCM sensors with small average fiber diameter had a higher sensitivity. And the sensitivity of FM-QCM sensors was much higher than that of CF-QCM sensors, they can detect ammonia at ppb level with the assistance of pre-adsorbed water in the coating materials. The FM-QCM sensors can not detect low level of concentration of ammonia gas at low relative humidity. Moreover, the sensing properties of the FM-QCM sensors indicated the concentration of ammonia, coating load of the fibrous membranes on QCM, and relative humidity were important parameters to influence the sensitivity of the FM-QCM sensors for ammonia. The FM-QCM sensors were found to have cross-sensitivity to ammonia and H_2O, and the sensitivity of this sensor to humidity was much higher than ammonia. Hence, it has the potential application to use as a humidity sensor. Additionally, a good stability was displayed in the preliminary study of the stability of FM-QCM sensors within 10 days.

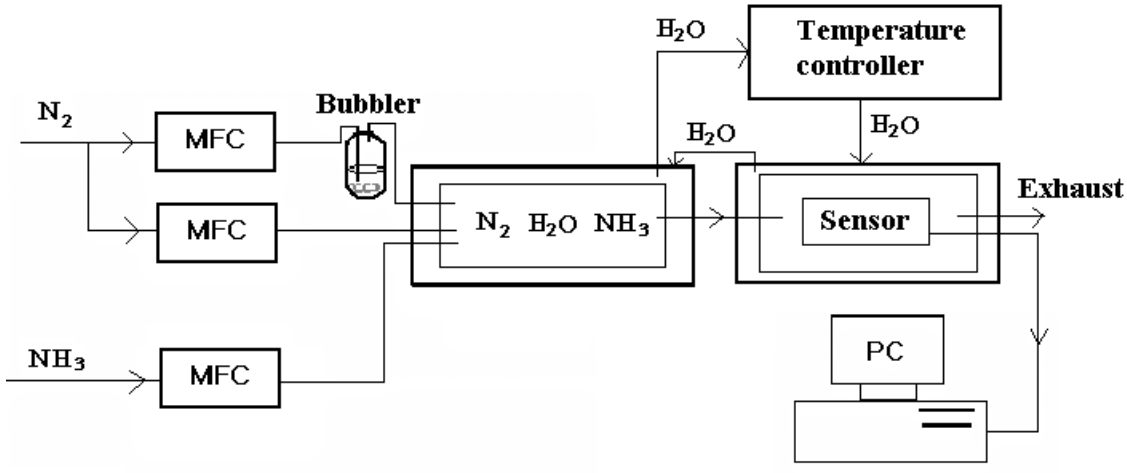

Fig. 8-1. Schematic diagram of a gas testing system for ammonia detection.

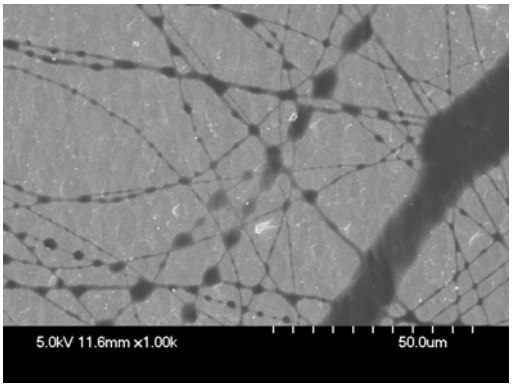

(a)

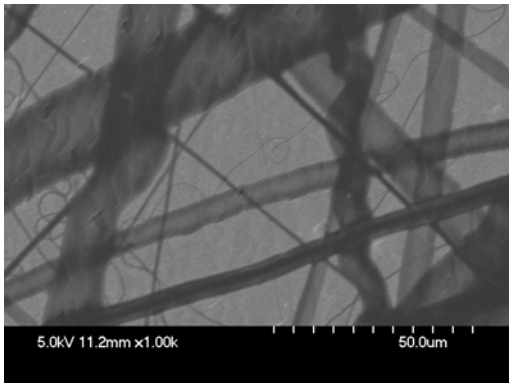

(b)

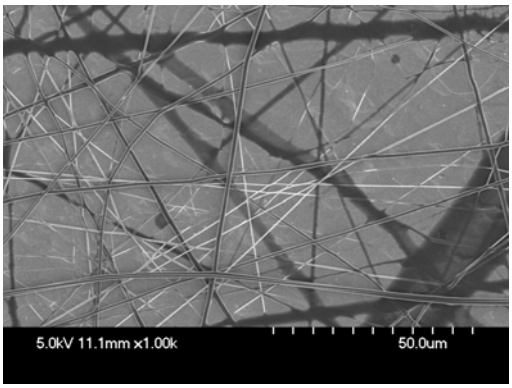

(c)

Fig. 8-2. FE-SEM images of the fibrous PAA membranes deposited on QCM as a function of the weight ratio of H_2O/ethanol in solvent. (a) 100/0; (b) 50/50 and (c) 0/100.

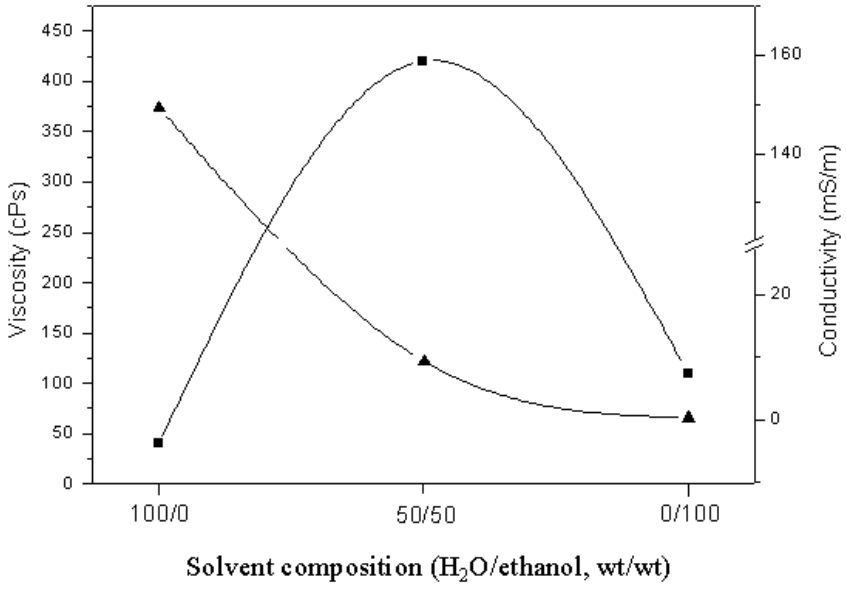

Fig. 8-3. Viscosity and conductivity of PAA solutions as a function of solvent composition (■, viscosity; ▲, conductivity).

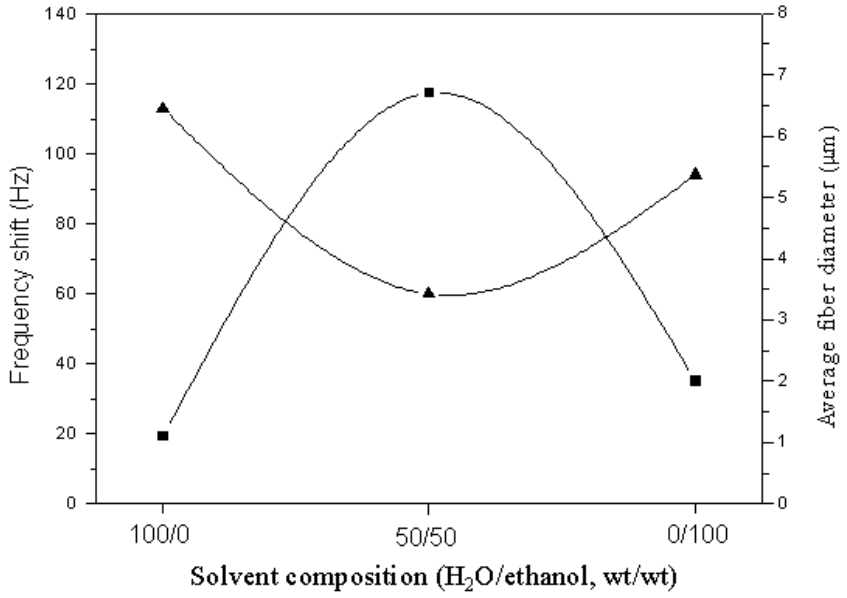

Fig. 8-4. Average fiber diameter and response of the FM-QCM sensors exposed to 1 ppm of ammonia as a function of solvent composition (■, average fiber diameter; ▲, frequency shift). The coating load of PAA fibrous membranes was 20000 Hz and the relative humidity was 40 %.

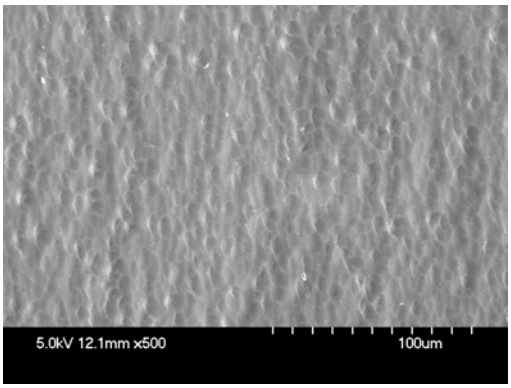

Fig. 8-5. An FE-SEM image of the PAA casting film on QCM.

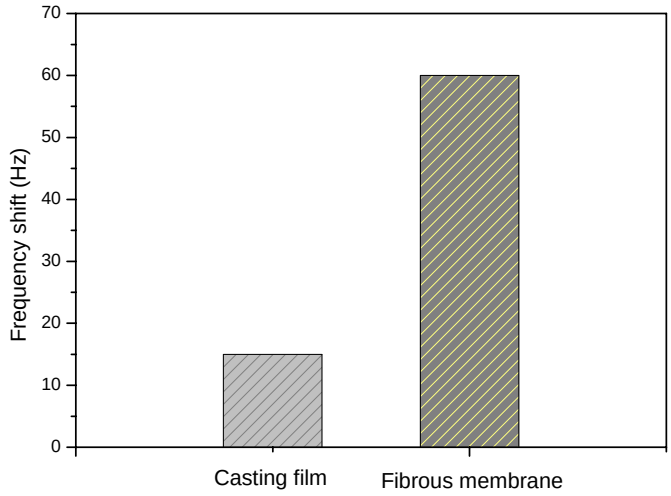

Fig. 8-6. Response of the FM-QCM and CF-QCM sensors with same coating load (10000 Hz) exposed to 1 ppm of ammonia at the relative humidity of 40 %. The PAA fibrous membrane was obtained from the solvent of H_2O.

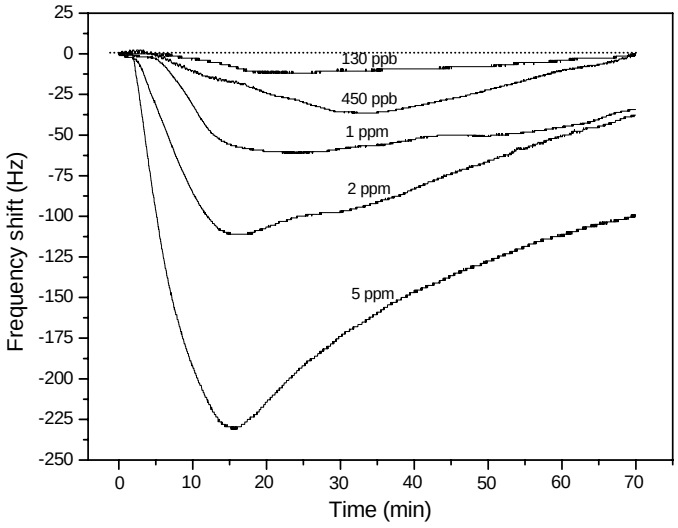

Fig. 8-7. Response of the FM-QCM sensors with 10000 Hz coating load exposed to various concentration of ammonia. The PAA fibrous membrane was obtained from the solvent of H_2O and the relative humidity was 40 %.

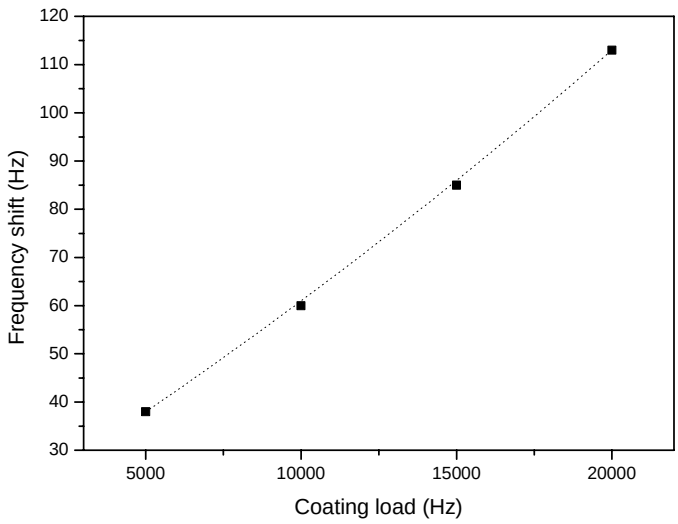

Fig. 8-8. Response of the FM-QCM sensors exposed to 1 ppm of ammonia as a function of coating load of fibrous PAA membranes on QCM. The PAA fibrous membrane was obtained from the solvent of H_2O and the relative humidity was 40 %.

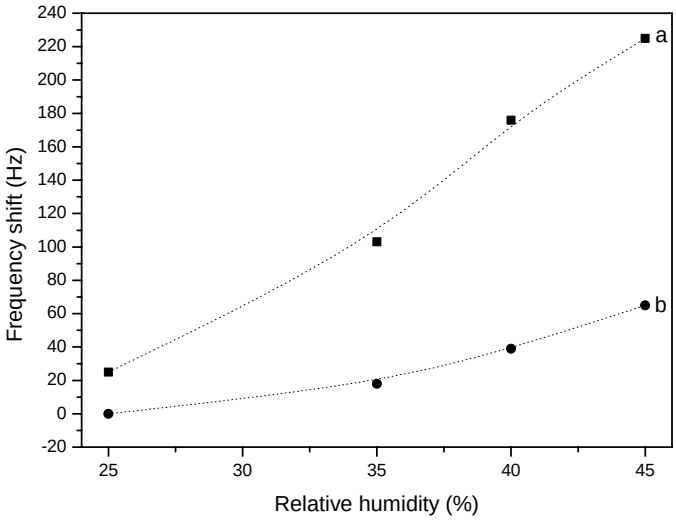

Fig. 8-9. Response of the FM-QCM sensors (a) stabilized at various relative humidity and (b) exposed to 450 ppb of ammonia at various relative humidity. The PAA fibrous membrane was obtained from the solvent of H_2O and the coating load was 10000 Hz.

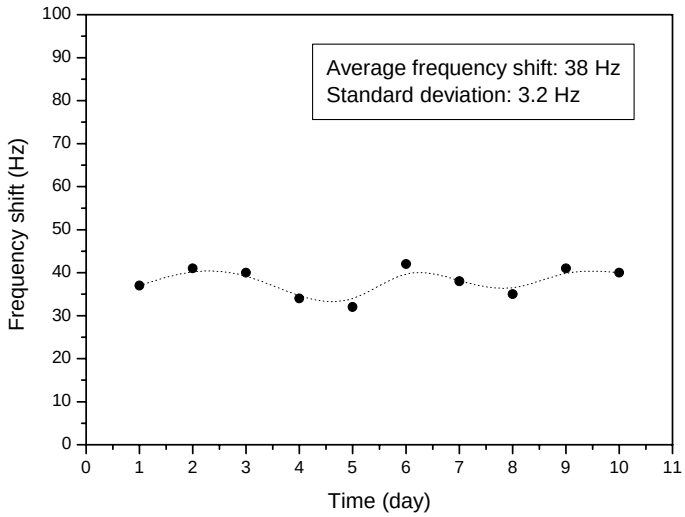

Fig. 8-10. The stability of FM-QCM sensors with 10000 Hz coating load exposed to 450 ppb of ammonia. The PAA fibrous membrane was obtained from the solvent of H_2O and the relative humidity was 40 %.

References

[8-1] M. Bendahan, P. Lauque, C.L. Mauriat, H. Carchano and J.L. Seguin, *Sens. Actuator B* 84 (2002) 6.

[8-2] S. Sen, K.P. Muthe, N. Joshi, S.C. Gadkari, S.K. Gupta, Jagannath, M. Roy, S.K. Deshpande and J.V. Yakhmi, *Sens. Actuator B* 98 (2004) 154.

[8-3] O.K. Varghese, D. Gong, W.R. Dreschel, K.G. Ong and C.A. Grimes, *Sens. Actuator B* 94 (2003) 27.

[8-4] V.V. Chabukswar, S. Pethkar and A.A. Athawale, *Sens. Actuator B* 77 (2001) 657.

[8-5] A. Galdikas, A. Mironas, V. Strazdiene, A. Setkus, I. Ancutiene and V. Janickis, *Sens. Actuator B* 67 (2000) 76.

[8-6] E. Milella and M. Penza, *Thin Solid Films* 327 (1998) 694.

[8-7] C. Zhang, B.P. Cappleman, M. Defibaugh-Chavez and D.H. Weinkauf, *J. Polym. Sci., Polym. Phys.* 41 (2003) 2109.

[8-8] K.H. Kang, J.M. Kim, D.K. Kim, S.B. Jung, J.S. Chang and Y.S. Kwon, *Sens. Actuator B* 77 (2001) 293.

[8-9] M. Gomes, P. Nogueira and J. Oliveira, *Sens. Actuator B* 68 (2000) 218.

[8-10] D.H. Reneker and I. Chun, *Nanotechnology* 7 (1996) 216.

[8-11] A.G. MacDiarmid, W.E. Jones, I.D. Norris, J. Gao, A.T. Johnson, N.J. Pinto, J. Hone, B. Han, F.K. Ko, H. Okuzaki and M. Llaguno, *Synth. Met.* 119 (2001) 27.

[8-12] A. Theron, E. Zussman and A.L. Yarin, *Nanotechnology* 12 (2001) 384.

[8-13] J. Huang, S. Virji, B. Weiller and R. Kaner, *J. Am. Chem. Soc.* 125 (2003) 314.

[8-14] B. Ding, J. Kim, Y. Miyazaki and S Shiratori, *Sens. Actuator B* 101 (2004) 373.

[8-15] H. Fong, I. Chun and D. Reneker, *Polymer* 40 (1999) 4585.

[8-16] D. Santhiya, S. Subramanian, K.A. Natarajan and S.G. Malghan, *J. Colloid Interface Sci.* 216 (1999) 143.

[8-17] K.H. Lee, H.Y. Kim, Y.M. La, D.R. Lee and N.H. Sung, *J. Polym. Sci., Part B: Polym. Phys.* 40 (2002) 2259.

[8-18] Y. Wang, X. Wu, Y. Li and Z. Zhou, *Solid State Electron.* 48 (2004) 627.

[8-19] B. Ding, H. Kim, C. Kim, M. Khil and S. Park, *Nanotechnology* 14 (2003) 532.

[8-20] H. Ding, V. Erokhin, M.K. Ram, S. Paddeu, L. Valkova and C. Nicolini, *Thin Solid Films* 379 (2000) 279.

[8-21] H.B. Lin and J.S. Shih, *Sens. Actuator B* 92 (2003) 243.

[8-22] Y. Shingaya, H. Kubo and M. Ito, *Surf. Sci.* 427 (1999) 173.

[8-23] A. Bozkurt, W. H. Meyer and G. Wegner, *J. Power Sources* 123 (2003) 126.

CHAPTER 9

Concluding Remarks on Optimization and Functionallization of Electrospun Nanofibers

9.1 Optimization of Nanofibrous Mats via Multi-jet Electrospinning

In this study, the samples in chapter 3 were prepared via a new approach (multi-jet electrospinning). The FE-SEM, FT-IR, XRD, immersion test, and mechanical properties (modulus, tensile strength, and elongation) of blend biodegradable electrospun nanofibrous nonwoven mats of PVA and CA showed that the weight ratio of PVA/CA in blends can be well controlled by changing the number ratio of jets of PVA/CA, and the PVA and CA nanofibers dispersed into each other very well. This approach afforded a high potential possibility to produce the nanofibrous mats with uniform properties such as, dispersibility, thickness, and mechanical properties. Especially, it had the advantage for multi-component polymers or composite viscous solutions which cannot be dissolved in the same solvent or kept in the same container. Meanwhile, the mass production of electrospun nanofibrous mats with uniform properties also been realized. It opened a way for commercialization the novel electrospun nanofibrous mats with controllable thickness to human society.

9.2 Combination of Electrospinning and Electrostatic Layer-by-layer (LBL) Self-assembly Techniques

The electrostatic LBL self-assembly technique, based on alternate adsorption of oppositely charged polyelectrolytes or fine particles, shows the advantage of allowing stable films to be produced in air with the use of a simple and inexpensive apparatus and many different substrates. On the other hand, it is critical to select the suitable core polymer as the fiber template. The polymer fibers with negative or positive charges, low fiber density, and good water insolubility can be regarded as ideal fiber templates, such as poly(ethylene-co-vinyl alcohol) (EVAL), CA, and chitosan. In this study, the CA

nanofibers were employed as the fiber template for the electrostatic LBL deposition.

In chapter 4, oppositely charged anatase TiO_2 nanoparticles and PAA were alternately deposited on the surface of negatively charged cellulose acetate (CA) nanofibers using the electrostatic LBL self-assembly technique. The fibrous mats were characterized by XRD, FT-IR, FE-SEM, TEM, and BET surface area. The crystalline phase of anatase TiO_2 remained unchanged in the resultant TiO_2/PAA films coated on CA fibrous mats. Moreover, the TiO_2/PAA films coated fibers showed rough surface with grains due to the deposition of aggregated TiO_2 particles. The diameter of the films coated fibers was distributed in the broad range of 200 to 1700 nm. The region of diameter distribution of the films coated fibers was enlarged and the major region was moved to large diameter. After deposition of LBL films, the average diameter of fibers increased from 344 to 584 nm and the standard deviation increased from 98 to 192 nm. The calculated average thickness of 5 bilayers of TiO_2/PAA films coated on CA nanofibers was approximately 120 nm, and thus the average thickness of one bilayer of TiO_2/PAA film was estimated to be about 24 nm. The BET surface area of fibrous mats increased from 2.5 to 6.0 m^2/g after being coated with 5 bilayers of TiO_2/PAA films because of the rough surface of the film coated fibers.

The typical LBL polyelectrolytes films, multilayered PAH/PAA films, were prepared in chapter 5. By controlling the amount of bilayers on nanofibers, a series of PAH/PAA films coated nanofiber samples were obtained. The average diameters of nanofibers and films thickness gradually increased with increasing the amount of bilayers on the surface of nanofibers. Meanwhile, the influence of pH value of polyelectrolyte solutions to the formation of LBL films on CA nanofibers was investigated. It was found that the film with low growing speed was suitable for coating on nanofibers.

The combination of these two techniques opened one way to make high efficient functional materials with high surface area using a simple, inexpensive, and clean process. Considering our developments in chapter 3, it had high potential possibility to make mass production of such functional materials. A number of functional coating materials can be used to coat the nanofibers such as, polyelectrolytes, charged organic and inorganic nanoparticles, and charged proteins, enzymes and dyes.

Encourgaed by the recent success in the fabrication of LBL films on electrospun

nanofibers using the electrostatic LBL self-assembly technique (chapter 4 and 5), we have developed a straightforward and highly versatile template method for the production of nanotubes. The concept is to coat the electrospun negatively charged CA nanofibers with oppositely charged PAH and polyoxometalate (POM) using LBL self-assembly technique. POM nanotubes are subsequently formed via selective removal of the core fiber template and PAH by thermal degradation.

In chapter 6, we have fabricated the Keggin-type polyoxometalate ($H_4SiW_{12}O_{40}$) nanotubes by calcining the LBL structured ultrathin hybrid films coated electrospun fibrous mats. The hybrid films coated electrospun fibrous mats were obtained from the alternate deposition of positively charged PAH and negatively charged $H_4SiW_{12}O_{40}$ on the surface of negatively CA nanofibers using the electrostatic LBL self-assembly technique. It was found that the morphology of hybrid PAH/$H_4SiW_{12}O_{40}$ films coated fibrous mats was strongly influenced by the number of deposition bilayers and the pH of dipping solutions. The fibrous mats were contracted and the $H_4SiW_{12}O_{40}$ nanotubes with a wall thickness about 50 nm can be fabricated after calcination at high temperature. Additionally, the FT-IR and WAXD results indicated that the pure $H_4SiW_{12}O_{40}$ nanotubes were gotten with a Keggin structure.

9.3 Sensing Properties of Electrospun Polyelectrolyte Nanofibers

The sensing properties of electrospun polyelectrolyte nanofibers were studied in chapter 7 and 8. The thin membrane composed of electrospun nanofibers, which obtained from electrospinning technique, has the strong potential application for sensor because the nanofibers have surface area approximately 1-2 orders of the magnitude larger than continous films. Different from the most of known sensors composed electrospun nanofibers which used as fluorescent optical sensors, the new sensing model adopted a QCM with high mass sensitivity as substrate, and polyelectrolytes with high sensitivity to polarized gases as sensing materials. For example, the polyanions can be used as sensing materials for basic gases, and the polycations can be used as sensing materials for acid gases. QCM is highly sensitive to mass changes in the presence of a coating that interacts

with the target gas. In this research, electrospun nanofibrous polyelectrolytes membranes were employed as sensing materials and combined with QCM to form a super-high sensitive gas sensor.

In chapter 7, the new sensing model was built up. The conductivity of blend electrospinning solution of PVA and PAA was increased with increasing the content of PAA because of the high conductivity of PAA in water. Meanwhile, the viscosity of blend solutions sharply increased and much higher than the original viscosity of PAA and PVA, which caused by the partial crosslinking of PVA and PAA due to the formation of hydrogen bond between the carboxyl groups of PAA and hydroxyl groups of PVA. As expected, the morphology of electrospun nanofibers was gradually changed corresponding to the change of electrospinning solution properties.

The anti-water solubility of sensing materials was reinforced by crosslinking of PAA and PVA. However, the sensitivity of sensors to ammonia decreased with increasing the content of PVA because PVA is not sensing materials to ammonia. The responses of sensors were reinforced with increasing the concentration of ammonia from 50 to 200 ppm. However, all the frequencies of sensors couldn't return to the original position after adsorption and desorption processes due to the excessive ammonia was kept inside the 3D structures of nanofibrous membranes which led to the desorption lag. The base lines of frequency shifts gradually decreased with increasing the concentration of ammonia. Meanwhile, the maximum frequency shift gradually increased with increasing the exposure cycles. The relative humidity was proved to be an important parameter to influence the sensor sensitivity. It can be observed that the responses of sensors were sharply increased with increasing the relative humidity after introducing ammonia. Moreover, the sensitivity of electrospun nanofibrous membranes was confirmed to be much higher than that of the continuous layer-by-layer films.

In chapter 8, a practical ammonia sensor with super-high sensitivity at ppb level was fabricated. The high molecular weight of PAA was chosen as sensing material to ammonia. The fibrous membranes with different morphology can be deposited on the electrode of QCM by electrospinning the PAA solutions with various solvent composition of water and ethanol. It was observed that the morphology of PAA fibers was strongly related with the

solution properties. The frequency shifts of sensors have an opposite trend with the average fiber diameter. In general, the sensitivity of sensors increases with increasing the surface area. And the surface area increases with decreasing the average fiber diameter. Hence, the sensors with small average fiber diameter had a higher sensitivity. The results of sensing experiments also indicated that the sensitivity of the fibrous membranes was 4 times higher than that of the casting films with the same coating load on QCM.

The responses of ammonia sensors were reinforced, and the response time was decreased from 6 to 1.5 min with increasing the concentration of ammonia from 130 ppb to 5 ppm. The maximum frequency shift of the sensors increased on increasing the coating load from 5 000 to 20 000 Hz. The sensors with a larger coating load of fibrous PAA membranes exhibited a larger frequency response for the same concentration of ammonia because there were more absorption sites in the sensors with large coating load. The responses of sensors were increased with increasing the relative humidity. The sensors were found to have cross-sensitivity to ammonia and water. Moreover, the response of sensors to humidity was much larger than to ammonia when ammonia was in low concentration. As a result, the FM-QCM sensors have the potential application to use as a humidity sensor.

9.4 The Future Prospect Regarding the Present Research

Firstly, the conventional wound dressing can be insteaded by the fibrous nonwoven mats which prepared via the multi-jet electrospinning fashion. To date, one of the commercial processes of producing some biopolymers for medical applications is the braiding of multiple melt/solution-spun filaments. These braided, multiple-strained fibers are either used as suture material or woven into mats to serve as tissue dressings. These constructs have also been used as scaffolds in tissue engineering. One limitation of these commercially prepared products is the relatively large fiber sizes (10-12 μm) that are due to the limitation of traditional extrusion. Therefore, there is a demand to reduce the fiber size as low as nanoscale for wound dressings.

The goal of wound dressing is the production of an ideal structure, which gives higher porosity and good barrier. To reach this goal, wound dressing materials must be selected

carefully, and the structure must be controlled to confirm that it has good barrier properties and oxygen permeability. Electrospun nanofibrous membranes have the advantages to be the candidate for wound dressings such as higher gas permeability and protection of wound from infection and dehydration.

Hence, we want to develop a novel nanofibrous wound dressing which is biodegradable, biocompatibility and releasable for drugs. The biodegradable polymeric nanofibrous membranes containing drugs can be obtained through the electrospinning of the blend solutions of biodegradable polymers and drugs. The drugs contained nanofibrous membranes have some merits for wound dressings such as the decreasing of the severe infiltration of inflammatory cells and forming thick scab.

Many biodegradable and biocompatible polymers can be used to for wound dressings materials such as polyglycolide (PG), polylactide (PLA), poly(p-dioxanone) (PDO), poly(lactide-co-trimethylene carbonate) (Poly(LA-co-TMC), poly(ε-caprolactone) (PC), poly(trimethylene carbonate) (PTMC), thermoreversible gelatins, etc. The drugs for drug delivery system include cefazolin, gentamicin, erythromycin, antibiotic, paclitaxel, rapamycin, hydroxypropyl-β-cyclodextrin, rifampin and so on. These above biodegradable and biocompatible materials blended with drugs can be electrospun into nanofibrous membranes after dissolving them into organic solvents such as methylene chloride (MC), chloroform, *N*,*N*-dimethylformamide (DMF), tetrahydrofuran (THF), and ethanol.

The different morphology and properties of drugs contained nanofibrous membranes can be fabricated by adjusting the solution properties and process parameters. The solution properties including surface tension, viscosity and conductivity can be affected by the average molecular weight of polymers, kinds of solvents, polymer concentration, drug concentration, applied voltage, distance between tip to collector, temperature and humidity. The positive electrode of a high voltage power supply is connected with a copper wire, is immersed into a pipette containing blend solution. The pipette was fixed to a stand which was above a grounded metal collector, and the distance between the tip of pipette to collector is about 15 cm. The applied voltage is kept as 20 kV. The nanofibrous membranes are obtained on the surface of the metallic collector. The nanofibrous membranes are dried

24 h at 80 ^{o}C under vacuum for prior to the subsequent characterizations.

The resultant nanofibrous membranes can be examined by field emission scanning electron microscopy (FE-SEM), Fourier transform infrared spectroscopy (FT-IR), wide-angle X-ray diffraction (WAXD), differential scanning calorimetry (DSC), tensile test, gel permeation chromatography (GPC), nuclear magnetic resonance (NMR), gas permeation analysis (GPA), thermogravimetric analysis (TGA), UV–vis spectroscopy, in vitro and vivo test, and Brunauer-Emmett-Teller (BET) surface area regarding their morphology, composition, crystallinity, mechnical properties, gas permeability, thermal stability, degradation speed, biocompatibility, surface area and porosity. The electrospun nanofibrous wound dressings are expected to have thin fiber diameter, high surface area, controllable degradation speed, stable release speed of drugs, good biocompatibility, good mechanical properties and good gas permeability. The modified wound dressings comprising drugs contained nanofibrous membranes have the strong potential ability to instead of the current market available wound dressings.

This novel products and technologies can make it through the regulatory hurdles and now face the daunting task of changing traditional wound care practices. Although traditional practices continue to dominate many sectors of wound care, advanced wound dressings and related technologies offer impressive, often lifesaving, advancements being increasingly accepted by both the hospital and alternative care markets.

Secondly, the high efficient nano- biosensors can be fabricated by using the combinations of electrospinning, electrostatic self-assembly LBL and QCM techniques. Biosensors are finding use in increasingly broader ranges of application such as clinical diagnosis and biomedicine, farm, garden and veterinary analysis, food and drink production and analysis, microbiology: bacterial and viral analysis, pharmaceutical and drug analysis, pollution control and monitoring, etc. It is reported that the market size for worldwide biosensors at yearend 2003 was about $7.3 billion. Even with scary geopolitical events unfolding and a stubborn weak global economy, the market is projected to improve and grow to about $10.8 billion in 2007 with a growth rate of about 10.4%. However, the sensitivity of some biosensors is poor due to various reasons. Many researchers are attempting to increase the biosensor performance by using different techniques.

It is well known that the ultrahigh sensitivity of QCM sensors can accurately detect mass uptake on the order of nanograms. The QCM is highly sensitive to mass changes in the presence of a coating that interacts with the target. The QCM biosensor performance such as sensitivity, selectivity and time response is largely influenced by the properties of the sensing materials. A number of materials such as oligonucleotides, proteins, antibodies, enzymes and glucose oxidase have been successfully employed in the coating of QCM biosensors by using electrostatic LBL self-assembly technique. This technique, based on alternate adsorption of oppositely charged polyelectrolytes or particles, shows the advantage of allowing stable films to be produced in air with the use of a simple and inexpensive apparatus and many different substrates. The stability of the deposited layers has been shown to be improved in the presence of salt (NaCl).

In general, the sensitivity of biosensors increases with increasing the surface area. The nanofibrous membranes, which obtained from electrospinning technique, have the strong potential application for sensors because the nanofibrous membranes have surface area approximately one to two orders of the magnitude larger than continuous films. Additionally, the method of electrostatic LBL self-assembly is ideally suited for growing thin films with controllable thickness on the 3D structured nanofibrous membranes. Meanwhile, it is critical to select the suitable core polymer as the nanofiber template. The polymer nanofibers with negative or positive charges, low fiber density and good water insolubility can be regarded as ideal nanofiber templates, such as poly(ethylene-co-vinyl alcohol) (EVAL), CA, and chitosan. In this study, the CA nanofibers were employed as the nanofiber template for the electrostatic LBL deposition.

The hydrophobilization of QCM surface is achieved by dipping the QCM in thiol solution. Then, the hydrophobic surface of QCM is used as collector to deposit the CA nanofibers during the electrospinning process. The applied voltage is 15 kV, and the tip-to-QCM distance is 10 cm. Nanofibrous CA membranes are in continuously collected on the electrode surface of QCM until the required frequency shift is got. The resonance frequencies are measured by a frequency counter. The CA nanofibrous membranes coated QCM (NM-QCM) is dried at 80 ^{o}C in vacuum for 2 h to remove the trace solvent. The zeta potential of CA had a negative value in the range pH 2-10. Next, the NM-QCM is used as

substrate for the electrostatic LBL deposition. The different biosensing materials with various types of charges such as oligonucleotides, proteins, antibodies, enzymes and glucose oxidase can be deposited on the nanofiber surface by assistance the oppositely charged polyelectrolytes, respectively. Negatively charged PAA can be sued as polyanion and positively charged poly(ethyleneimine) (PEI) and PAH can be used as polycations. Due to the hydrophobilization of QCM surface, the LBL films can not be formed on the surface of QCM. Therefore, the LBL films only can grow along the surface of nanofibers. The thickness of the sensing LBL films is closely related to the deposition conditions, i.e., molecular weight of PAA, concentration, pH value and zeta potential of the dipping solution, the deposition time, and the amount of bilayers. The inner diameter of LBL films is controlled by the size of the electrospun template CA nanofibers.

This route might open a new door to making high efficient biosensors. These novel biosensors comprising QCM and sensing films coated nanofibrous membranes with high surface area are expected to have much higher sensitivity to the target than the current market available biosensors.

CHAPTER 10

Summary

In this thesis, the optimization and functionallization of nanofibrous mats/membranes prepared by electrospinning were discussed to obtain the uniform properties of nanofibrous nonwoven mats, functional films coated nanofibrous mats, inorganic nanotubes, and high sensitive fibrous sensing membranes.

Firstly, a fashion was built up to overcome the changllege in electrospinning field, that the mulit-component blend nanofibrous mats can not be obtained if the materials can not be dissolved in the same solvent or kept in the same container. Another challenge was also solved. The mass production of electrospun nanofibrous mats with uniform properties also been realized.

As a example, blend biodegradable nanofibrous nonwoven mats with different weight ratio of poly(vinyl alcohol) (PVA)/cellulose acetate (CA) were fabricated via multi-jet electrospinning. These nanofibrous mats were examined regarding their morphology, dispersibility, and mechanical properties. The results showed the blend nanofibrous mats have good dispersibility because the blend nanofibrous mats have uniform properties for each sample and regular transforms with changing the number ratio of jets of PVA/CA. As a result, the PVA and CA nanofibers were homogenously dispersed into each other. FT-IR results demonstrated that there was no chemical reaction between PVA and CA nanofibers, just physical blending. Additionally, the mechanical properties of CA nanofibrous mats were improved by increasing the content of PVA nanofibers. Furthermore, the multi-component blend nanofibrous mats also can be obtained by increasing the electrospinning jets in this multi-jet electrospinning fashion. Based on this fashion, any electrospinable materials can be electrospun into blend nanofibrous mats despite their interactions in solvents.

Secondly, we prepared the functional films coated nanofibrous mats by the combination of electrospinning and electrostatic layer-by-layer (LBL) self-assembly techniques. The technique, based on alternate adsorption of oppositely charged polyelectrolytes, shows the

advantage of allowing stable films to be produced in air with the use of a simple and inexpensive apparatus and many different substrates. The method of electrostatic LBL self-assembly is ideally suited for growing thin nanoparticle films with controllable thickness on the 3D structured nanofibrous mats. It is critical to select the suitable core polymer as the fiber template. The polymer fibers with negative or positive charges, low fiber density, and good water insolubility can be regarded as ideal fiber templates, such as poly(ethylene-co-vinyl alcohol) (EVAL), CA, and chitosan. In this study, the CA nanofibers were employed as the fiber template for the electrostatic LBL deposition.

Oppositely charged anatase TiO_2 nanoparticles and poly(acrylic acid) (PAA) were alternately deposited on the surface of negatively charged CA nanofibers using the electrostatic LBL self-assembly technique to form a LBL structured ultrathin hybrid films on electrospun nanofibers. The crystalline phase of anatase TiO_2 remained unchanged in the resultant TiO_2/PAA films coated on CA fibrous mats. Moreover, the TiO_2/PAA films coated fibers showed rough surface with grains due to the deposition of aggregated TiO_2 particles. The average diameter of fibers increased from 344 to 584 nm and the BET surface area of fibrous mats increased from 2.5 to 6.0 m^2/g after being coated with 5 bilayers of TiO_2/PAA films. And such LBL films coated fibrous mats would show great potential to be used as catalysts, filters and sensors. Furthermore, the LBL structured tubes might be made by thermal degradation or solvent extraction of the template nanofibers.

Self-assembled polyelectrolyte multilayered (PEM) films were fabricated on electrospun CA nanofibers via the electrostatic LBL adsorption of oppositely charged poly(allylamine hydrochloride) (PAH) and PAA. The growth of PEM films on CA nanofibers was studied by regulating the pH value of polyelectrolyte solutions and the number of PAH/PAA bilayers. The results indicated that the growth of PEM films fabricated at a PAH pH of 7.5 and a PAA pH of 3.5 (PAH7.5/PAA3.5) was much quicker than that of films of PAH and PAA adsorbed at pH 5 (PAH5/PAA5). The CA nanofibers were embedded in the thick PAH7.5/PAA3.5 films. The average diameter of PAH5/PAA5 films coated fibers and average PAH5/PAA5 film thickness gradually increased with increasing the number of PEM bilayers. Moreover, the surface roughness of fibers was increased after deposition of PAH/PAA films.

Furthermore, we have recently fabricated the Keggin-type polyoxometalate ($H_4SiW_{12}O_{40}$) nanotubes by calcining the LBL structured ultrathin hybrid films coated electrospun fibrous mats. The hybrid films coated electrospun fibrous mats were obtained from the alternate deposition of positively charged PAH and negatively charged $H_4SiW_{12}O_{40}$ on the surface of negatively charged CA nanofibers using the electrostatic LBL self-assembly technique. It was found that the morphology of hybrid PAH/$H_4SiW_{12}O_{40}$ films coated fibrous mats was strongly influenced by the number of deposition bilayers and the pH of dipping solutions. The fibrous mats were contracted and the $H_4SiW_{12}O_{40}$ nanotubes with a wall thickness about 50 nm can be fabricated after calcination at high temperature. Additionally, the FT-IR and WAXD results indicated that the pure $H_4SiW_{12}O_{40}$ nanotubes were gotten with a Keggin structure.

As a result, the polymer nanofibers were functionalized by the LBL coating on surface of fibers with functional materials. Most of the LBL films applications can be inherited and expanded by taking the advantage of the high surface-to-volume ratio of nanofibrous mats. Additionally, it opens a way to fabricate the functional inorganic nanotubes.

Finally, the thin membranes composed of electrospun nanofibers, which obtained from electrospinning technique, have the strong potential application for sensor because the nanofibers have surface area approximately one to two orders of the magnitude larger than continuous films. Quratz crystal microbalance (QCM) is highly sensitive to mass changes in the presence of a coating that interacts with the target gas. The characteristics of QCM gas sensors depend on the kinds of sensing films coated on their electrodes.

A novel gas sensor composed of electrospun nanofibrous membranes and QCM was fabricated. The electrospun nanofibers with diameter of 100-400 nm can be deposited on the surface of QCM by electrospinning the homogenous blend solutions of cross-linkable PAA and PVA. A series of nanofibrous membranes with various weight percentage of PAA to PVA were fabricated and characterized regarding their morphology and sensitivity to NH_3. The average diameter and rigidity of nanofibers was increased due to the increasing of viscosity and conductivity of the blend solutions by increasing the content of PAA component. Sensing experiments were examined by measuring the resonance frequency shifts of QCM which due to the additional mass loading. The results showed that the

sensing properties were mainly affected by the content of PAA component in nanofibrous membranes, concentration of NH_3, and relative humidity. Additionally, the sensitivity of nanofibrous membranes was much higher than that of continuous layer-by-layer (LBL) films. Additionally, the nanofibrous membranes have the potential application to use as a humidity sensor.

Additionally, electrospun fibrous PAA membranes were studied as sensing material coated on QCM for ammonia detection at ppb level. The fibrous membranes with different morphology can be deposited on the electrode of QCM by electrospinning the PAA solutions with various solvent composition of H_2O and ethanol. The results of sensing experiments indicated that the sensitivity of the fibrous membranes coated QCM (FM-QCM) sensors was 4 times higher than that of the casting films coated QCM (CF-QCM) sensors. Meanwhile, the FM-QCM sensors exhibited high sensitivity towards low concentration of ammonia, as low as 130 ppb at the relative humidity of 40 %. The pre-sorbed water in fibrous membranes was proved to be the key factor to affect the sensitivity of FM-QCM sensors for ammonia. The sensor performance has been found to depend on the morphology of the fibrous membranes, concentration of ammonia, coating load of the fibrous membranes on QCM, and relative humidity. Preliminary study of the stability investigation was also presented. Based on the new established model for gas sensors, a series of gas sensors with different charged fibrous polyelectrolytes coated on QCM can be fabricated to detect the oppositely charged gases, such as H_2S, $(CH_3)_2S$, N_2O, NO_2, etc.

Publication list regarding the present thesis

Original Papers

1. Bin Ding, Eiji Kimura, Tomokazu Sato, Shiro Fujita and Seimei Shiratori, "Fabrication of blend biodegradable nanofibrous nonwoven mats via multi-jet electrospinning". Polymer 45 (2004) 1895-1902.
2. Bin Ding, Jinho Kim, Yasuo Miyazaki and Seimei Shiratori, "Electrospun nanofibrous membranes coated quartz crystal microbalance as gas sensor for NH_3 detection", Sensors and Actuators B: Chemical 101 (2004) 373-380.
3. Bin Ding, Jinho Kim, Eiji Kimura and Seimei Shiratori, "Layer-by-layer hybrid films of poly(acrylic acid) and titania on electrospun nanofibers", Nanotechnology 15 (2004) 913-917.
4. Bin Ding, Michiyo Yamazaki and Seimei Shiratori, "Electrospun fibrous polyacrylic acid membrane-based gas sensors", Sensors and Actuators B: Chemical, (In press).
5. Bin Ding, Kouji Fujimoto and Seimei Shiratori, "Preparation and characterization of self-assembled polyelectrolyte multilayered films on electrospun nanofibers", Thin Solid Films, (Revised).
6. Bin Ding, Jian Gong, Jinho Kim and Seimei Shiratori, "Polyoxometalate nanotubes from layer-by-layer coating and thermal removal of electrospun nanofibers", Nanotechnology, (In review).
7. Kouji Fujimoto, Shiro Fujita, Bin Ding and Seimei Shiratori, "Fabrication of layer-by-layer self-assembly films using roll-to-roll process", Japanese Journal of Applied Physics, (In press).
8. Katsuhiro Onozuka, Bin Ding, Shinichiro Sugi, Shingo Ohno, Masato Yoshikawa and Seimei Shiratori, "Dye-sensitized solar cells based on electrospun nanofibrous membranes" Nanotechnology, (In review).

International Conference

1. Bin Ding, Jinho Kim, Kouji Fujimoto and Seimei Shiratori, "Electrospun nanofibrous polyelectrolyte membranes for advanced chemical sensors", The 10^{th} international

meeting on chemical sensors (2004, Tsukuba, Japan). (Oral presentation)

2. Bin Ding, Masashi Kikuchi, Michyo Yamazaki and Seimei Shiratori, "Ammonia sensors based on electrospun poly(acrylic acid) fibrous membranes", The 3rd IEEE conference on sensors (2004, Vienna, Austria). (Oral presentation)
3. Katsuhiro Onozuka, Bin Ding, Seimei Shiratori, Shinichiro Sugi, Shingo Ohno and Masato Yoshikawa, "Application of electrospun titanium dioxide nanofiber to dye-sensitized solar cells", The 6th international conference on nano-molecular electronics (ICNME 2004) (2004, Kobe, Japan). (Poster)

Domestic Conference

1. Bin Ding, Jinho Kim and Seimei Shiratori, "Composite nanofiber interface for chemical and biochemical sensor", The technical meeting on chemical sensor, IEE Japan, (2003, Tokyo, Japan). (Oral presentation)
2. Bin Ding and Seimei Shiratori, "Generation of biodegradable nanofibrous membranes via electrospinning", The 53rd symposium on macromolecules, (2004, Sappro, Japan). (Poster)
3. Bin Ding and Seimei Shiratori, "Layer-by-layer structured films on electrospun nanofibrous membranes", The 53rd symposium on macromolecules, (2004, Sappro, Japan). (Poster)
4. Kouji Fujimoto, Bin Ding, Jinho Kim and Seimei Shiratori, "abrication of layer-by-layer ultrathin films by roll-to-roll method" The 64th symposium of applied physics, (2003, Fukuoka, Japan). (Poster)
5. Kouji Fujimoto, Bin Ding, Jinho Kim and Seimei Shiratori, "reparation of layer-by-layer ultrathin films by roll-to-roll method" IEICE, (2003, Niigata, Japan). (Poster)

Patents

1. 光触機能を持つナノファイバージートおよびその製造方法。特願：２００４－

８０１８１
（理・助教）白鳥世明（理・学生） Bin Ding

2. セラミックスハニカム製H_2S除去の方法。特願：２００４－８０１８０
（理・助教）白鳥世明（理・学生） Bin Ding（理・学生）木村英司
（学外）大林昌則（学外）野田　究

3. 色素増感型金属酸化物半導体電極及びその製造方法並べに色素増感型太陽電池。
特願：２００４－３０１７０７
（理・助教）白鳥世明（理・学生）丁彬（理・学生）大野塚克弘
（学外）杉信一郎（学外）大野信吾（学外）吉川雅人

Other publications

Papers

1. Bin Ding, Hak-Yong Kim, Se-Chul Lee, Chang-Lu Shao, Douk-Rae Lee, Soo-Jin Park, Gyu-Beom Kwag and Kyung-Ju Choi, “Preparation and characterization of a nanoscale poly (vinyl alcohol) fiber aggregate produced by an electrospinning method”, Journal of polymer science Part B: Polymer physics, 40 (2002)1261-1268.
2. Bin Ding, Hak-Yong Kim, Se-Chul Lee, Douk-Rae Lee and Kyung-Ju Choi, “Preparation and characterization of nanoscaled poly(vinyl alcohol) fibers via electrospinning”, Fibers and Polymers, 3 (2002) 73-79.
3. Se Chul Lee, Hak-Yong Kim, Duck Rae Lee, Bin Ding and Soo Jin Park, “Morphological characteristics of electrospun poly(vinyl alcohol) nonwoven”, Journal of the Korean Fiber Society, 39 (2002) 316-322.
4. Bin Ding, Hak-Yong Kim, Chul-Ki Kim, Myung-Seob Khil and Douk-Rae Lee, “Morphology and crystalline phase study of electrospun TiO_2-SiO_2 nanofibers”, Nanotechnology, 14 (2003) 532-537.
5. Jian Gong, Xiang-Dan Lee, Chang-Lu Shao, Bin Ding, Douk-Rae Lee and Hak-Yong Kim, “Photochromic and thermal properties of poly(vinyl alcohol) /$H_6P_2W_{18}O_{62}$ hybrid membranes”, Materials chemistry and physics, 79 (2003) 87-93.
6. Chang-Lu Shao, Hak-Yong Kim, Jian Gong, Bin Ding, Douk-Rae Lee and Soo-Jin

Park, “Fiber mats of poly(vinyl alcohol)/silica composite via electrospinning”, Materials Letters, 57 (2003) 1579-1584.

7. Jian Gong, Xiang-Dan Li, Bin Ding, Douk-Rae Lee and Hak-Yong Kim, “Preparation and characterization of fiber mats of $H_4SiMo_{12}O_{40}$/PVA via electrospinning”, Journal of Applied Polymer Science, 89 (2003) 1573-1578.
8. Yong Tang Jia, Hak-Yong Kim, Jian Gong, Douk-Rae Lee, Bin Ding and Narayan Bhattarai, “Synthesis and characterization of ABA type block copolymer of trimethylene carbonate and epsilon-caprolactone”, Polymer International, 53 (2004) 312-319.
9. Bin Ding, Chulki Kim, Hakyong Kim, Minkang Se and Soojin Park, “Titanium dioxide nanofibers prepared by using electrospinning method” Fibers and Polymers, 5 (2004) 105-109.

International conference

1. Bin Ding, Hakyong Kim, Jian Gong, Changlu Shao and MinGang Su, “A novel method for making titanium dioxide nanofibers by using electrospun method” 39th International symposium on macromolecules, (2002, Beijing, China).
2. Bin Ding, Jian Gong, Xiangdan Li, Duckrae Lee and Hakyong Kim, “Preparation and characterization of photochromic ultrafine fiber mats of $H_4SiMo_{12}O_{40}$/PVA via electrospinning”, International conference for inauguration of SOTSEA (2002, Daegu, South Korea).

Acknowledgements

This dissertation and the related study were completed under the devoted guidance and supervision of Prof. Shiratori of Keio University in Japan. First of all, I would like to express my cordial gratitude to Prof. Shiratori for his valuable advice, helpful instruction, warm encouragement and important financial support.

I sincerely thank Prof. Tomita, Prof. Hatayama and Prof. Kawaguchi for their peer reviewing and valuable comments.

I gratefully acknowledge Dr. Fujita, Dr. Kim, Dr. Higuchi, Dr. Kikuchi, Dr. Fujimoto and other friends in the same lab for their warm and kind help in my research work and daily life in Japan.

This work was partly funded by Keio Life Conjugate Chemistry (LCC) Program of COE Research Project sponsored by Japanese Ministry of Education, Science Culture, and Sports.

Plusto and Ebara Co., Ltd. are acknowledged for their financial support for MF project.

Partial support from Marubun Research Promotion Foundation of Japan is appreciated.

I am grateful to my wife C.R. Li and my son R.D. Ding for their many years of full support and continuous encouragement.

Finally, I would like to delicate this dissertation to my parents for their love and support.